

UNIVERSITY OF SALERNO



DEPARTMENT OF CHEMISTRY AND BIOLOGY "A. Zambelli"

Ph. D. Course in Chemistry – XXXIV Cycle

Ph. D. Thesis in Chemistry

## **Synthesis of Eco-Friendly Additives for Sustainable Tanning Processes**

**Academic tutors:**

Prof. Placido Neri

**PhD Student:**

Ilaria Quaratesi

Prof. Carmine Gaeta

**Industrial tutor:**

Dr. Rocco Gliubizzi

**Serial number:**

8800100053

**PhD coordinator:**

Prof. Claudio Pellecchia

Academic years 2018/2021





# Summary

|  |           |
|--|-----------|
| <b>Summary .....</b>   | <b>4</b>  |
| <b>Abstract .....</b>  | <b>8</b>  |
| <b>Glossary of terms .....</b>   | <b>10</b> |
| <b>1. Introduction.....</b>  | <b>11</b> |
| 1.1 Tanning Industry.....  | 11        |
| 1.2 Tanning Process.....   | 12        |
| 1.3 The properties of leather in tanning .....   | 15        |
| 1.3.1 The hide .....   | 15        |
| 1.3.2 The isoelectric point and the shrinkage temperature.....   | 19        |
| 1.3.3 Tannage .....  | 21        |
| 1.3.3.1 Vegetable tanning .....  | 22        |
| 1.3.3.2 Chrome tanning.....  | 24        |
| 1.3.3.3 Aldehydic tanning.....   | 26        |
| 1.3.3.4 Synthetic tanning.....   | 27        |
| <b>2. Research aims and thesis outline .....</b>   | <b>32</b> |
| <b>3. <math>\beta</math>-Cyclodextrin-Based Tanning Materials: <i>SupraSynt</i> Additives as an eco-friendly alternative .....</b> | <b>35</b> |
| 3.1 General overview .....   | 35        |
| 3.1.1 Cyclodextrins .....  | 35        |
| 3.1.2 Molecular recognition .....  | 38        |
| 3.1.3 Bisphenol S and related syntans .....  | 40        |
| 3.2 Synthesis and characterization.....  | 41        |
| 3.2.1 Synthesis and characterization of new supramolecular tanning systems ( <i>SupraSynts</i> ).....                              | 41        |

|           |   |           |
|-----------|---|-----------|
| 3.2.2     | <sup>1</sup> H NMR characterization of the obtained supramolecular tanning systems.....       | 43        |
| 3.2.3     | ATR-FTIR characterization of the obtained SupraSynts .....                                    | 46        |
| 3.3       | Tanning Tests.....  | 48        |
| 3.3.1     | Laboratory scale tests.....   | 48        |
| 3.3.1.1   | Micro- DSC measurements: evaluation of the efficiency of the tanning interaction.....         | 52        |
| 3.3.1.2   | ATR-FTIR characterization of L-SS <sub>i</sub> products.....                                  | 57        |
| 3.3.2     | Pilot scale tests: characterisation of L-SS <sub>i</sub> samples by standard methods .....    | 60        |
| 3.4       | Conclusion .....  | 66        |
| 3.5       | Experimental section.....   | 67        |
| <b>4.</b> | <b>Selective recognition of bisphenol S isomers in water by β-cyclodextrin .....</b>          | <b>71</b> |
| 4.1       | General overview .....  | 71        |
| 4.2       | Synthesis and characterization.....   | 72        |
| 4.2.1     | Complexation study of 4,4'-BPS and 2,4'-BPS in solution via 1D and 2D NMR .....               | 73        |
| 4.2.2     | Thermodynamic insights on the complexation of 4,4'-BPS and 2,4-BPS in solution by ITC.....    | 79        |
| 4.2.3     | Complexation study of 4,4'-BPS and 2,4'-BPS in the gas phase by FT ICR MS investigation ..... | 84        |
| 4.2.4     | DSC and TGA analysis of the inclusion complexes 4,4'-BPS@β-CD and 2,4'-BPS@β-CD.....          | 86        |
| 4.2.5     | FT IR spectra of BPSs@β-CD complexes.....   | 89        |
| 4.2.6     | Complexation study of 4,4'-BPS and 2,4'-BPS in the solid state                                | 92        |
| 4.3       | Conclusions.....  | 95        |
| 4.4       | Experimental section.....   | 96        |

|           |  |            |
|-----------|--|------------|
| <b>5.</b> | <b>Bio-based re-tanning agent by sodium alginate .....</b>   | <b>105</b> |
| 5.1       | General Overview .....   | 105        |
| 5.1.1     | Sodium alginate as a green alternative .....   | 105        |
| 5.1.2     | The ultrasounds and the cavitation phenomenon .....  | 110        |
| 5.1.3     | Ultrasonic transducer .....  | 113        |
| 5.2       | Synthesis and characterization of SADs .....   | 114        |
| 5.2.1     | Preliminary tests.....   | 114        |
| 5.2.2     | Synthesis of samples .....   | 118        |
| 5.2.2.1   | Experiments with the ultrasonic horn Sonic vibracell VCX 750   | 118        |
| 5.2.2.2   | Experiments with bath type transducers .....   | 119        |
| 5.2.3     | SADs characterization.....   | 121        |
| 5.2.3.1   | The oxidation degree.....  | 121        |
| 5.2.3.2   | Viscosity.....   | 122        |
| 5.2.3.3   | ATR-FTIR analysis.....   | 123        |
| 5.3       | Lab-scale tanning tests .....  | 125        |
| 5.4       | Sodium alginate derivatives SADs tanning ability - Denaturation temperature evaluation by micro- DSC ..... | 126        |
| 5.5       | Upscaling the US reactor .....   | 132        |
| 5.6       | Optimisation of depolymerisation and aldehyde group formation. 133   |            |
| 5.6.1     | Sodium alginate derivatives SADs tanning ability - Denaturation temperature evaluation by micro- DSC ..... | 136        |
| 5.7       | Conclusion .....   | 140        |
| 5.8       | Experimental section.....  | 141        |
| <b>6.</b> | <b>Final conclusions .....</b>   | <b>143</b> |
|           | <b>Scientific contributions:.....</b>  | <b>144</b> |



## Abstract

Sustainability is a global level challenge for tanning industry whose production is based on Cr(III) salts for more than 90%, negatively impacting both biotic and abiotic factors in an ecosystem. Societal challenges are strongly pushing tanning industry to develop a more sustainable leather value chain. In fact, over the past 100 years, a lot of synthetic tannins have been developed for trying to replace chrome and to make the process more sustainable.<sup>1</sup> An alternative tanning system, in fact, should not only satisfy environmental criteria, but should be also able to match the properties of chrome tanned leathers.<sup>2</sup> For this reason, the *wet white* tanning process seems, nowadays, the only alternative to develop a less polluting process obtaining high quality products. In this respect, many efforts have been focused on the design of new environmental friendly and high-performance tanning products for industrial applications.

This industrial PhD project has been developed in collaboration with the *BI-QEM SPECIALTIES S.P.A.*, *Leather and Footwear Research Institute (ICPI)*, *Politehnica University of Bucharest*, and *FGL International S.P.A.*

In the first phase of this PhD project, a new supramolecular system based on bisphenol S and  $\beta$ -cyclodextrin was synthesized and used as a tanning agent and as an eco-friendlier and sustainable alternative to tannins currently on the market. Firstly, we investigated the formation of the supramolecular system, using 1D and 2D NMR, FT-IR, and high-resolution mass spectrometry and we studied the different interaction between  $\beta$ -cyclodextrin and the two isomers of bisphenol S. Secondly, we tested the obtained systems on raw hide to evaluate their efficiency in the tanning process on both a laboratory and pilot scale, in collaboration with *FGL International S.P.A.*

In the project phase carried out at the *Leather and Footwear Research Institute (ICPI)*, Bucharest, under the supervision of Dr. Elena Badea, the

---

<sup>1</sup> (a) A. D. Covington, *Chem. Soc. Rev.*, **1997**, 26, 111. (b) A.D. Covington, W.R. Wise, *Tanning Chemistry The science of Leather*, Ed. Royal Society of Chemistry, Croydon, **2020**.

<sup>2</sup> N. Nishad Fathima, T. Prem Kumar, D. Ravri Kumar, J. Raghava Rao, B. Unni Nair, *J. Am. Leather Chem. Assoc.*, **2005**, 100, 58-65.

goal was to obtain a fully eco-sustainable re-tanning agent from sodium alginate, a biodegradable, renewable biomass, using the ultrasonic technology. The efficacy of the obtained sodium alginate products (SAD) was evaluated by micro-differential scanning calorimetry (micro-DSC)<sup>3</sup> and attenuated total reflection mode infrared spectroscopy (FTIR-ATR).<sup>4</sup> The results so far obtained have confirmed the suitability of the various SADs as non-toxic and biodegradable re-tanning agents.

---

<sup>3</sup> C. Carşote, E. Badea, L. Miu, G. Della Gatta, *J. Therm. Anal. Calorim.*, **2016**, *124*, 1255–1266.

<sup>4</sup> C. Sendrea, C. Carsote, E. Badea, A. Adams, M. Niculescu, H. Iovu, *Series Chemistry*, **2016**, *78*, 27-38.

## Glossary of terms

**$\beta$ -CD** –  $\beta$  cyclodextrin

**SS** – SupraSynt

**4,4'-BPS** – 4,4'-dihydroxydiphenyl sulfone

**2,4-BPS** – 2,4-dihydroxydiphenyl sulfone

**$T_s$**  – Shrinkage temperature

**$T_d$**  – Denaturation temperature

**US** – Ultrasound treatment

**SA** – Sodium alginate

**OSA** – Oxidized sodium alginate

**SADs** – Sodium alginate derivatives

**OD** – Oxidation degree

# 1. Introduction

## 1.1 Tanning Industry

The leather tanning industry is the sector that recovers and enhances a by-product of slaughter into a versatile and valuable final product. Raw hide is mostly obtained from the processing of adult bovine hides, which accounts for 71% of total production, followed by sheep (11%), goats (10%), and calves (8%).<sup>5</sup>

The Italian tanning sector is considered one of the most profitable sectors of our economy. About 1200 companies are active on the Italian territory according to the data provided by the National Union of the Tanning Industry (UNIC). Italian production plays an important role on the international scene, covering about 22% of global tanning production and 65% of European production. The main customers of Italian tanneries have always been footwear manufacturers (42%), followed by leather goods (24%), furniture industry (27%), car interiors (11%), and clothing (5%).

The Italian tanning sector has four main districts:

- Arzignano district: located in the Chiampo valley (Vicenza), it is the most important district in Italy in terms of production and number of employees, as well as one of the largest districts worldwide. It covers an area of about 130 km<sup>2</sup> and UNIC estimates that the production of the Veneto district covers more than half of the national turnover in the sector, with more than half going to foreign markets. On the production level, the district is specialized in the processing of large bovine leathers destined for automotive interiors, footwear, leather goods, and furnishings.
- Santa Croce sull'Arno district: located in Tuscany, it covers about 233 km<sup>2</sup>. According to UNIC data, about 35% of national production is concentrated in the district, with an overall turnover that accounts for 28% of the national total. The workings, destined

---

<sup>5</sup> <https://www.unic.it/>

mainly for the fashion sector, are characterized by a high degree of craftsmanship and concern above all medium and small cow hides, many of which are used for the specialty of sole leather. In the Tuscan district is concentrated 98% of the national production of sole leather, which represents about 70% of that of the countries of the European Union.

- Solofra district: located in Campania in an area of about 115 km<sup>2</sup>. The companies are mainly located in Solofra's area (Avellino), Montoro Inferiore, Montoro Superiore and Serino, with some important presences also in the surroundings of Naples (Arzano, Casandrino, Casoria). The tanneries of the district of Solofra are specialized in the tanning of small sheep and goat skins, whose production is mainly destined to the clothing, footwear, and leather goods sectors. Currently worth about 7% of the national tanning production.
- Lombardy district: is located in the province of Milan, mainly in the Magenta area and is responsible for over 5% of total national production. The tanneries belonging to the Lombardy district are specialized in the sheep and goat sector for high fashion.

## 1.2 Tanning Process

The term tannage refers to the treatment for transforming animal hide into leather. The purpose of tannage is to guarantee, through chemical processes, that the leather is breathable and rot-proof. At the same time, it ensures the preservation of the natural fibrous structure from which strength and flexibility are derived. A satisfactory tanning effect is characterized by a complete penetration and uniform distribution of the tanning compounds. This is achieved through the action of special products called *tanning agents*, which irreversibly attach themselves to the hide and consolidate its internal structure, giving each hide specific characteristics. These characteristics are due to the intrinsic properties of the animal's hide when it is still alive.<sup>6</sup>

---

<sup>6</sup> E. Kamla Nagar, *Leather Processing & Tanning Technology*, Niir Project Consultancy Services, Delhi, 2011.

The tanning cycle starts with the arrival at the tannery of animal skins of various types and origins, preserved by methods such as salting or drying. Preservation must be carried out as quickly as possible in order to create conditions within the leather that make it impossible for bacteria and microorganisms that produce the enzymes of putrefaction to live and develop.

The tanning process consists of a series of long and complex chemical and mechanical operation. The entire process can be divided into three macro-phases (Figure 1):<sup>7</sup>

1. Pre-Tanning
2. Tanning
3. Post Tanning

---

<sup>7</sup> A.D. Covington, W.R. Wise, *Tanning Chemistry The science of Leather*, Ed. Royal Society of Chemistry, Croydon, 2020.

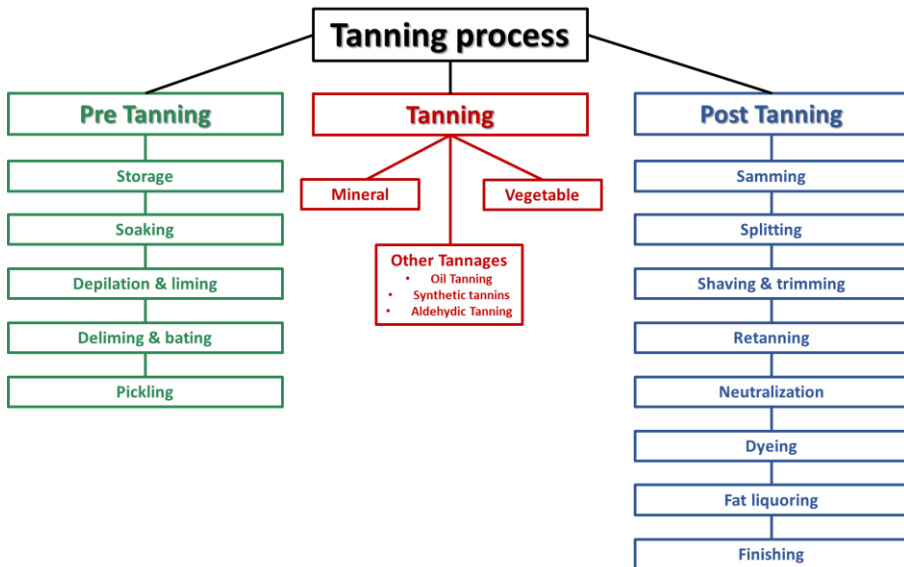


Figure 1. Scheme of the tanning process.

All chemical operations, up to post-tanning treatments, are carried out inside the tanning drum, a machine consisting of a large cylinder that rotates around its own axis (Figure 2). The hides, water, and chemicals are introduced into the tanning drum, so that the mechanical action of rotation can promote the penetration of the products into the leather and thus the tanning process.



Figure 2. Tanning drum.

### 1.3 *The properties of leather in tanning*

#### 1.3.1 *The hide*

The term *hide* refers to the outer covering of the body of vertebrate animals which not only protects the organism from environmental influences, but also for the perception of general external sensations, excretion and secretion. This covering can be easily separated from the rest of the body and constitutes the tanner's raw material.

There are three separate and distinct layers in hide: the epidermis, the thin outer layer, the dermis (or corium), and the fatty subcutaneous layer (Figure 3).<sup>8</sup>

---

<sup>8</sup> <https://beljoly.com/blogs/news/what-is-full-grain-leather>

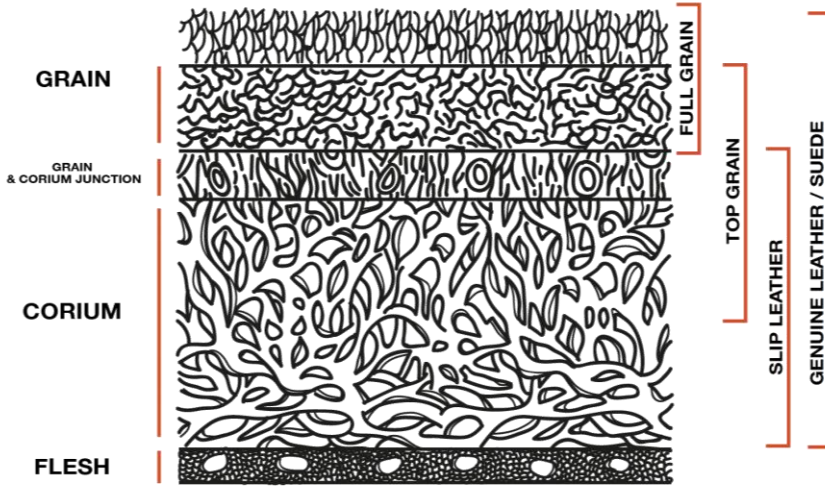


Figure 3. Diagram of a hide section.

The dermis is the element which is used to produce leather while the other parts are removed during the pre-tanning process (beamhouse operations). It represents about 85% of the thickness of the skin. The outer layer is called the grain and is the area where the collagen fibres are most compact. It constitutes the outer layer of the tanned leather, from which the quality of the grain can be deduced. The inner side is called flesh side and is the part which is directly connected with the body tissue.<sup>9</sup>

The protein which constitutes the dermis and who reacts directly in the tanning process, is collagen. The collagen family consist of trimeric molecules of the extracellular matrix that are used, primarily, to provide structural integrity to cells.<sup>10</sup>

Each collagen molecule is composed of a precise combination of three polypeptide  $\alpha$ -chains that vary according to the type of collagen. Presently,

<sup>9</sup> J.H. Sharpouse, *Leather Technician's Handbook*, Ed. Leather Producer's Ass., Northampton, 1983.

<sup>10</sup> M.K. Gordon, R.A. Hahn, *Cell Tissue Res*, 2010, 339, 247–257.

no less than 28  $\alpha$ -chains have been reported, each encoded by a unique gene.<sup>11,12</sup>

Each of the three  $\alpha$ -chains within the molecule forms an extended left-handed helix with a pitch of 18 amino acids per turn, stabilised by numerous hydrogen bonds.<sup>13</sup> The assembly into a triple helix is driven by the presence of the glycine residue, the smallest amino acid, which is present in every third position of the polypeptide chains. The  $\alpha$ -chains are assembled in such a way that all the glycine residues are positioned in the centre of the triple helix, with the other bulkier amino acids occupying the outer positions.<sup>14</sup> All chains are characterized by containing repetitions of the tripeptide Gly-X-Y where Gly represents glycine, and the X and Y positions can be any residue but are commonly proline and hydroxyproline, respectively.<sup>15</sup> Glycine makes up one third of the total amino acids, while proline and hydroxyproline together make up another third (Figure 4). The remaining 40% is made up of the other amino acids. This sequence is repeated in a segment about 1400 amino acids long.<sup>16</sup>

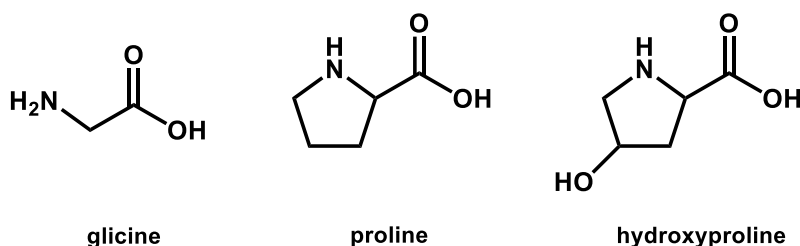


Figure 4. Main amino acids of the collagen.

Three intertwined polypeptides constitute the tropocollagen molecule, the basic structural unit of collagen fibrils.<sup>17</sup>

---

<sup>11</sup> M.H. Kerkhof, L. Hendriks, H.A.M. Brölmann, *Int. Urogynecol. J.*, **2009**, 20, 461–474.

<sup>12</sup> M.A. Cremer, E.F. Rosloniec, A.H. Kang, *J. Mol. Med.*, **1998**, 76, 275–288.

<sup>13</sup> H. Hofmann, P.P. Fietzek, K. Kuhn, *J. Mol. Biol.*, **1978**, 125, 137 – 165.

<sup>14</sup> K. Gelsea, E. Poschlb, T. Aigner, *Adv. Drug Deliv. Rev.*, **2003**, 55, 1531–1546.

<sup>15</sup> L.D. Muiznieks, F.W. Keeley, *Biochim Biophys Acta.*, **2013**, 1832, 866–875.

<sup>16</sup> P.Li, G. Wu, *Amino Acids*, **2018**, 50, 29-38.

<sup>17</sup> G. Meisenberg, W.H. Simmons, *Principles of medical biochemistry e-book*. Elsevier Health Sciences, **2016**.

Several tropocollagen molecules join to form thin filaments (60-100 nm) called microfibrils and more microfibrils aggregate (in bundles) to form fibrils (0.2  $\mu\text{m}$ ) and more fibrils to form collagen fibres (Figure 5).

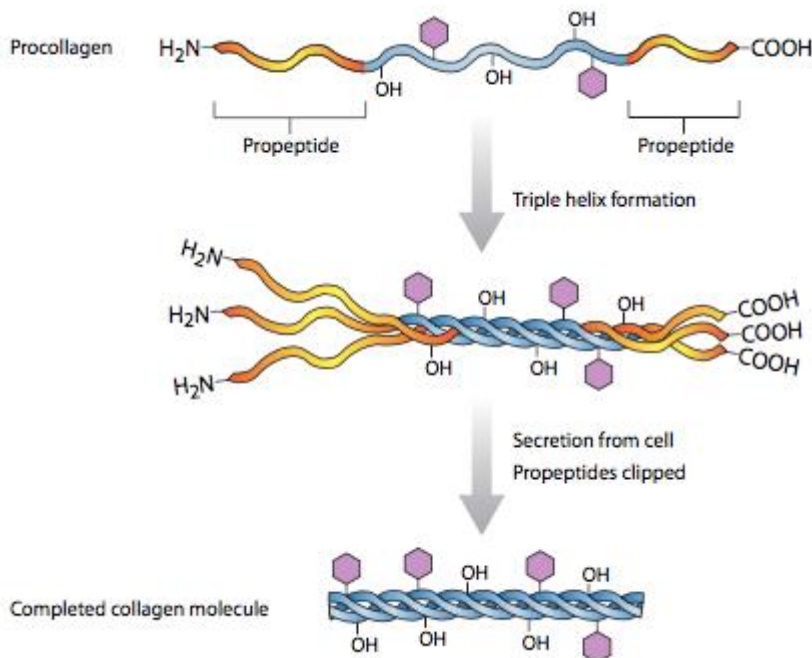


Figure 5. Collagen structure.<sup>18</sup>

The aim of tannage is to increase the hydrothermal stability of native collagen, increase its biological inertness, and improve the hide's physical properties.<sup>19</sup>

The covalent cross-links that are established between the side chains also act on the stabilisation of the collagen structure, but not on its formation: the aim of the tanning process is precisely to increase the number of these links in the dermis in order to improve the mechanical properties and contraction temperature of the leather (Figure 6). Tannage, therefore, must be intense as the process by which the tanning products combine

<sup>18</sup> <https://bio.libretexts.org/@go/page/16171>.

<sup>19</sup> C. Carsote, E. Badea, *Herit. Sci.*, **2019**, 7, 48.

irreversibly with the collagen, leading to the consolidation of its structure by stabilising the crosslinking between the collagen polypeptide chains. The consequence of these bonds is that the leather, once tanned, will possess great thermal stability, great resistance to attack by chemical and bacterial agents and the ability not to harden in the dry state.<sup>20</sup>

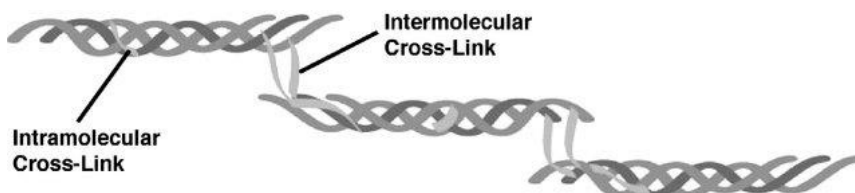


Figure 6. Collagen cross-links.<sup>21</sup>

### 1.3.2 The isoelectric point and the shrinkage temperature

The isoelectric point and the shrinkage temperature are the characteristics that most influence the diffusion and fixation of tanning agents in collagen.

The isoelectric point IEP is a fixed pH where the sum of positive and negative charges of a substrate, in this case collagen, are equal and thus there is no overall charge.<sup>22</sup> Like amino acids, proteins are also amphoteric in character. That means that at pH values below the isoelectric point the overall charge will be positive as progressively more carboxylates are protonated, reducing the negative charge component (cationic skin). Vice versa, when collagen is placed in an alkaline bath, the positive charges are neutralised by the OH<sup>-</sup> ions in the medium, resulting in the protein being negatively charged overall (anionic skin). Consequently, by varying the pH value of the medium it is possible to reach the isoelectric point (Figure 7).<sup>23</sup>

---

<sup>20</sup> P. Neri, C. Gaeta, B. Pirolò, *Processi di lavorazione delle pelli mediante p-solfonatocalix(n)areni*. SA2008A000038, **2008**.

<sup>21</sup> R. Diegelmann, *Wounds*, **2001**, *13*, 177-182.

<sup>22</sup> A.D. Ballantyne, S. J. Davis, *modelling the charge across pH and isoelectric point of bovine collagen during leather manufacture*, IULTCS Congress, Dresden, **2019**.

<sup>23</sup> J.H. Highberger, *J. Am. Chem. Soc.*, **1939**, *61*, 2302-2303.

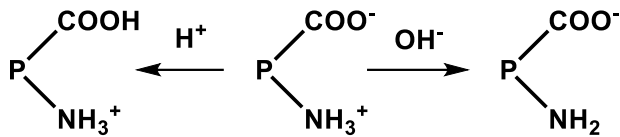


Figure 7. Amphoteric behaviour of collagen (P=protein).

The pH of collagen, and its isoelectric point, is between 7-7.5. It follows that at pH values corresponding to its isoelectric point, collagen is characterised by great chemical-physical inertia: it has the least tendency to react, the least viscosity and the least swelling.<sup>24</sup>

The other important property of collagen is that it exhibits a sudden shrinkage in length when heated in water. Skin collagen that has not received chemical processing shrinks at about 50°C. There is little variation in this temperature with different mammalian species or different regions of the skin. This shrinkage is due to the fact that the backbone chains of the molecule exist in an extended form, held in this form by hydrogen bonding. Thus, when the hide is heated, is reached a point at which the energy input exceeds that of the hydrogen bonding.<sup>25</sup>

The shrinkage temperature of leather ( $T_s$ ) is the most commonly measurement of hydrothermal stability. The principle of the method is to suspend the test piece in water, in the form of a strip, then to heat the water at a rate of 2°C min<sup>-1</sup>, according to the ISO 3380:2015 [IULTCS/IUP 16]. The shrinkage temperature is noted when the sample visibly shrinks (Figure 8).

<sup>24</sup> G. Manzo, *Chimica e tecnologia del cuoio*, Ed. Media Service, Legnano (MI), 1998.

<sup>25</sup> M. Kite, R. Thomson, *Conservation of leather and related materials*, Ed. Elsevier Ltd, Burlington, 2006.

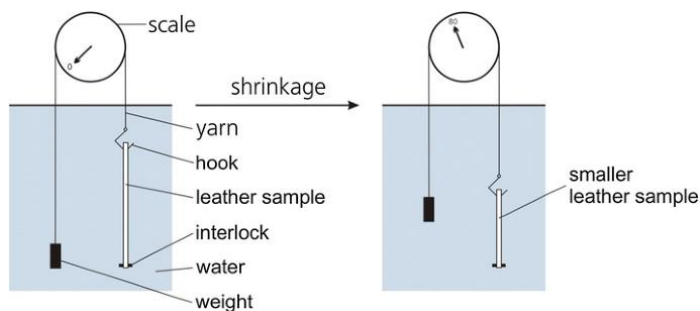


Figure 8. Test for shrinkage temperature.<sup>26</sup>

Karavana<sup>27</sup> demonstrated that the thermal behaviour of tanned leathers can be studied using differential scanning calorimetry as there is a correlation between this measurement and the conventional shrinkage temperature test. Furthermore, the results obtained from DSC analysis can be correlated with the theoretical binding mechanisms of each type of tanning agent. In fact, according to Covington, the hydrothermal stability of collagen increases as the number of stable bonds and bond strengths increase.<sup>28</sup>

### 1.3.3 Tannage

The first step in the tanning process is the *Beamhouse operations*. They are a set of chemical, chemical-physical, enzymatic and mechanical processes which aim to prepare the raw hide for tanning. These processes take different names according to their function: soaking, liming, deliming and pickling.<sup>29</sup> The pickling phase is one of the most important because allows to obtain the best conditions of reactivity towards the tanning products using acid condition. To obtain a pH of about 2-3, the hides are left in contact with the tanning bath for about 16 hours in a float consisting of

<sup>26</sup> M. Prokein, M. Renner, E.E. Weidner, T. Heinen, *Clean Technol. Environ. Policy*, **2017**,19.

<sup>27</sup> E. Onem, A. Yorgancioglu, H.A. Karavana, O. Yilmaz, *J. Therm. Anal. Calorim.*, **2017**, 129, 615–622.

<sup>28</sup> A.D. Covington, *Tanning chemistry, the science of leather*. Northampton: The University of Northampton; **2009**.

<sup>29</sup> <https://www.conceriaf3.com/processi-di-concia-della-pelle/>

sulphuric acid or mixtures of acids such as formic and sulphuric. At this point the tanning phase can start.<sup>30</sup>

### 1.3.3.1 Vegetable tanning

Vegetable tanning is one of the oldest methods to convert animal hides into a biomaterial. It is thought to date back to prehistoric times, when men learned to transform the hides of animals killed during hunting into clothing and tools. Vegetable tanning has evolved over the centuries, through the selection of the most suitable plants for tannin extraction and the improvement of the efficiency of production methods. However, the basic steps have remained unchanged until today, handed down between generations as a precious craft tradition. In particular, the vegetable tanning process produces a hard leather which, thanks to its resistance, can be used for leather soles and in some furniture components.<sup>31</sup>

The term *tannins* refers to a very complex set of natural compounds, widely distributed in the plant kingdom, whose most interesting quality for the tanner is the stabilisation of proteins, which allows the transformation of hides into leather. These products are characterised by the presence of phenolic groups and form complex molecular assemblies, whose molecular weight is generally high. They can be more or less soluble in water. Tannins can be divided into two large families: hydrolysable tannins, in which the main constituent of the molecule is gallic acid and its derivatives, and condensed tannins, in which the main constituents are complex polyphenolic structures similar to catechins (Figure 9).<sup>32</sup>

---

<sup>30</sup> I.A. Ioannidis, R.A. Hancock, A.D. Convington, XX Congresso internazionale, *Union Leather Techn. Chem.Soc.*, Phyladelphia, 15-19 October, **1989**.

<sup>31</sup> <https://www.tannins.org/the-vegetable-tanning-process/>

<sup>32</sup> P. Schofield, D.M. Mbugua, A.N. Pell, *Anim Feed Sci Technol*, **2001**, *91*, 21-40.

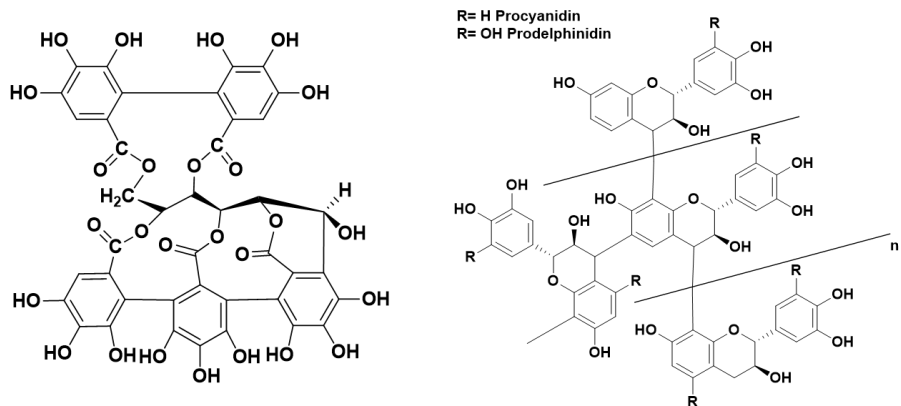


Figure 9. Example of hydrolysable tannin (left) and condensed tannin (right).

For vegetable tannins, the primary reaction is mainly through multiple hydrogen bonding, while the subsequent reaction is to crosslink the tannin molecules together, thus creating matrices of crosslinked poly-phenolic species bound to collagen effectively working as a single moiety (Figure 10).<sup>33</sup>

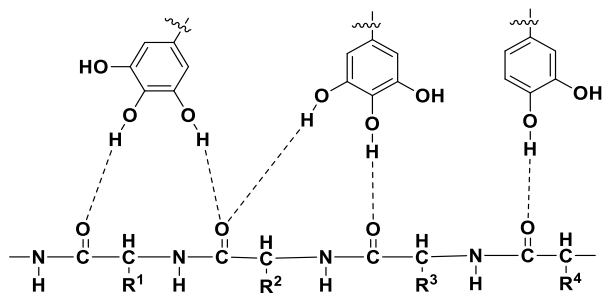


Figure 10. Model of hydrogen bonding between plant polyphenols and collagen.

Vegetable tanning involves the slow penetration of large reactive molecules and long processing time, which is one of biggest disadvantages of using natural tannins. On average, the vegetable tanning process can take up to 60 days. Consequently, it is not practical and, at the same time, expensive.

<sup>33</sup> Z. Sebestyén, E. Jakab, E. Badea, E. Barta-Rajnai, C. Şendrea, Zs.Czégény, *J. Anal. Appl. Pyrolysis*, **2019**, 138, 178–187.

On the other hand, the properties that vegetable tannins impart to the leather are manifold and the tanning process is the one with the lowest environmental impact.

### 1.3.3.2 Chrome tanning

In the last decades, chrome tanning has been the dominant method of making leather due to its economic advantages and ease to achieve leather with very good performances. It accounts for 85% of the world's leather production. The leather so obtained gives a comfortable feel, it's lighter, soft, brighter and have high hydrothermal stability. The leathers obtained by this process involve the use of trivalent chromium and in particular the basic chromium sulphate  $\text{Cr}(\text{OH})(\text{SO}_4)$ . Trivalent chromium has the capability to form complexes with the carboxyl groups of leather collagen (Figure 11).

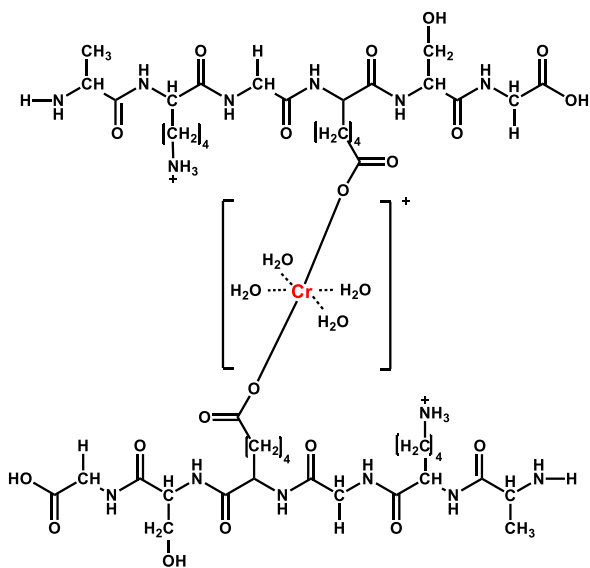


Figure 11. Coordinating cross-linkage between collagen carboxyl groups and trivalent chromium.

The chromium-tanned leathers have a bluish colouring, in fact the leather obtained with this method are called *wet blue* (Figure 12).



Figure 12. Wet blue leather.

Nevertheless, chrome tanning has a major disadvantage: the possible oxidation of Cr(III) to Cr(VI), classified as a human carcinogen.<sup>34,35,36</sup> This conversion may occur during the fabrication or storage of leather, leading to polluted tannery effluents during incineration<sup>37</sup> and landfill.<sup>38</sup>

It has already been proved that, in some areas, the tannery effluents and waste contributed to changing the chemistry of soil solution by introducing toxic metals into the soil environment.<sup>39</sup> All wastes containing chromium are therefore considered hazardous and their disposal is mainly made by burial (landfill) and incineration with high impact on soil and air pollution.

REACH regulation,<sup>40</sup> consumers growing concerns, as well as the environmental concerns<sup>41</sup> resulted in an increasing demand for chrome free leather, substitution of dangerous chemicals and reduced chemical consumption, with health and safety considerations playing the major role for both humans and environment. Using organic-based tannins has been

---

<sup>34</sup> H. Sun, J. Brocato, M. Costa, *Curr. Environ Health Rep.*, **2015**, 2, 295-303.

<sup>35</sup> F. Ma'arfi, M.Y. Khan, A. Husain, A. Khanam, Z. Hasan, *Contamination of water resources with potentially toxic elements and human health risk assessment*, Chapter 9, Pages 123-141, **2021**.

<sup>36</sup> S. Mishra, R.N. Bharagava, *J. Environ. Sci. Health C*, **2016**, 34(1), 1-32.

<sup>37</sup> M. Velusamy, B. Chakali, S. Ganesan, F. Tinwala, S. Shanmugham Venkatachalam, *Environ. Sci. Pollut. Res.*, **2019**, 27, 29778-29790.

<sup>38</sup> J. Liang, X. Huang, J. Yan, Y. Li, Z. Zhao, Y. Liu, J. Ye, Y. Wei, *Sci. Total Environ.*, **2021**, 774, 145762.

<sup>39</sup> A.S. Sallam, A.R.A. Usman, H.A. Al-Makrami, M.I. Al-Wabel, A. Al-Omran, *Arab. J. Geosci.*, **2015**, 8, 11019-11029.

<sup>40</sup> [https://www.hsa.ie/eng/Your\\_Industry/Chemicals/Legislation\\_Enforcement/REACH/](https://www.hsa.ie/eng/Your_Industry/Chemicals/Legislation_Enforcement/REACH/)

<sup>41</sup> <https://www.unep.org/resources/report/international-declaration-cleaner-production-implementation-guidelines>

considered a step-change toward a sustainable and chrome-free leather production.

### 1.3.3.3 Aldehydic tanning

The most important collagen functional group involved in aldehyde crosslinking is the amino group. Aldehyde tannages form stable covalent imine-based crosslinking through the relatively limited number of amine groups available. While other aldehydes have been investigated for their tanning ability, only formaldehyde and glutaraldehyde are used industrially. Natural polymers containing an aldehyde, or a masked aldehyde group, have also been employed for tanning.<sup>42</sup>

This type of tanning is based on the nucleophilic addition reaction between an aldehyde and an amine leading to the formation of methylene derivatives according to the reaction in Figure 13.

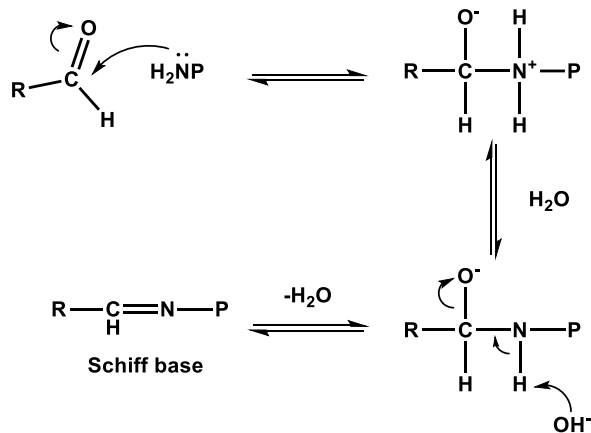


Figure 13. General aldehyde reaction with protein amino group ( $P$ =protein)

Although it is a tanning method which produces chrome free leather the crosslink between aldehyde and collagen is weaker than the crosslink between collagen and chrome salt. Aldehyde tanning, as synthetic tanning, gives *wet white* leather due to the pale cream colour it imparts to the skins.

<sup>42</sup> J.W. Harlan, S.H. Fearheller, *Chemistry of the Crosslinking of Collagen during Tanning*, Ed. Springer, Boston, 1977.

Nowadays pure formaldehyde is no longer used because of its high toxicity to animals and humans. At concentrations below 2 ppm it is an irritant to the eyes and cause problem to breathing, repeated contact with solutions may cause eczematoid dermatitis. The upper tolerance limit for formaldehyde in finished leather articles for adults is 150 ppm and for children is 75 ppm. Glutaraldehyde also has toxicity issues and can cause similar problems. This method is not normally used often but can be used with other materials in the process of tanning.<sup>43</sup>

For this reason, aldehyde tanning is not a viable alternative today due to toxicological and environmental concerns.

#### 1.3.3.4 Synthetic tanning

The term *syntan*<sup>36</sup> means synthetic tanning agent. Using organic-based tannins has been considered a step-change toward a sustainable and chrome-free leather production. This class of reagents is wide ranging, but typically they are polymeric materials constituted by aromatic monomers, such as phenol or naphthol derivatives bearing anionic sulfonate groups. Although the reaction conditions may be precisely controlled, the chemical structure of syntans, are relatively non-specific and are rarely analysed in detail. They are classified into two types, according to their primary properties: auxiliary syntans and replacement syntans.<sup>44</sup>

As the name implies, the auxiliary syntans are relatively unreactive in a tanning sense, so their performance functions are limited to aiding the tanning process. This type of syntans is frequently based on naphthalene (Figure 14). They have the capacity to increase the speed of diffusion of other tannins and favour the penetration of dyes in order to obtain more uniform colouring. They allow to obtain more separated and swollen fibres (thicker leather), to improve the softness of the leather and make possible to obtain a better distribution of the tanning agent throughout the section and the use of smaller quantities of them, like in the case of chromium.<sup>45</sup>

---

<sup>43</sup> P. Maina, M.A. Ollengo, E.W. Nthiga, *Int. J. Sci. Res.*, **2019**, 9, 212-223.

<sup>44</sup> A.D. Covington, W.R. Wise, *Tanning Chemistry The science of Leather*, Ed. Royal Society of Chemistry, Croydon, **2020**.

<sup>45</sup> H. Traeubel, K.H. Rogge, *J. Am. Leather Chem. Ass.*, **1988**, 83, 193- 205.

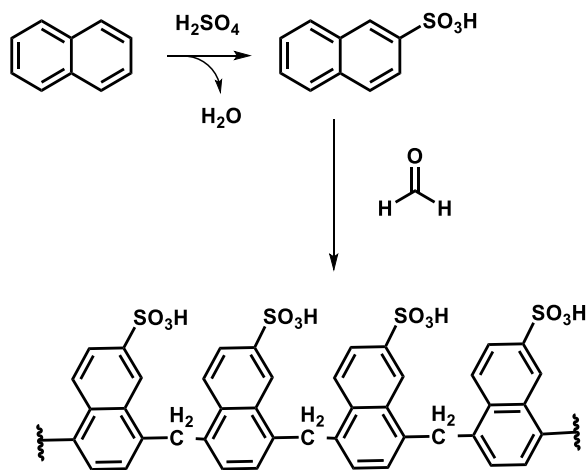


Figure 14. Synthesis of auxiliary syntans.

The replacement syntans are used as tanning and re-tanning agents. These syntans can be used for tanning alone because their properties of tanning are comparable with plant polyphenols, in fact their shrinkage temperature is usually between 70-75 °C. These syntans are usually based on simple phenolic compounds and interacts with collagen with the same type of interactions of the vegetable tannins, such as hydrogen bonding and electrostatic interaction (Figure 15).

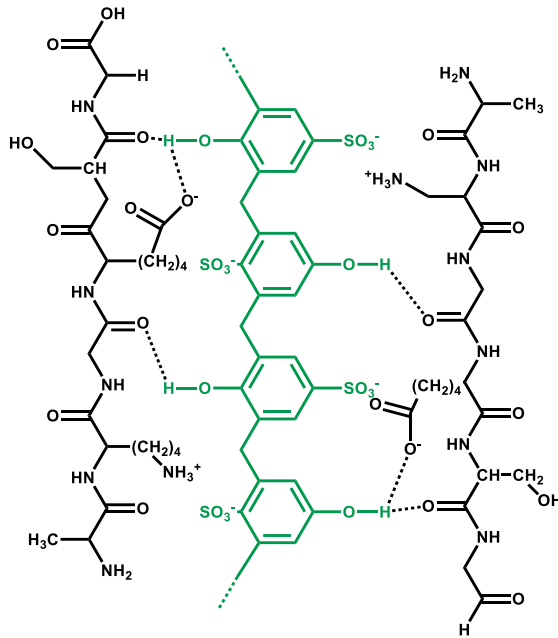


Figure 15. Interaction between collagen and a replacement sytan.

This class mainly consists of aromatic condensates with functional groups (Ar-OH) capable of forming a stable bond with the leather. Usually, there are two steps in the synthesis of syntans: sulfonation and polymerisation. As the number of the sulphonate groups increases, the water solubility increases but the tanning power decreases (Figure 16).

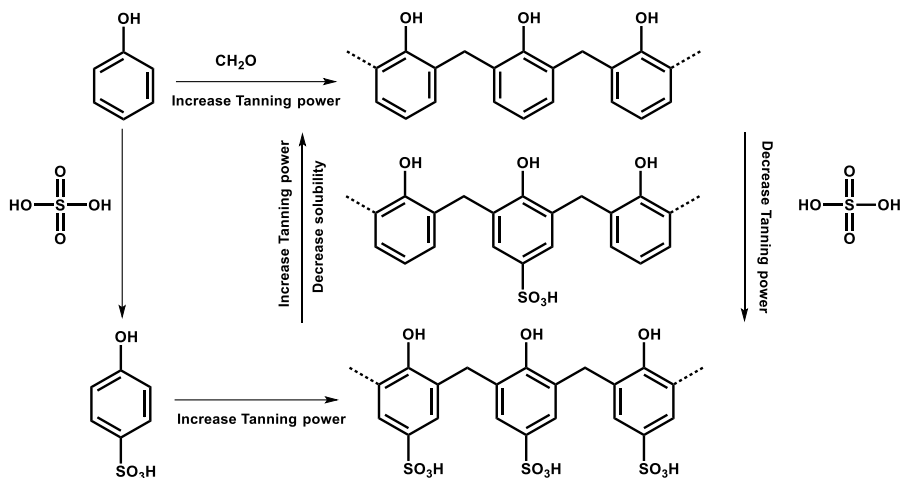


Figure 16. Syntans related tanning ability.

The syntans available on the market have high molecular weight, ranging from 200 to 15000.<sup>46</sup> Their properties vary according to the number of -OH groups, their position on the aromatic ring, the ratio between -OH and - $\text{SO}_3\text{H}$  groups and their position within the polymer chain. They also have lightening power and improve the dyeability of leather (Figure 17).

<sup>46</sup> J. Raghava Rao, M. Kanthimathi, P. Thanikaivelan, K.J. Sreeram, R. Ramesh, S. Ramalingam, N.K. Chandrababu, B.U. Nair, T. Ramasami, *Clean. Techn. Environ. Policy*, **2004**, *6*, 243–249.



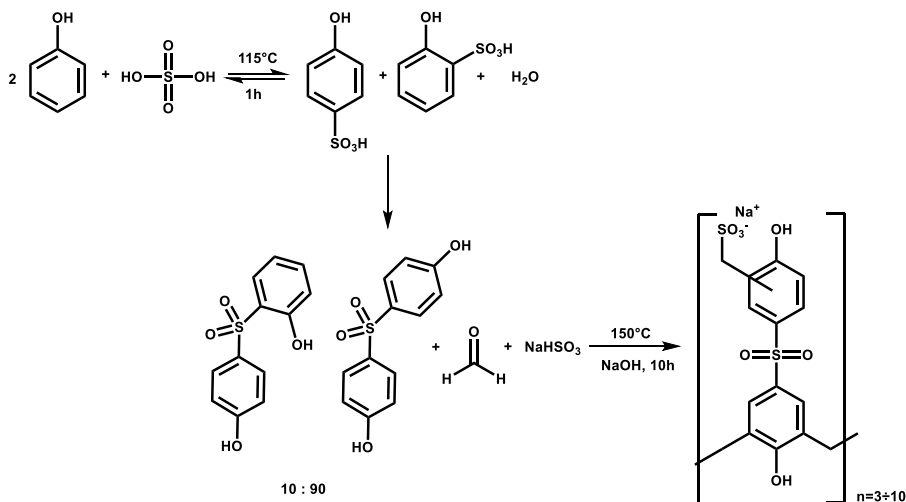


Figure 18. Industrial synthesis of BPS based syntans.

## 2. Research aims and thesis outline

The overall aim of this PhD thesis project is to carry out the synthesis and development of new tannins with high industrial performance and different types of applications.

The main objective of the work (Chapter 3) was to develop a new tanning agent that could be an efficient and really used product from an industrial point of view. The thesis work was therefore developed directly by evaluating its applicability on an industrial scale in collaboration with the company BI-QEM SPECIALTIES S.P.A. at its plant in Buccino (SA). BI-QEM SPECIALTIES S.P.A. is an industry that produces and markets chrome tanning agents, dispersants, synthetic tannins and auxiliaries for the chemical tanning, cement, and concrete industry (Figure 19).



Figure 19. Plant of BI-QEM SPECIALTIES S.P.A. (Buccino, SA).

The first part of this work aimed at obtaining “*supramolecular syntans*” (*suprasynts*) based on a bisphenol S polymer and  $\beta$ -cyclodextrin to be used as tanning agents. The *suprasynts* (SS) were initially characterized by NMR and FTIR measurements to evaluate the effective formation of the inclusion complexes. The *suprasynts* were tested in the tanning process in a laboratory scale at the *Leather and Footwear Research Institute (ICPI)*, located in Bucharest, Romania) under the supervision of Prof. Elena Badea to attest the efficiency of the new products using Micro DSC and ATF-FTIR analysis. Furthermore, in order to evaluate the real applicability of the products, a pilot scale test was carried out at the *FGL international SPA* (Figure 20). The physical and mechanical tests were performed in order to establish the quality of the final product obtained (crust leather).



Figure 20. Logo of FGL International S.P.A. (Castelfranco di Sotto, PI).

Chapter 4 deals with a study on the selective recognition of BPSs isomers by  $\beta$ -CD in water. In fact, during the synthesis of bisphenol S based polymer, used for tannage, a mixture of both isomeric dihydroxy diphenyl sulfones is obtained as the purification of the pure bisphenol S (4,4'-isomer) from mixtures with the 2,4'-isomer cannot be easily achieved.<sup>48</sup>

In Chapter 5, as part of the European Eureka project E!13427 “*Biodegradable and Antimicrobial Re-tanning Agent and Coating for Ecological and Safe Leather - BIOSAFE LEATHER*”, a re-tanning agent from

---

<sup>48</sup> G.C.Vegter, M.M. de Brabander, US 3065274 19621120, 1962.

alginate was developed to enable a greener re-tanning process. The research was performed within the interdisciplinary team made of researchers from the *Leather and Footwear Research Institute (ICPI)* and the *Politehnica University of Bucharest (UPB)* (Figure 21). As a result, novel safe and non-toxic agents based on sodium alginate (SA) derivatives, from 100% renewable sources have been developed. SA derivatives (SADs) were obtained using radical degradation by H<sub>2</sub>O<sub>2</sub> under ultrasound<sup>49</sup> and ultrasonic treatment.<sup>50</sup> Various treatment conditions (oxidants' concentration, treatment duration, ultrasound frequency and intensity) were tested to obtain the appropriate depolymerization degree and aldehyde content for ensuring re-tanning and tanning properties. The ability of the SADs to crosslink collagen in hide was tested at laboratory level.<sup>51</sup>

---

<sup>49</sup> A. Dodero, S. Vicini, M. Castellano, *Food Hydrocoll.*, **2020**, *109*, 106128.

<sup>50</sup> L. Feng, Y. Cao, D. Xu, S. Wang, J. Zhang, *Ultrason. Sonochem.*, **2017**, *34*, 609-615.

<sup>51</sup> E. Badea, M. Crudu, C. Carsote, C. Sendrea, M.C. Lupas, L. Miu, Stabilisation of collagen by alginate dialdehyde for eco-sustainable tanning. XL National Conference on Calorimetry, Thermal Analysis and Chemical Thermodynamics, Pisa, Italy. 17-19 December **2018**.



IL PASSO



*Curtidos Badia*

Figure 21. Partners of the Eureka project BIOSAFE LEATHER.

### 3. $\beta$ -Cyclodextrin-Based Tanning Materials: *SupraSynt* Additives as an eco-friendly alternative

#### 3.1 General overview

##### 3.1.1 Cyclodextrins

Cyclodextrins (CDs) are naturally occurring cyclic oligosaccharides formed from monomeric D-glucopyranose units, joined by an  $\alpha$ -1,4-glycosidic bond and closed to form a toroidal ring.<sup>52,53</sup> Depending on the number of glucose units in the ring, they are called  $\alpha$ - (6 units),  $\beta$ - (7 units) and  $\gamma$ - (8 units) – cyclodextrins, respectively. They are obtained through the enzymatic degradation of starch, so from renewable resources, and are practically nontoxic.<sup>54</sup> By adding a biological catalyst, the enzyme glucosyl transferase, to a cold dextrin solution, a linear oligosaccharide is formed which undergoes intramolecular cyclization to form cyclodextrins. Therefore, the technology used to synthesise cyclodextrins, on an industrial scale, is both economical and environmentally friendly. In addition, they are already on

---

<sup>52</sup> J. Szejtli, *Chem. Rev.*, **1998**, 98, 1743–1753.

<sup>53</sup> G. Crini, *Chem. Rev.*, **2014**, 114, 10940–10975.

<sup>54</sup> E.M.M. Del Valle, *Process Biochem.* **2004**, 39, 1033–1046.

the market in such large quantities that they can be widely used.<sup>55</sup> Indeed, due to their versatile nature, CDs are widely used in various fields such as pharmaceuticals,<sup>56</sup> food,<sup>57</sup> and cosmetics. In the food industry, CDs are often used in food packaging<sup>58</sup>, but also in improving the antioxidant and antibacterial properties of additives when they are included in the cavity.<sup>59</sup> CDs are used in cosmetics as they have the ability to increase stability and preserve guests from biological oxidative phenomena. They are used to solubilise fragrances, to suppress their volatility, and as stabilisers.<sup>60</sup>

Although the potential of cyclodextrins is vast, the literature on their application in the tanning process is very limited and their use mainly concerns the finishing or dyeing stage.<sup>61</sup> In 2006, the Bayer Company reported results on cyclodextrin-based fragrance microcapsule used in leather finishing.<sup>62</sup> In 2013, Chen developed a  $\beta$ -cyclodextrin-based coloured fragrance agent prepared with a reactive dye.<sup>63</sup> Other patents were developed concerning the use of  $\beta$ -CD for the gradual release of fragrances from leather.<sup>64,65</sup>

Cyclodextrins are useful hosts in supramolecular chemistry and are capable to form inclusion complexes.<sup>66</sup> The formation of inclusion complexes between the cyclodextrin and hydrophobic guests occurs by inclusion of the guest inside the hydrophobic cavity of the cyclodextrin. The thermodynamic driving forces of this supramolecular process is the *hydrophobic effect*, that

---

<sup>55</sup> N. Sharma, A. Baldi, *Drug Deliv.*, **2016**, *23*, 729- 757.

<sup>56</sup> P. Jansook, N. Ogawa, T. Loftsson, *Int. J. Pharm.*, **2018**, *535*, 272–284.

<sup>57</sup> É. Fenyvesi, M. Vikmon, L. Szente, *Crit. Rev. Food Sci. Nutr.*, **2016**, *56*, 1981–2004.

<sup>58</sup> B. Tian, D. Xiao, T. Hei, R. Ping, S. Hua, J. Liu, *Polym. Int.* **2020**, *69*, 597–603.

<sup>59</sup> R.V. Stick, S.J. Williams, Disaccharides, Oligosaccharides and Polysaccharides. In *Carbohydrates: The Essential Molecules of Life*. Elsevier, **2009**, 321–341.

<sup>60</sup> H. Hashimoto, *J. Incl. Phenom.*, **2002**, *44*, 57–62.

<sup>61</sup> W. Ding, Y. Wang, J. Zhou, B. Shi, *Carbohydr. Polym.*, **2018**, *201*, 549- 556.

<sup>62</sup> K. Martin, K., W. Jurgen, K. Friedrich, US 2006/0216509 A1, **2006**.

<sup>63</sup> X. Liu, X. Zhang, W. Chen, C.C. Gaidau, L. Miu, *Leather Footwear J.*, **2013**, *13*, 139-148.

<sup>64</sup> C. Long, H. Guohua, L. Zhihai, Y. Kaishen, Z. Lichuan, CN103114459B, **2013**.

<sup>65</sup> W. Chen, X. Liu, X. Zhang, CN101857908B, **2010**.

<sup>66</sup> G. Chen, M. Jiang, *Chem. Soc. Rev.* **2011**, *40*, 2254-2266.

drives the aggregation of nonpolar molecules in an aqueous solution.<sup>67</sup> The resulting complex has its own chemical/physical properties that are different from the guest organic molecule which, in an aqueous environment, is released in a controlled manner over time (without losing its properties once released). The affinity between the cyclodextrin and the guest molecule is regulated mainly by secondary interactions and the size of the guest molecule in relation to the size of the cavity (Figure 22).

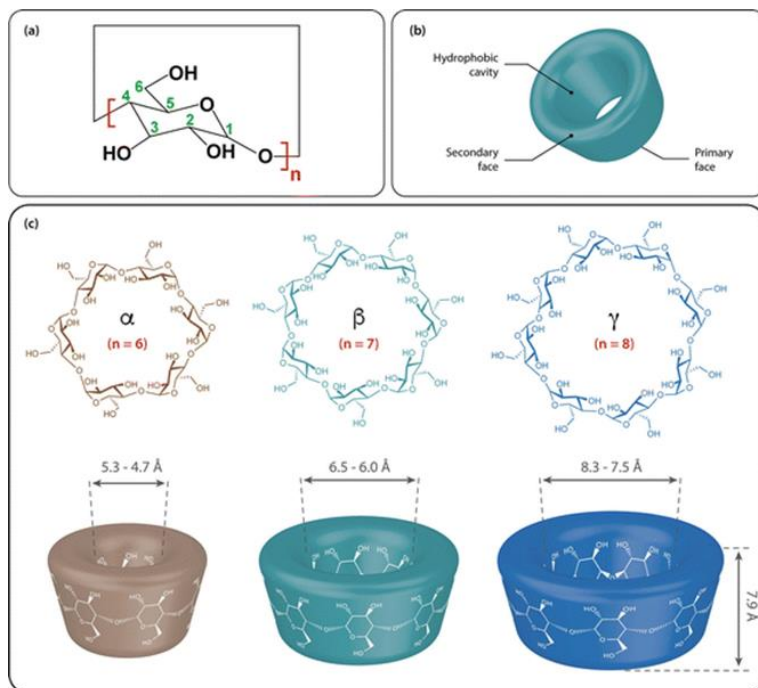


Figure 22. (a) monomeric unit of cyclodextrins, (b) hydrophobic cavity of cyclodextrins, (c)  $\alpha$ -cyclodextrin (brown),  $\beta$ -cyclodextrin (green),  $\gamma$ -cyclodextrin (blue).<sup>68</sup>

As previously said, an effective tanning process is based on two important processes: good dispersion/penetration of the tanning agent in the collagen matrix of the leather (in section) and formation of strong and stable

<sup>67</sup> E. Dodziuk, *Cyclodextrins and their Complexes: Chemistry, Analytical Methods, Applications*. Wiley-VCH, 2006.

<sup>68</sup> J. Lee, S. Lee, S. Lee, H.B. Oh, *Molecules*, 2020, 25.

chemical interactions with the functional groups of the leather proteins. It is generally recognised that a uniform dispersion of the tanning agent is an essential prerequisite for a uniform tanning process. The tanning power of syntans mainly depends on the availability of -OH groups to form hydrogen bonds with collagen and their distribution through it.

From these premises, it's easy to understand that cyclodextrins could pave the way for the development of completely new sustainable tanning agents thanks to the presence of numerous -OH groups and their molecular recognition abilities in aqueous solvent.

### 3.1.2 Molecular recognition

In contrast to classical chemistry, which concerns the synthesis of molecules by forming and breaking covalent bonds between atoms, *supramolecular chemistry* aims at developing complex chemical systems from components interacting by noncovalent intermolecular forces.<sup>69</sup>

Macrocyclic compounds have shown enormous potential in the supramolecular field. Indeed, they can create highly organised and functional structures through secondary interactions with smaller molecules (*guests*) by acting as *hosts* due to the presence of preformed cavities in their structure.<sup>70</sup> The chemical forces involved in host-guest interactions are the classical secondary interactions such as ion-ion interaction (100-350 kJ/mol), dipole-ion (50-200 kJ/mol) and dipole-dipole (5-50 kJ/mol) interactions, hydrogen bond (4-120 kJ/mol), and van der Waals forces (< 5 kJ/mol). The binding site is the region of the *host* that has the right size, geometry, and chemical and electronic nature to interact with complementary species.<sup>71</sup> Figure 23 schematically shows a process of host-guest complexation.

---

<sup>69</sup> J.M. Lehn, *Proc. Natl. Acad. Sci. U.S.A.*, **2002**, *99*, 4763.

<sup>70</sup> T. Ogoshi, P. Gale, J. Steed, *Pillararenes (Monograph in Supramolecular Chemistry)*, Royal Society of Chemistry: Londra, **2015**.

<sup>71</sup> J.W. Steed, D.R. Turner, K. Wallace, *Core Concepts in Supramolecular Chemistry and Nanochemistry*, **2007**.

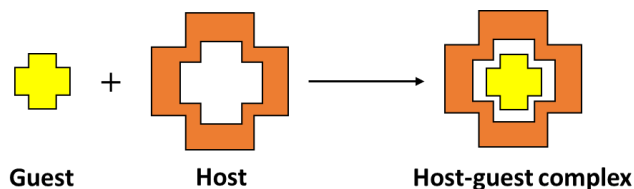


*Figure 23. Host-guest complexation.*

Clearly, a simple secondary chemical bonding interaction cannot be regarded as a recognition. Recognition is an interaction with a purpose and requires a set of secondary chemical interactions. In this way, the supramolecule that is generated will have its own kinetic and thermodynamic stability. The stability of a host-guest complex is therefore a combination of enthalpic ( $\Delta H$ ) and entropic ( $\Delta S$ ) factors that lower the total complexation free energy ( $\Delta G$ ).

It is therefore obvious that for a *host-guest* interaction to take place it is necessary for the *host* to have the appropriate binding sites to complex the *guest*. A *host* may have a certain degree of selectivity towards certain guests (or families of *guests*), which may result from the complementarity of *host* and *guest* binding sites or the pre-organisation of the *host* conformation.<sup>72,73</sup>

Selectivity can then be defined in terms of the ratio of the equilibrium constants of the complexation reactions between the host and two different guest species, as shown in the equation:

$$\text{Selectivity} = \frac{K_{\text{guest-1}}}{K_{\text{guest-2}}}$$

Where  $K_{\text{guest-1}}$  and  $K_{\text{guest-2}}$  are the association constants of *host/guest-1* and *host/guest-2* complexes, respectively.

---

<sup>72</sup> J.M. Lehn, *Supramolecular Chemistry: Concepts and Perspectives*, VCH Publishers Inc.: Weinheim, 1995.

<sup>73</sup> J.W. Steed, J.L. Atwood, *Supramolecular Chemistry*, 2nd edition, John Wiley & Sons: Chichester, 2009.

### 3.1.3 Bisphenol S and related syntans

As stated in chapter 1.3.3.4, among the alternative tanning agents investigated for replacing chromium, bisphenol S (BPS) based polymers are the most promising substitutes in today's leather industry.<sup>74,75,76</sup> However, bisphenol S has shown endocrine and estrogenic activity which may damage fertility<sup>77,78,79</sup> according to the classification provided by companies to ECHA.<sup>80</sup> It has been reported that the metabolic interference triggered by bisphenol S has the potential to induce metabolic diseases, immune diseases, clonal diseases, ocular diseases, and neurological diseases.<sup>81</sup>

Furthermore, these types of syntans do not have the ability to completely exhaust the tanning float and a large amount of these materials remains in the wastewater. Considering that bisphenol S polymer-based tanning agents are derived from non-renewable petroleum source this contribute to increase the environmental impact due to the use of fossil fuels.

In addition, during the synthesis of 4,4'-dihydroxydiphenyl sulphone (4,4'-BPS) large quantities of the isomeric 2,4'-dihydroxydiphenyl sulphone (2,4'-BPS) are formed as by-product. Consequently, the commercial product known as bisphenol S is in fact a mixture of both isomeric dihydroxy diphenyl sulphones, as the purification of the pure 4,4'-isomer from mixtures with the 2,4'-isomer cannot be easily achieved. Unfortunately, the presence of the 2,4'-isomer complicates the issue of molecular control in the field of application of bisphenol S and increases the related pollution problems.

It is therefore crucial to increase the sustainability of the tanning process involving bisphenol S-based tannins. This could be achieved either by

---

<sup>74</sup> A. D. Covington, *Chem. Soc. Rev.*, **1997**, 26, 111.

<sup>75</sup> S. Lipowski Newark, C.A. Fetscher, S. Hills, *Synthetic tanning Agent and process for preparing same*, US3029212, **1962**.

<sup>76</sup> J. Ammenn, C. Huebsch, E. Schilling, B. Dannheim, *J. Am. Leather Chem.*, **2015**, 110 (11), 349-354.

<sup>77</sup> L.N. Vandenberg, R. Hauser, M. Marcus, N. Olea, W.V. Welshons, *Reprod. Toxicol.*, **2007**, 24, 139-177.

<sup>78</sup> L.H. Wu, X.M. Zhang, F. Wang, C.J. Gao, D. Chen, J.R. Palumbo, E.Y. Zeng, *Sci. Total Environ.*, **2018**, 615, 87-98.

<sup>79</sup> D. Crump, S. Chiu, L.K. Williams, *Environ. Toxicol. Chem.*, **2016**, 35, 1541-1549.

<sup>80</sup> <https://echa.europa.eu/substance-information/-/substanceinfo/100.001.137>.

<sup>81</sup> A. Beronius, C. Ruden, H. Hakansson, A. Hanberg, *Reprod. Toxicol.*, **2010**, 29, 132-146.

replacing bisphenol S-based tannins with new tanning agents derived from bio-organic renewable sources <sup>82</sup> or significantly reducing the quantity of bisphenol S-based tannins. The latter solution has the advantage of not requiring the development of a new tanning technology, but only the minimal modification of the technology already in use.

Thus, in this work, we developed a new supramolecular system derived by  $\beta$ -CD and a bisphenol S based polymer (MIDA DD<sup>®</sup>) in order to obtain blends with preponderant bio-based products by adding increasing amounts of  $\beta$ -cyclodextrin.

The products obtained were tested on laboratory and pilot scale to verify their tanning action. In particular, the shrinkage temperatures, the stability of the hides under artificial light and the physical properties of the finished product were determined.

## *3.2 Synthesis and characterization*

### *3.2.1 Synthesis and characterization of new supramolecular tanning systems (SupraSynts)*

The polymer used (MIDA DD<sup>®</sup>) consists of a water-soluble blend of oligomers industrially obtained by polymerization of bisphenol S (BPSs) with formaldehyde (Figure 24).

---

<sup>82</sup> W. Ding, X. Pang, Z. Ding, D.C.W. Tsang, Z. Jiang, Bi Shi, *J. Hazard. Mater.*, **2020**, 396, 122771.

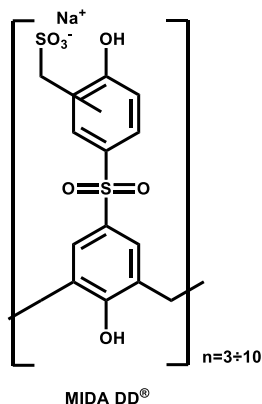


*Figure 24. MIDA DD®.*

Different amounts of polymer and  $\beta$ -CD were used to develop five different supramolecular tanning systems. The  $\beta$ -CD/MIDA DD® ratio ranged from 0.3:1 to 4.5:1 (Table 1). The choice of these ratios was based on a preliminary GPC study made on MIDA DD® (Experimental section 4.4).

In every sample is present 15% w/w of sodium sulphate and 10% w/w of a mixture of dicarboxylic acids to make the products comparable with the product sold industrially (Table 2). For the synthesis of each system, the appropriate quantity of  $\beta$ -cyclodextrin and MIDA DD® were put in a flask at 85°C for 15 minutes. The reaction is allowed to cool to 75°C and dicarboxylic acids and sodium sulphate are added and mixed for other 15 minutes until complete dissolution. The product is brought to dryness in an oven at 80°C. The pH of the product ( $4.5 \pm 0.5$ ) is measured by preparing a 20% w/w solution in distilled H<sub>2</sub>O.

Table 1. Weight ratio between  $\beta$ -CD and MIDA DD<sup>®</sup>

| SupraSynt (SS) | Ratio (w/w)                                    |
|----------------|--|
| 1              | 0.3: 1 ( $\beta$ -CD : MIDA DD <sup>®</sup> )  |
| 2              | 0.56: 1 ( $\beta$ -CD : MIDA DD <sup>®</sup> ) |
| 3              | 0.8: 1 ( $\beta$ -CD : MIDA DD <sup>®</sup> )  |
| 4              | 2.3: 1 ( $\beta$ -CD : MIDA DD <sup>®</sup> )  |
| 5              | 4.5: 1 ( $\beta$ -CD : MIDA DD <sup>®</sup> )  |

Table 2. Percentage composition of the new supramolecular syntans.

|                                 | SS1  | SS2 | SS3  | SS4  | SS5  |
|---------------------------------|------|-----|------|------|------|
| $\beta$ -CD                     | 17.5 | 27  | 33.5 | 52.5 | 61.4 |
| MIDA DD <sup>®</sup>            | 57.5 | 48  | 41.5 | 22.5 | 13.6 |
| Na <sub>2</sub> SO <sub>4</sub> | 15   | 15  | 15   | 15   | 15   |
| Dicarboxylic acids              | 10   | 10  | 10   | 10   | 10   |

### 3.2.2 <sup>1</sup>H NMR characterization of the obtained supramolecular tanning systems

Usually, upon formation of a supramolecular *guest@host* complex, <sup>1</sup>H NMR signals of both host and guest experience a variation of chemical shift.<sup>83</sup> Proton NMR shifts reflect interactions across space between different molecules or between parts of a larger molecular entity. For this reason, <sup>1</sup>H NMR titrations are widely used to characterise supramolecular complexes

<sup>83</sup> J. Hu, T. Xu, Y. Cheng, *Chem. Rev.*, **2012**, *112* (7), 3856–3891.

in solution, and the complexation induced shift (CIS,  $\Delta\delta = \delta_{compl} - \delta_{free}$ ) is commonly used to this purpose.<sup>84</sup>

Hence, the complexation ability of  $\beta$ -CD towards MIDA DD<sup>®</sup> was evaluated by the CIS of  $\beta$ -CD signals for each supramolecular tanning systems.

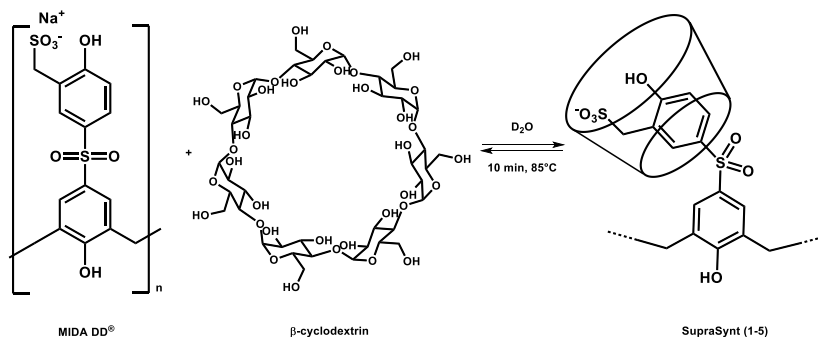


Figure 25. Scheme of interaction between  $\beta$ -CD and MIDA DD<sup>®</sup>.

In Figure 27, a single set of averaged  $^1\text{H}$  NMR signals was observed for the SupraSynt 1 (Table 2), indicating a fast exchange between free and bound species on the NMR time scale. A significant complexation induced shift was found for the protons inside the cavity of  $\beta$ -CD, namely H3 and H6 protons (Figure 26), which both present a CIS of -0.1 ppm. In addition, the H5-atom, which is the deepest located in the cavity, has a CIS of -0.31.

<sup>84</sup> V. Rüdiger, H.J. Schneider, *Chem. Eur. J.*, **2000**, 6: 3771-3776.

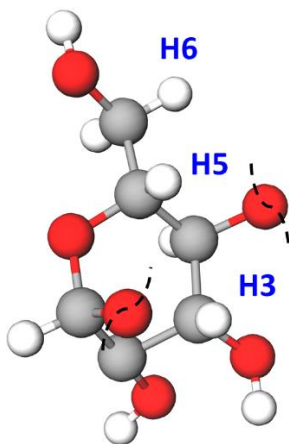


Figure 26. Proton inside the cavity of  $\beta$ -cyclodextrin.

Smaller CIS were observed for H1, H2, and H4: -0.04, -0.027, and 0.02 ppm, respectively. MIDA DD<sup>®</sup> signals were also affected by the formation of the pseudorotaxane structure: all polymer signals, contrary to what happens to  $\beta$ -cyclodextrin ones, were down-field shifted.

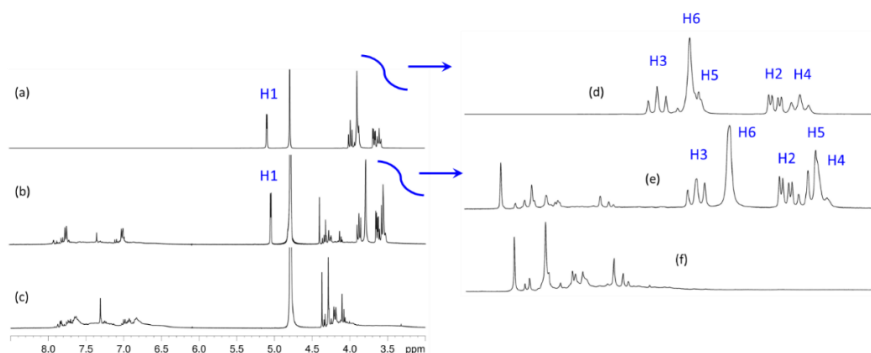


Figure 27. a-e)  $^1\text{H}$  NMR spectra (400 MHz, 298 K,  $\text{D}_2\text{O}$ ) of: a)  $\beta$ -CD; b) SupraSynt 1 c) MIDA DD<sup>®</sup>, d) Expansion from 3.4 to 4.5 ppm of the  $^1\text{H}$  NMR spectrum of  $\beta$ -CD in (a); e) Expansion from 3.4 to 4.5 ppm of the  $^1\text{H}$  NMR spectrum of the SupraSynt 1 in (b); f) Expansion from 3.4 to 4.5 ppm of the  $^1\text{H}$  NMR spectrum of MIDA DD<sup>®</sup>.

The  $^1\text{H}$  NMR spectra of the other four systems in Table 2 show a similar behaviour confirming the formation of the inclusion complex between  $\beta$ -CD and MIDA DD<sup>®</sup>.

### 3.2.3 ATR-FTIR characterization of the obtained SupraSynts

The ATR-FTIR bands in the MIDA DD<sup>®</sup> spectrum (Figure 28a) were mainly assigned on the basis of the molecular vibrations identified for BPS by Ullah and Wang.<sup>85</sup> The signal at 553 cm<sup>-1</sup> indicates out-of-plane bending of the C-C bonds on the aromatic rings and wagging of the hydrogen atoms bonded on them. The signal at 691 cm<sup>-1</sup> is indicative of S-C stretching, and that at 833 cm<sup>-1</sup> of C-C-C bending of the aromatic ring. The signal at 1124 cm<sup>-1</sup> and 1282 cm<sup>-1</sup> identifies the S-O stretching. At 1440 cm<sup>-1</sup> there is HC-C bending and at 1586 cm<sup>-1</sup> C-C stretching. The signals at 619 and 1043 cm<sup>-1</sup> are typical of sodium sulphate while the signals at 1711 cm<sup>-1</sup> and 2946 cm<sup>-1</sup> belong to the dicarboxylic acids used.

The ATR-FTIR spectrum of  $\beta$ -CD presents the characteristic bands of the hydroxyl groups at 3278 cm<sup>-1</sup>, the C-H stretching vibrations at 2923 cm<sup>-1</sup> and C-O stretching vibration at 1151, 1022, 942, 575 cm<sup>-1</sup>.<sup>86</sup> The anomeric band at 858 cm<sup>-1</sup> essentially consists of C<sub>1</sub>-H deformation coupled to other motions (Figure 28c).

All five SupraSynts show all the characteristics bands of both host and guest molecules, with slight shifts. For example, in the spectrum of SupraSynt 1, the C-O stretching bands of  $\beta$ -CD shifted from 1151 and 1022 cm<sup>-1</sup> to 1143 and 1027 cm<sup>-1</sup>, respectively (Figure 28b). As can be seen in Figure 29, the signals of the SupraSynts were shifted depending on the relative amount of  $\beta$ -CD and MIDA DD<sup>®</sup>.

---

<sup>85</sup> R. Ullah, X. Wang, *Applied Optics*, **2018**, *57*, D20-26.

<sup>86</sup> T. Simsek, B. Rasulev, C. Mayer, S. Simsek, *Molecules*, **2020**, *25*, 4275.

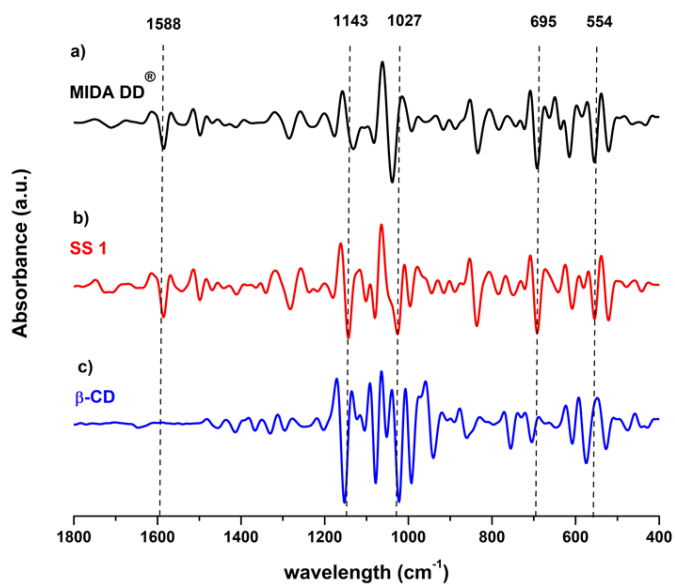
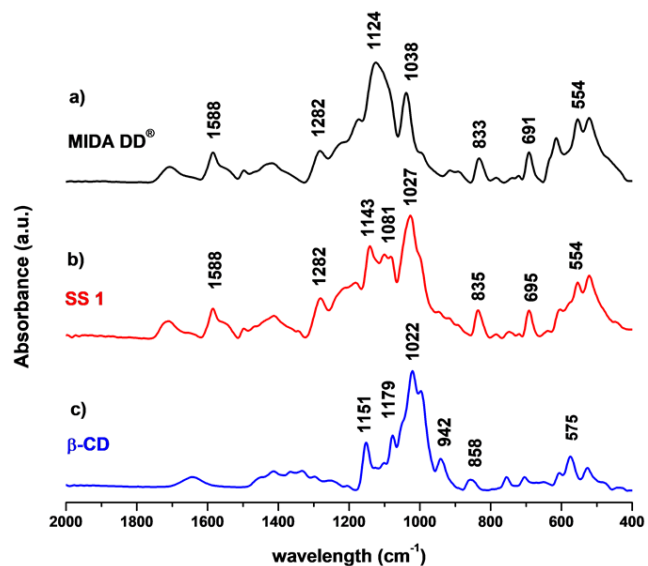


Figure 28. (top) Detail of ATR- FTIR spectra of (a) MIDA DD®, (b) SS 1, (c)  $\beta$ -CD. (bottom) ATR-FTIR second derivative spectra of (a) MIDA DD®, (b) SS1, (c)  $\beta$ -CD.

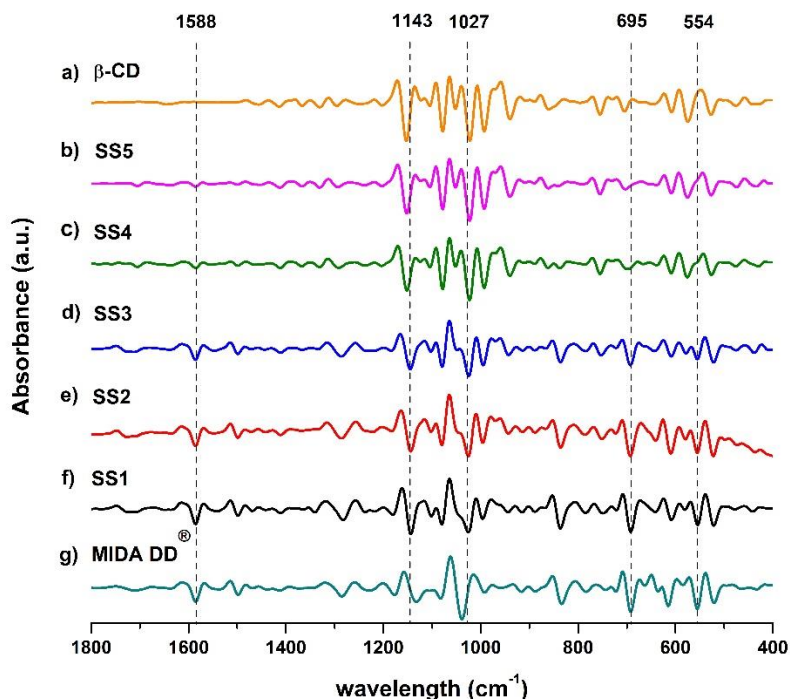


Figure 29. ATR-FTIR second derivative spectra of (a)  $\beta$ -CD, (b) SS5, (c) SS4, (d) SS3, (e) SS2, (f) SS1, (g) MIDA DD<sup>®</sup>.

In summary, both <sup>1</sup>H NMR and ATR-FTIR studies show supramolecular interaction between  $\beta$ -CD and MIDA DD<sup>®</sup> (see also Chapter 4.2.1) confirming the formation of the inclusion complexes.

### 3.3 Tanning Tests

#### 3.3.1 Laboratory scale tests

The tanning efficacy of the novel SupraSynts was evaluated by performing tanning tests at laboratory level at the Leather and Footwear Research Institute, Bucharest, under the supervision of Prof. Elena Badea. A rotator drive stirrer STR4 (Stuart) with speed 4 was used to this purpose and glass beads were added in the tannin bath to simulate the mechanical effect of the tanning drum. All five SupraSynts and their precursors, MIDA DD<sup>®</sup> and

$\beta$ -CD, were tested. The chemicals used in the operations were those normally used in the leather industry.



*Figure 30. Rotator drive stirrer STR4 used for simulating the tanning drum.*

The test was carried out on the same piece of hide and divided for all the samples tested to allow us to better compare the results considering the heterogeneity of the source material. The process follows the scheme reported in Figure 31.

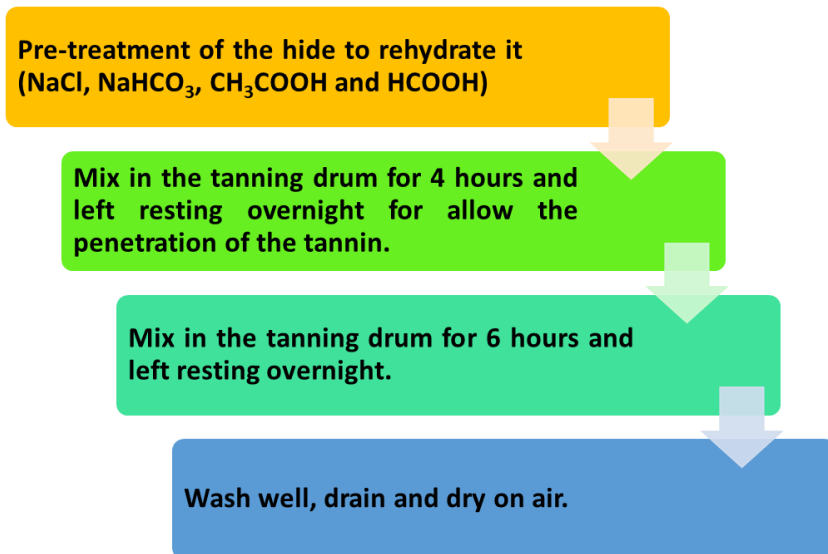


*Figure 31. Scheme of the tanning process.*

The hide was initially pre-treated according to the quantities shown in Table 3. This step is necessary in order to rehydrate the raw hide and bring it to a pH level that favours the penetration of the synthetic tannins in the study. The final pH of the hide was adjusted at around 4.5.

Table 3. Pre-treatment of defrosted hide

| Pre-treatment formulation on defrosted raw hide <sup>a</sup>  |       |   |
|---|-------|---|
| Products  | % w/w |   |
| Water   | 100   | $T = 30\text{ }^{\circ}\text{C}$              |
| NaCl  | 10    | Rotate 10 min                                 |
| Hide  | 100   | Rotate 20 min                                 |
| CH <sub>3</sub> COONa   | 1     |   |
| NaHCO <sub>3</sub>  | 1     | Rotate 30 min, pH = $6.0 \pm 0.5$ at 25°C     |
| Drain and wash  |       |   |
| Water   | 80    |   |
| NaCl  | 8     |   |
| HCOOH   | 0.15  | Rotate 120 minutes, pH= $4.5 \pm 0.5$ at 25°C |
| Rest overnight in the lab drum  |       |   |
| <sup>a</sup> The percentage of added products is calculated based on the hide weight. That is, for 100 g hide, 100 g of water is added. |       |   |

After the pre-treatment, the tanning test were carried out following the process described in Table 4. For each test, we used 10 g of raw hide and 4 g of novel tanning product. The hide was mixed in the tanning drum for 4 hours and was left resting overnight to allow a better penetration of the tanning product. Considering that the test is conducted on a laboratory scale, the hide was left to shake for a further 6 hours and soaked in the tanning drum overnight to maximise the tannin penetration.

At the end of the process the hide was washed with plenty of water, drained and air dried before micro-DSC measurements were taken.

Table 4. Tanning test- laboratory scale

| Tanning of pre-treated raw hide <sup>a,b</sup>  |       |  |
|---|-------|--|
| Products  | % w/w |  |
| Water   | 400   | $T = 30\text{ }^{\circ}\text{C}$   |
| NaCl  | 10    |  |
| Hide  | 100   | Rotate 10 minutes  |
| Product tested (SS1, SS2, SS3, SS4, SS5, MIDA DD <sup>®</sup> , $\beta$ -CD)  | 40    | pH = $4.5 \pm 0.5$<br>Rotate 4 hours and then rest overnight.<br>Rotate 6 hours and then rest overnight. |
| Wash, drain and dry.  |       |  |
| <sup>a</sup> The percentage of added products is calculated based on the hide weight. That is, for 100 g hide, 400 g of water is added.<br><sup>b</sup> The actual weight of the leather is calculated on half of the real weight since the leather is weighed wet. |       |  |

### 3.3.1.1 Micro- DSC measurements: evaluation of the efficiency of the tanning interaction

As previously reported (chapter 1.3.2), the efficiency of the tanning processes and in particular of tanning agents is generally assessed by measuring the hydrothermal stability of leather. The Standard Test Method for Shrinkage Temperature of Leather, ISO 3380:2015 [IULTCS/IUP 16], is the most widely used method from laboratory to industry level. However, the tanning reaction is very complex at the molecular level, to the extent that there is no clear model of its effect on hydrothermal stability.<sup>87,88</sup> As micro-differential scanning calorimetry (micro-DSC) is the classical tool to study the thermodynamics of protein folding and unfolding processes, we applied this experimental technique to characterise the hydrothermal stability of fibrillar collagen upon treatment with the SupraSynts and find insights into the interaction of collagen with the novel five SupraSynts.

<sup>87</sup> A.D. Covington, *Global J. Inorg. Chem.*, **2010**, 1(2), 119-31.

<sup>88</sup> A. Covington, L. Song, O. Suparno, H. Koon, M.J. Collins, *J. Soc. Leather Technol. Chem.*, **2008**, 92, 1-7.

Table 5 reports the calorimetric parameters (Figure 32) featuring fibrillar collagen denaturation for all samples tested.

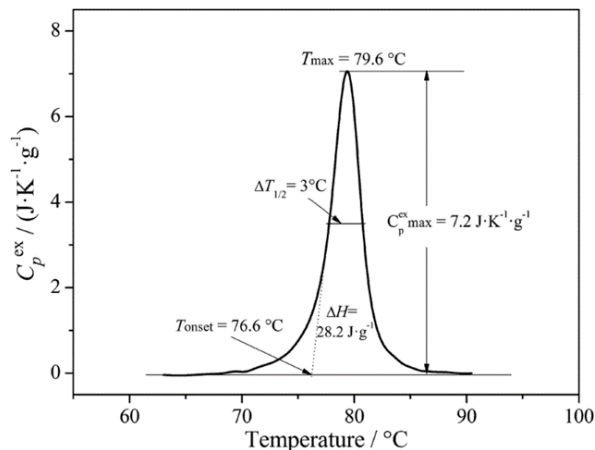


Figure 32. Typical denaturation curve of leather measured by micro-DSC with the denaturation parameters and their calculation. *Errore. Il segnalibro non è definito.*

The  $T_{max}$  refers to the denaturation temperature of the various collagen populations present in the investigated sample while the onset temperature  $T_{onset}$  refers to the overall thermal transition.  $T_{onset}$  reflects the structural destabilisation occurring within the fibrils prior to the denaturation of the collagen population showing the lowest hydrothermal stability.<sup>19,89</sup> The peak halfwidth  $\Delta T_{1/2}$  characterises the asymmetry of the denaturation peak and its increase reveals an increase of thermal heterogeneity of the analysed sample, namely the presence of various collagen populations with distinct thermal stability.<sup>90,91</sup> The enthalpy of denaturation of collagen fibres is an extensive parameter directly related to the forces stabilising the fibrillar structure of collagen, not dependent on scan rate.<sup>90</sup> The overall enthalpy of denaturation is calculated as the sum of the enthalpies  $\Delta H_i$  corresponding to the various collagen populations with distinct thermal stabilities within each investigated sample. Accordingly,

<sup>89</sup> A.D. Covington, *Chem. Soc. Rev.*, **1997**, 26, 111–126.

<sup>90</sup> E. Badea, G. Della Gatta, T. Usacheva, *Polym. Degrad. Stab.*, **2012**, 97, 346-353.

<sup>91</sup> H.R. Tang, A.D. Covington, R.A. Hancock, *J. Agric. Food Chem.*, **2003**, 51(23), 6652-6.

$\% \Delta H_i$  is assumed as the percentage of the various collagen populations within the investigated sample.

Table 5. Micro-DSC parameters of thermal denaturation of collagen within non-tanned and tanned hide

| Product tested  | Test's name    | $T_{onset}$ (°C) | $T_{max i}$ (°C)   | $\Delta T_{1/2}$ (°C) | $\Sigma \Delta H_i$ (J·g <sup>-1</sup> ) | $\% \Delta H_i$   |
|---|----------------|------------------|--|-----------------------|--|---|
| Row hide  | R.H.           | 50               | $T_1 = 54$   | 8.0                   | 44.7                                     | $\Delta H_1 = 100$  |
| $\beta$ -CD   | L- $\beta$ -CD | 50               | $T_1 = 54$<br>$T_2 = 62$   | 8.3                   | 39.6                                     | $\Delta H_1 = 68.3$<br>$\Delta H_2 = 31.7$  |
| MIDA DD®  | L-MIDA DD®     | 62               | $T_3 = 65$<br>$T_4 = 73$   | 12.8                  | 37.1                                     | $\Delta H_3 = 53.0$<br>$\Delta H_4 = 47.0$  |
| SS 1  | L-SS1          | 62               | $T_3 = 65$<br>$T_4 = 74$<br>$T_5 = 78$                             | 15.5                  | 32.2                                     | $\Delta H_3 = 19.8$<br>$\Delta H_4 = 53.9$<br>$\Delta H_5 = 26.3$   |
| SS 2  | L-SS2          | 62               | $T_3 = 65$<br>$T_4 = 73$<br>$T_5 = 77$                             | 15.1                  | 38.5                                     | $\Delta H_3 = 28.0$<br>$\Delta H_4 = 41.0$<br>$\Delta H_5 = 31.0$   |
| SS 3  | L-SS3          | 62               | $T_3 = 65$<br>$T_4 = 74$<br>$T_5 = 78$                             | 14.7                  | 32.4                                     | $\Delta H_3 = 26.5$<br>$\Delta H_4 = 38.0$<br>$\Delta H_5 = 35.5$   |
| SS 4  | L-SS4          | 62               | $T_2 = 62$<br>$T_3 = 66$<br>$T_4 = 74$<br>$T_5 = 78$               | 15.6                  | 26.6                                     | $\Delta H_2 = 12.9$<br>$\Delta H_3 = 27.5$<br>$\Delta H_4 = 28.6$<br>$\Delta H_5 = 31.0$                        |
| SS 5  | L-SS5          | 55               | $T_1 = 56$<br>$T_2 = 61$<br>$T_3 = 65$<br>$T_4 = 71$<br>$T_5 = 75$ | 20.9                  | 36.0                                     | $\Delta H_1 = 15.2$<br>$\Delta H_2 = 24.9$<br>$\Delta H_3 = 21.1$<br>$\Delta H_4 = 17.6$<br>$\Delta H_5 = 21.2$ |
| i=1-5 represents the index of collagen populations within the analysed samples, from the least to the most stable |                |                  |  |                       |  |   |

In Figure 33 the denaturation peaks of the hides treated with  $\beta$ -CD (L-  $\beta$ -CD) and MIDA DD® (L- MIDA DD®) are compared with that of raw hide (R.H.), a narrow and rather symmetrical calorimetric signal with a maximum at  $T_1 = 54$  °C. Considering that the thermal stabilisation of collagen is due to the

linking reaction between elements of collagen structure and other molecules, one can infer that the peak component visible as a shoulder at  $T_2 = 61\text{ }^\circ\text{C}$  on L- $\beta$ -CD peak (Figure 33b) represents the denaturation of a population of collagen that interacted with  $\beta$ -CD. The denaturation peak of L-MIDA DD<sup>®</sup> (Figure 33c) is characterised by the presence of two components corresponding to two thermally stabilised collagen populations denaturing at  $T_3 = 65\text{ }^\circ\text{C}$  and  $T_4 = 73\text{ }^\circ\text{C}$ , respectively. The broad temperature range of the overall denaturation transition  $\Delta T_{1/2}$  could be attributed to the wide distribution of the molecular weights of MIDA DD<sup>®</sup>.<sup>92</sup>

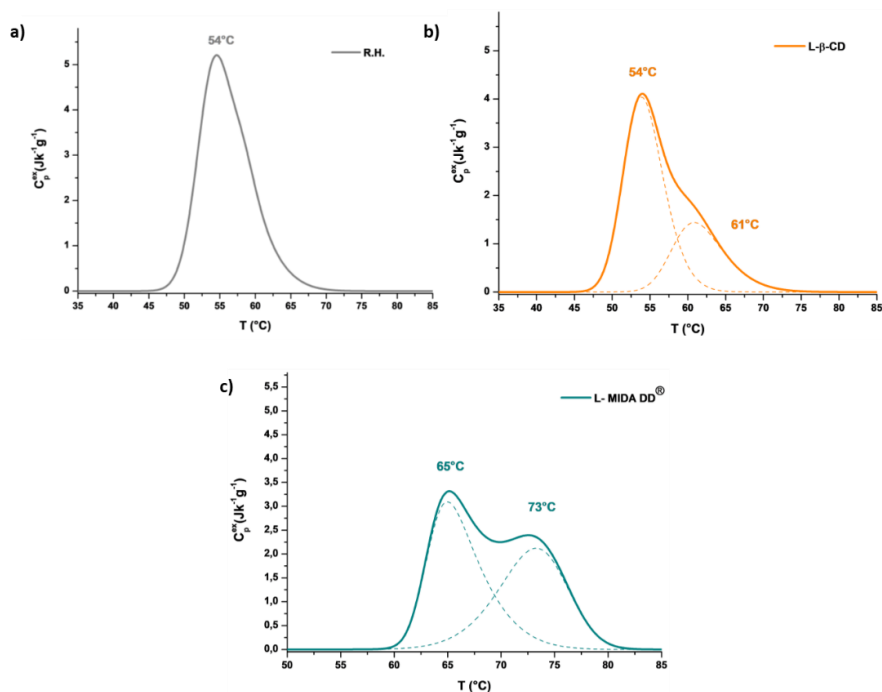


Figure 33. Denaturation curves for (a) raw hide, (b) leather tanned with  $\beta$ -cyclodextrin and (c) leather tanned with MIDA DD<sup>®</sup> obtained by micro-DSC.

The denaturation peaks of the hides tanned with the SupraSynt mixtures exhibit three to five distinct components depending on the  $\beta$ -CD / MIDA DD<sup>®</sup> ratio (Figure 34). The group formed by L-SS1, L-SS2, and L-SS3 (Figure

<sup>92</sup> C. Carșote, E. Badea, L. Miu, G. Della Gatta, *J. Thermal. Anal. Calorim.*, **2016**, 124, 1255-1266.

34a-b-c) is characterised by the presence of three thermally stabilised collagen populations showing denaturation at about 65°C ( $T_3$ ), 73°C ( $T_4$ ), and 78°C ( $T_5$ ), respectively. As we already found that the  $T_3$  and  $T_4$  populations result from the interaction of collagen with MIDA DD<sup>®</sup>, the  $T_5$  population can be assigned to the interaction of collagen with the supramolecular system MIDA DD<sup>®</sup>@ $\beta$ -CD. It is worth noting that the percentage of the enthalpy corresponding to the  $T_5$  population increases as  $\beta$ -CD/MIDA DD<sup>®</sup> ratio increases (Figure 34e). This indicates that these supramolecular systems have an improved tanning ability compared to MIDA DD<sup>®</sup> itself and their tanning efficiency increases as  $\beta$ -CD/MIDA DD<sup>®</sup> ratio increases. On the other hand, an excess of  $\beta$ -CD no longer benefits to the tanning ability of the supramolecular complexes as indicated by the denaturation behaviour of L-SS4 (Figure 34d) and L-SS5 (Figure 34e). In fact, in the L-SS4 denaturation peak shows the component at 62°C associated to the interaction of the  $\beta$ -CD with collagen, while an unreacted (not tanned) collagen component denaturing at 56°C is present in the L-SS5 denaturation peak.<sup>93</sup> Contrary to what we observed in the case of L-SS1, L-SS2 and L-SS3, the percentage of the most stable population ( $T_5 > 75$  °C) decreases as  $\beta$ -CD/MIDA DD<sup>®</sup> ratio increases for L-SS4 and L-SS5 (Figure 34d-e). In conclusion, the micro-DSC results indicate system SS3 as the most effective tanning agent.

---

<sup>93</sup> A.D. Covington, *Chem. Soc. Rev.*, **1997**, *26*, 111–126.

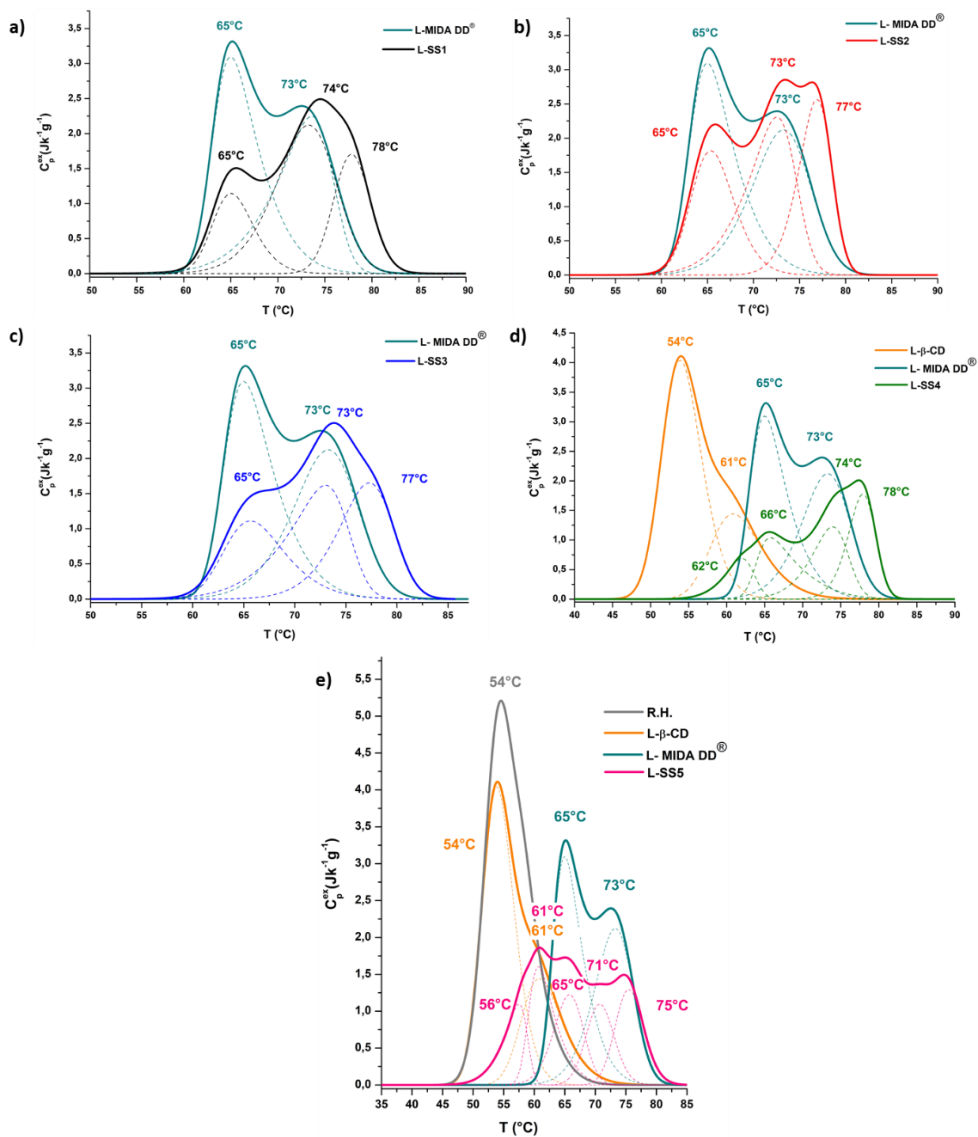


Figure 34. Deconvolution of multi-component denaturation peaks of the hides tanned with (a) SS1, (b) SS2, (c) SS3, (d) SS4, (e) SS5.

### 3.3.1.2 ATR-FTIR characterization of L-SS<sub>i</sub> products

The interaction between collagen and the five products was also studied using FTIR-ATR analysis.<sup>94</sup> In Figure 35, the FTIR-ATR spectrum of L-SS1 in

the region of 1000-1800  $\text{cm}^{-1}$  is compared to raw hide and SS 1 spectra and further processed using the second derivative method. The resolution of the absorption peaks in the second derivative spectra is significantly enhanced, allowing us to separate and identify the overlapping peaks (Figure 36). L-SS1 spectrum shows both the typical signals of MIDA DD<sup>®</sup> and SS 1. For example, C-C (benzene ring) stretching at 1586  $\text{cm}^{-1}$ , S-O stretching at 1142  $\text{cm}^{-1}$  and C-C-C bending at 833  $\text{cm}^{-1}$ . Furthermore, there is also a sharp peak at 1027  $\text{cm}^{-1}$  which confirms the interaction of the  $\beta$ -CD component with collagen.

---

<sup>94</sup> C. Carsote, C. Şendrea, M.C. Micu, A. Adams, E. Badea, *Radiat. Phys. Chem.*, **2021**, *189*, 109712.

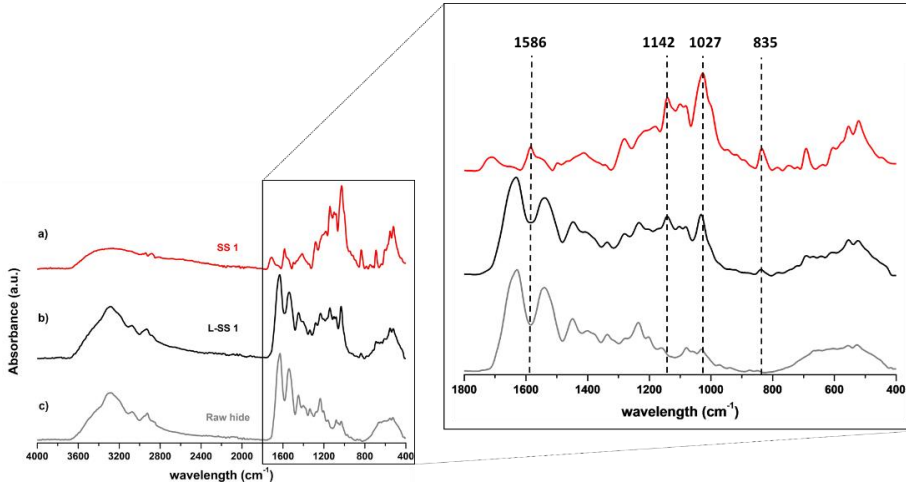


Figure 35. ATR- FTIR spectra of (a) SS 1, (b) L-SS1 and (c) raw hide.

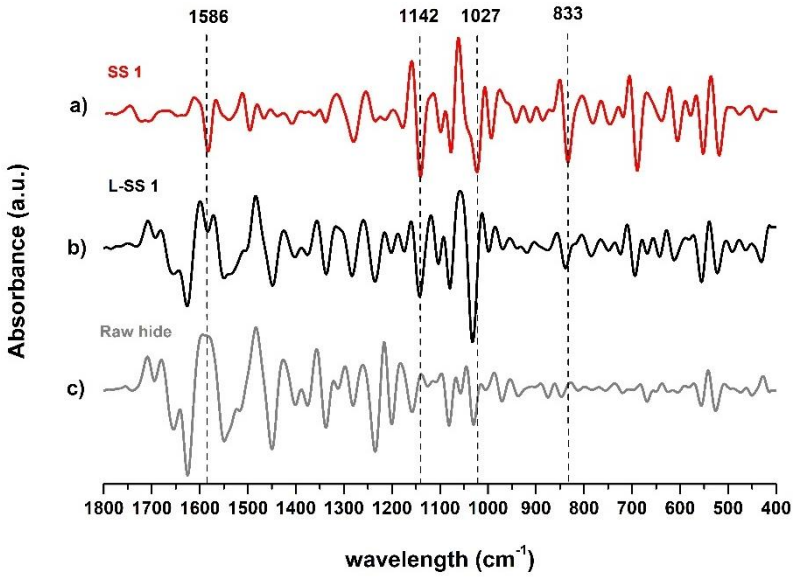


Figure 36. ATR- FTIR second derivative spectra of (a) SS 1, (b) L-SS1, (c) Raw hide.

The same bands can be observed in all investigated samples (Figure 37). It is important to note that L-SS5 spectrum shows very attenuated bands at 833 and 1586  $\text{cm}^{-1}$ . This correlates very well with the micro-DSC results that indicated L-SS5 as having the lowest tanning ability.

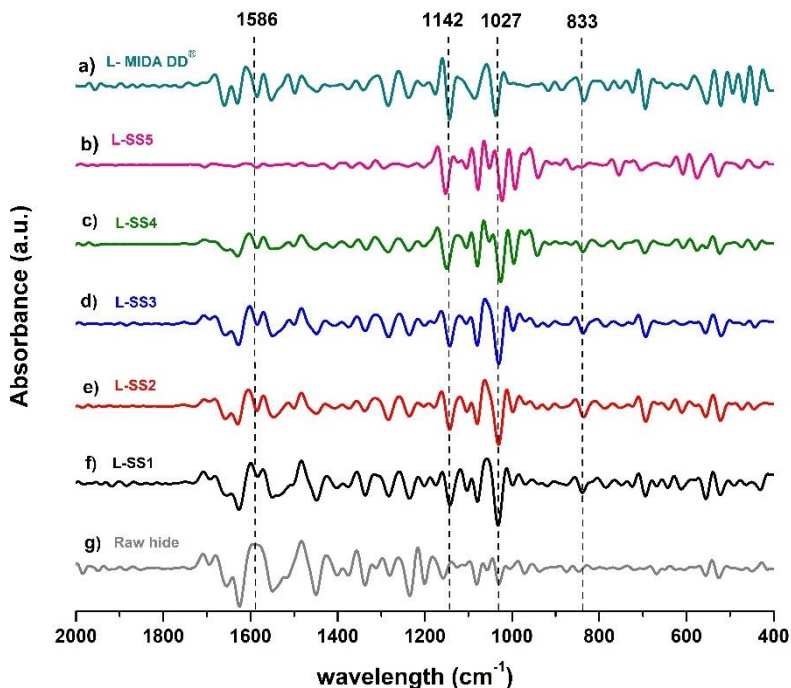


Figure 37. ATR-FTIR second derivative spectra of hide tanned with (a) MIDA DD<sup>®</sup> (b) SS 5, (c) SS 4, (d) SS 3, (e) SS 2, (f) SS1, (g) Raw hide.

### 3.3.2 Pilot scale tests: characterisation of L-SS<sub>i</sub> samples by standard methods

All the SupraSynts were tested at pilot scale to verify their actual tanning effectiveness after scaling-up the tanning process. The pilot scale tanning test was carried out at *FGL International S.P.A.* (Figure 38).

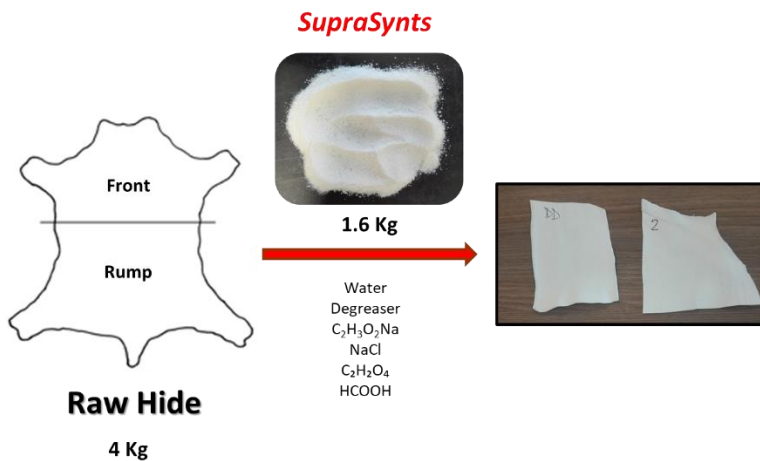


Figure 38. Pilot scale process.

The pilot-scale tanning process is reported in Table 6. Calf hides were used for the tests and a quantity of 4Kg of raw hide was used for each SupraSynt tested. A test using MIDA DD<sup>®</sup> was done to better compare the results obtained.

Table 6. Tanning formulation on pilot scale

| Tanning formulation on calf hide <sup>a,b</sup>  |       |  |
|--|-------|--|
| Products   | % w/w |  |
| Water  | 100   | T=30°C   |
| NaCl   | 10    |  |
| Hide   | 100   | 10 minutes   |
| IDROSIN JK <sup>®</sup>  | 0.5   |  |
| Tannin tested (SupraSynt 1, 2, 3, 4, 5 or MIDA DD <sup>®</sup> )   | 40    | pH= 4.5± 0.5<br>240 minutes and then leave resting overnight |
| HCOONa   | 0.5   |  |
| ECOGRIN 30LR <sup>®</sup>  | 0.1   | 60 minutes   |
| Leave resting overnight then wash, drain and dry.  |       |  |
| <sup>a</sup> The percentage of added products in each process is related to weight of hides. That is, if we are working with 100 g of hides, we add 100 g of water per each process.<br><sup>b</sup> The actual weight of the leather is calculated on half of the real weight since the leather is weighed wet. |       |  |

The shrinkage temperatures  $T_s$  of the five L-SS<sub>i</sub> crust leather samples, determined using the shrinkage Tg tester (Figure 39) according to UNI EN ISO 3380: 2015 standard method, are reported in Table 7.



Figure 39. The shrinkage tester

Table 7. Shrinkage temperatures of the crust leather samples tanned with the five SupraSynts compared to that tanned with the commercial tanning agent MIDA DD®.

| Product tested | Test's name | $T_s$ (°C) |
|----------------|-------------|------------|
| MIDA DD®       | L- MIDA DD® | 70         |
| SS1            | L-SS1       | 74         |
| SS2            | L-SS2       | 72         |
| SS3            | L-SS3       | 75         |
| SS4            | L-SS4       | 68         |
| SS5            | L-SS5       | 56         |

As expected, the leather samples obtained using the SupraSynt 1, 2, and 3 show shrinkage temperatures higher than leather tanned with the commercial tanning agent MIDA DD®. L-SS4 crust leather has a lower  $T_s$  compared to L-MIDA DD® while the hydrothermal stability of L-SS5 sample

is similar to that of not-tanned hide. These results correlate very well with the percentage of the most stable collagen populations, i.e. those showing denaturation at  $T_4 \approx 74$  °C and  $T_5 \approx 78$  °C, as from the micro-DSC results (Table 5). These populations represent almost 50% of the total collagen in the reference sample L-MIDA DD<sup>®</sup>, increase their percentage to more than 70% within L-SS1, L-SS2 and L-SS3, while decreasing to 60% for L-SS4 and dropping to less than 40% for L-SS5. Consequently, the standard physical-mechanical tests were performed only for the most stable leather samples, i.e., L-SS1, L-SS2, and L-SS3 samples. The results are reported in Table 8.

*Table 8. Results of standard physical-mechanical test of the selected crust leather samples (pilot scale level)*

| <b>Crust leather sample</b>               | <b>L-MIDA DD<sup>®</sup></b> | <b>L-SS1</b> | <b>L-SS2</b> | <b>L-SS3</b> | <b>Standard method</b> |
|---|------------------------------|--------------|--------------|--------------|------------------------|
| Thickness (mm)                            | 1.6                          | 1.7          | 1.2          | 1.0          | UNI EN ISO 2589: 2016  |
| Tensile strength (N/mm <sup>2</sup> )     | 23.2                         | 25.1         | 33.9         | 32.9         | EN ISO 3376:2020       |
| Percentage elongation (%)                 | 34.6                         | 37.0         | 41.0         | 39.3         | EN ISO 3376:2020       |
| Resistance to grain cracking (Kg)         | 35.6                         | 30.1         | 43.2         | 49.2         | UNI EN ISO 3378: 2005  |
| Crack index (mm)                          | 5.9                          | 6.7          | 8.0          | 8.6          | UNI EN ISO 3378: 2005  |
| Force at crack (Kg)                       | 73.3                         | 80.3         | 58.4         | 65.1         | UNI EN ISO 3379: 2015  |
| Distention and strength of the grain (mm) | 10.2                         | 10.1         | 9.1          | 9.8          | UNI EN ISO 3379: 2015  |

It is well known that the specific applications of a leather assortment depend on the physical properties measured at the crust leather stage.<sup>95</sup> Hence, several physical-mechanical properties were measured to

<sup>95</sup> W. Ding, S. Guo, H. Liu, X. Pang, Z. Ding, *Mater. Today Chem.*, **2021**, *21*, 100508.

demonstrate the applicability of the leather assortment obtained with the newly synthesised derivatives. As shown in Table 8, the mechanical properties of crust leathers tanned with the three *SupraSynts* (L-SS1, L-SS2, L-SS3) clearly improved compared to the crust leather obtained using the commercial tannin MIDA DD®.

Tensile strength determines the maximum tension that a hide can withstand without breaking. The minimum acceptable tensile strength for a tanned leather is 20 N/mm<sup>2</sup>.<sup>96</sup> The observed increase in tensile strength of L-SS2 and L-SS3 leathers could be assigned to an increased percentage of β-CD compared to L-SS1 and L-MIDA DD® leathers. Elongation at break (percentage elongation) is the maximum extent to which the material can stretch without breaking. A low elongation value causes the resulting leather to tear easily, while too high elongation value causes it to deform too quickly and even lose its usability. A good percentage of elongation should be around 40%, as measured for L-SS2 and L-SS3.<sup>97</sup> The SS2 and SS3 have therefore the ability to produce a more thermostable leather while increasing its tensile strength and conferring the optimal elongation at break.

The colour fastness to artificial light of the three selected samples was evaluated using the xenon arc fading lamp standard test UNI EN ISO 105-B02:2014 (Table 9). This test evaluates the degree of yellowing of the tanned leather as a result of exposure to light. The evaluation is carried out by comparing the tanned leather not subjected to the test with those exposed to light and assessing the variation from the original colour numbered from 1 (higher contrast) to 5 (no contrast) on the grey scale. As shown in Table 9 the use of β-CD did not adversely affect the final leather colour resulting in a very good performance in terms of resistance to artificial light.

---

<sup>96</sup> K.M. Nalyanya, R.K. Rop, A. Onyuka, Z. Birech, A. Sasia, *Leather Footwear J.*, **2018**, *18*, 4.

<sup>97</sup> W.D. Kanuri, A. Onyuka, R. Tanui, *Int. j. sci. res. publ.*, **2019**, *9*, 12-17.

Table 9. Results of colour fastness to artificial light of the selected crust leather samples (pilot scale level)

| Crust leather sample | L-MIDA DD <sup>®</sup> | L-SS1 | L-SS2 | L-SS3 |
|----------------------|------------------------|-------|-------|-------|
| 24 hours             | 2/3                    | 2/3   | 2/3   | 2/3   |
| 48 hours             | 2/3                    | 2/3   | 2/3   | 2/3   |
| 72 hours             | 2                      | 2     | 2     | 2     |

Furthermore, the leather obtained with the new SupraSynts (L-SS<sub>i</sub>) had a more even grain surface, was softer and more elastic compared to that tanned with MIDA DD<sup>®</sup> (Figure 40).

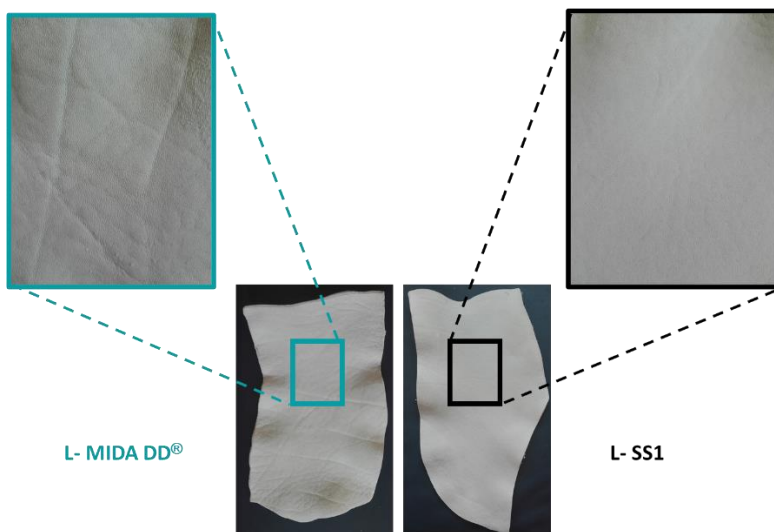


Figure 40. Grain surface of leather tanned with (left) MIDA DD<sup>®</sup> and (right) SS1.

### 3.4 Conclusion

In conclusion, this work presents an approach for a cleaner and more sustainable tanning process based on the enhancement of tanning ability of the widely used wet-white tannin MIDA DD<sup>®</sup>, while reducing its bisphenol S

polymer content and thus increase the safety and biodegradability of both the tanning process and final product.

A novel supramolecular system (*SupraSynt*) based on a pseudorotaxane motif was synthesized starting from  $\beta$ -CD and a commercial bisphenol S polymer called MIDA DD<sup>®</sup> currently used as a wet-white tanning agent in order to enhance the tanning sustainability. Different molar ratios of  $\beta$ -CD and MIDA DD<sup>®</sup> were used and five distinct inclusion complexes were synthesized. The formation of the pseudorotaxane supramolecular systems was confirmed by solution-state 1D NMR and FTIR-ATR spectroscopies. Their ability to interact with collagen within animal hide and to increase the collagen fibers thermal stability was tested by micro-DSC. Noteworthy, the  $\beta$ -CD/MIDA DD<sup>®</sup> ratio was shown to significantly influence the tanning ability. ATF-FTIR analysis confirmed the interaction between collagen and the novel supramolecular systems. All the new *SupraSynts* were tested on a pilot scale to verify their actual tanning effectiveness after scaling-up the tanning process. Three of the five crust leather samples showed higher thermal stability compared to that conferred by MIDA DD<sup>®</sup>. The physical-mechanical properties of these samples, as well as their colour fastness to artificial light was evaluated by the standard methods used in tanning industry. The results obtained in the physical tests clearly shows that the synergy between host and guest is also advantageous in terms of the quality of the finished product (crust leather).

The *SupraSynts* developed are now the object of an Italian patent with the name: "Composto conciante o rionciante di pellame con composto di inclusione a base di ciclodestrina" (application number 1020220000938). This thesis work will be published afterwards when the patent goes into the public domain.

### 3.5 *Experimental section*

$\beta$ -cyclodextrin ( $\beta$ -CD) was purchased from Roquette (Kleptose<sup>®</sup> GC grade  $\geq$  93%) and used without further purification. MIDA DD<sup>®</sup>, dicarboxylic acid and sodium sulphate used to prepare the derivatives were supplied by BI-QEM Specialties S.P.A.

**<sup>1</sup>H NMR spectra of the SupraSynts 1-5** (400 MHz, 298 K, D<sub>2</sub>O) were recorded on a Bruker 400 MHz spectrometer. Chemical shifts are reported relative to the residual solvent peak.

**GPC** spectrum of MIDA DD<sup>®</sup> was recorded on a Jasco spectrometer with UV-vis detector with three columns in series: GPC PL-Gel 5 μm (Guard column), PL-Gel 10000 Å (300 x 7.5 mm), PL-Gel 500 Å (300 x 7.5 mm). The flux was 0.6 ml/min at a pressure of 70-80 bar at a temperature of 40°C. The eluent used was a LiCl 0.10 M in DMF. The concentration of the sample is 0.3% wt in DMF + 10% H<sub>2</sub>O (volume of injection 10 μL).

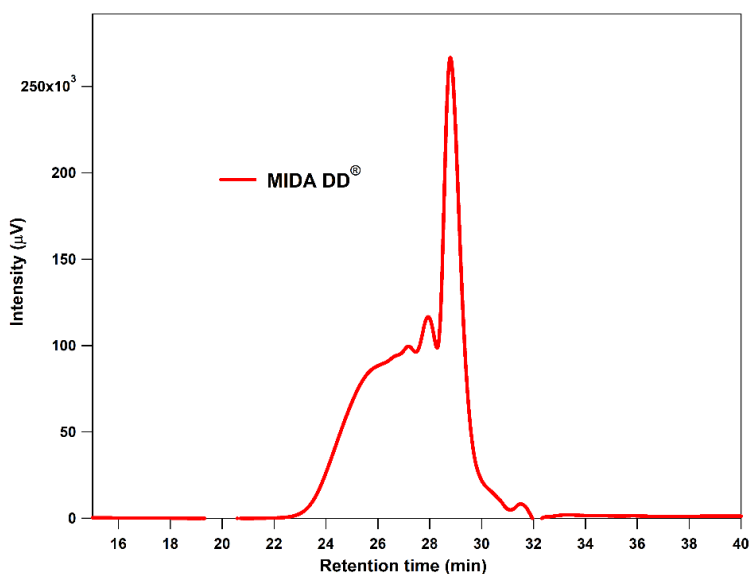


Figure 41. GPC MIDA DD<sup>®</sup>

Table 10. GPC results of MIDA DD<sup>®</sup>

| tR      | Mp  | Mn  | Mw   | Mz    | Mv   | Mw/Mn  | Mz/Mw  |
|---------|-----|-----|------|-------|------|--------|--------|
| 28.2200 | 538 | 985 | 3271 | 10759 | 3271 | 3.3258 | 3.2896 |

Table 11. MW percentage of MIDA DD®

| Mw Range        | %    |
|-----------------|------|
| 500 - 1         | 11.7 |
| 1000 - 501      | 31.9 |
| 5000 - 1001     | 37.6 |
| 10000 - 5001    | 10.9 |
| 1000000 - 10001 | 7.9  |

The hides used for tanning tests at laboratory scale were made available by the Leather and Footwear Research Institute (ICPI) of the National Research and Development Institute for Textiles and Lather (INCDTP), Bucharest. All reagents (i.e., sodium chloride, formic acid, sodium acetate and sodium bicarbonate) used in the tanning tests were from CHIMREACTIVE S.R.L. Tanning tests were performed using a rotator drive stirrer unit STR4/4 (Bibby Scientific Ltd) set for continuous operation at 35 rpm to simulate the movement of the tanning drum. Calf hides, reagents and chemicals used in the tanning process at pilot scale were made available by the FGL International S.P.A., Italy where the tanning tests were performed. The shrinkage temperature of crust leather samples was measured using a shrinkage Tg tester according to the standard method ISO 3380:2015 [IULTCS/IUP 16]. Physical-mechanical tests as well as colour fastness to artificial light were performed according to the specific standard tests used in the tanning industry.

**Micro-Differential Scanning Calorimetry (micro-DSC)** was employed to measure the hydrothermal stability of tanned hides. Measurements, carried out with a high-sensitivity Micro-DSC III calorimeter (SETARAM), were performed in the temperature range (25–85) °C at 0.5 K min<sup>-1</sup> heating rate, using 850 µl stainless steel (Hastelloy C) cells. This low scan rate was applied to provide the equilibrium condition for DSC analysis and accurately measure the denaturation parameters. Samples of about (5.0–10.0) mg were suspended in 0.5 M acetate buffer (pH = 5.0) directly in the measure

cell and left for 30 minutes to assure their fully hydration and avoid  $T_{\max}$  and enthalpy variation with hydration level. Experimental DSC data acquired with the SETARAM SetSoft2000 software were analysed using PeakFit 4.1 (Jandel Scientific). The DSC multiple peaks of the investigated samples were deconvoluted using the PeakFit asymmetric Gaussian fit function to improve the fit of the asymmetry in the peaks.

***The Infrared Spectroscopy in Attenuated Total Reflection mode (FTIR-ATR)***

analyses was carried out using an ALPHA spectrometer (Bruker Optics) equipped with a Platinum ATR module. The penetration depth, depending on the refractive indices of ATR crystal and sample, typically amounts to a few microns (ca. 0.5–3  $\mu\text{m}$ ). Spectra were recorded in the 4000–400  $\text{cm}^{-1}$  spectral range with a 4  $\text{cm}^{-1}$  resolution, using 32 scans. Opus software (Bruker Optics, Germany) was used for the acquisition and elaboration of the spectra. The second derivative spectra were applied to enable a better evaluation of variations in peak intensity and position and to more easily identify the individual bands in the complex spectra of tanned hides.

## 4. Selective recognition of bisphenol S isomers in water by $\beta$ -cyclodextrin<sup>98</sup>

### 4.1 General overview

During the industrial synthesis of MIDA DD<sup>®</sup>, in addition to the formation of 4,4'-dihydroxybiphenyl sulfone (4,4'-BPS), the isomeric 2,4'-dihydroxybiphenyl sulfone (2,4'-BPS) is also formed as a by-product. Consequently, the commercial product known as bisphenol S is actually a mixture of both isomeric dihydroxy diphenyl sulfones, since purification of the two isomers from the mixtures is not readily achievable.

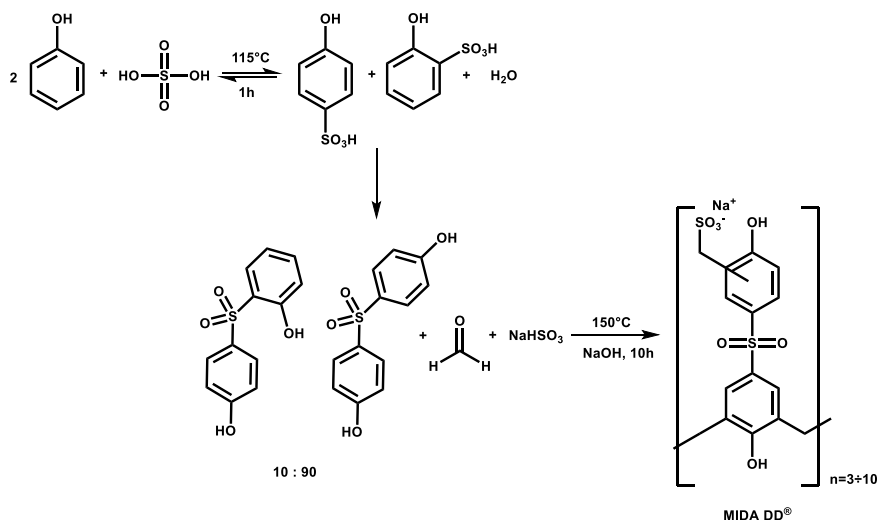


Figure 42. Industrial synthesis of MIDA DD<sup>®</sup>.

For this reason, synthetic BPS-based tannins contain a large percentage of 2,4-BPS that is not easily purified by conventional purification techniques such as crystallisation or chromatography. Therefore, many efforts are focused on designing supramolecular hosts that can selectively recognise

<sup>98</sup> I. Quaratesi, P. Della Sala, C. Capacchione, C. Talotta, S. Geremia, N. Hickey, R. Gliubizzi, I. Bruno, C. Sgarlata, R. Migliore, C. Gaeta, P. Neri, *Supramol. Chem.*, **2021**, 1-14.

one of the two BPS isomers. Molecular recognition of constitutively isomeric species is still a challenge in supramolecular chemistry<sup>99</sup> and this is particularly true for organic pollutants such as BPS isomers, which show very similar chemical and physical properties.

Although it is well known that  $\beta$ -CD has the ability to form an inclusion complex with 4,4'-BPS in an aqueous system,<sup>100,101</sup> to date no information has been reported regarding molecular recognition towards the 2,4-isomer. Therefore, in the second part of this work, to better assess the actual interaction between  $\beta$ -CD and MIDA DD<sup>®</sup>, we evaluated the complexation capabilities of  $\beta$ -CD towards the two isomeric dihydroxybiphenyl sulfones, in solution, solid state, and gas phase.

In addition, the study of supramolecular hosts capable of discriminating between the two isomeric hosts (4,4'-BPS and 2,4'-BPS) could pave the way for the construction of new materials for separating the two isomers, which could be interesting from both an economic and environmental point of view.

## 4.2 Synthesis and characterization

The synthesis of BPS@ $\beta$ -CD pseudorotaxane complexes was conducted in a flask at atmospheric pressure.  $\beta$ -CD (9.0 mg,  $8.0 \times 10^{-3}$  mmol) was solubilized in 10 mL of deionized water. Then, an appropriate amount of the BPS *guest* was added (1.8 mg,  $8.0 \times 10^{-3}$  mmol), and the resulting mixture was stirred at 25 °C for 30 min. Finally, water was evaporated under vacuum, and the product was further dried and stored at room temperature (Figure 43).

---

<sup>99</sup> M.J. Klemes, L.P. Skala, M. Ateia, B. Trang, D.E. Helbling, W.R. Dichtel, *Acc. Chem. Res.*, **2020**, *53*, 2314–2324.

<sup>100</sup> H. Kitano, H. Endo, M. Gemmei-Ide, M. Kyogoku, *J. Incl. Phenom. Macrocycl. Chem.*, **2003**, *47*, 83–90.

<sup>101</sup> T. Nakaji-Hirabayashi, H. Endo, H. Kawasaki, M. Gemmei-Ide, H. Kitano, *Environ. Sci. Technol.*, **2005**, *39*, 5414–5420.

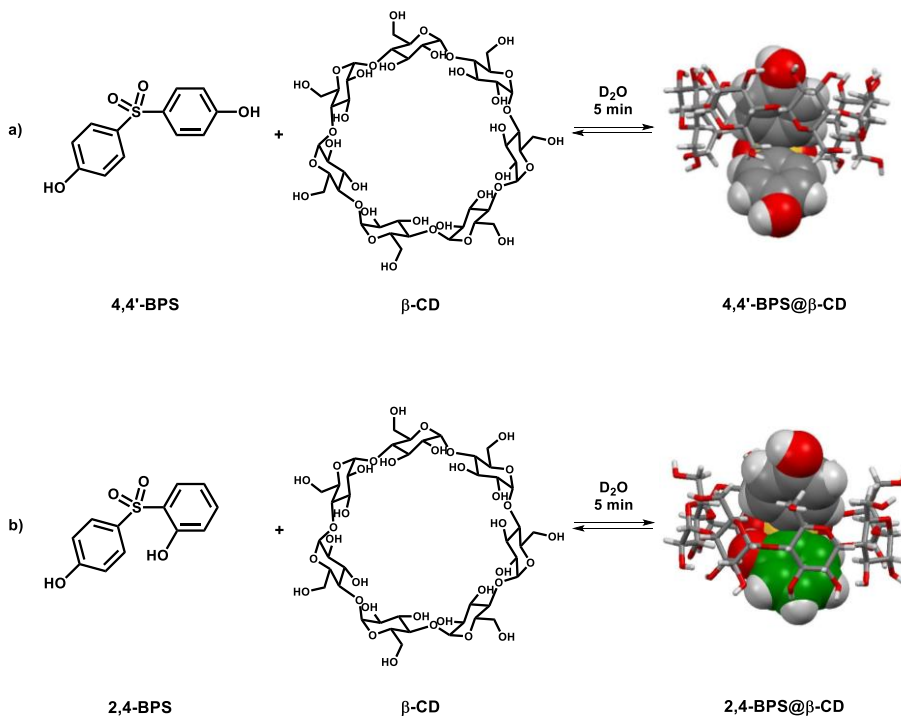


Figure 43. Synthesis of BPS@β-CD pseudorotaxane complexes.

#### 4.2.1 Complexation study of 4,4'-BPS and 2,4'-BPS in solution via 1D and 2D NMR

$^1\text{H}$  NMR titration experiments were used to evaluate the complexation abilities of β-CD toward the two isomeric 4,4'- and 2,4'-dihydroxydiphenyl sulfone.<sup>102,103</sup>

Substantial changes were observed in the respective  $^1\text{H}$  NMR signals when a  $\text{D}_2\text{O}$  solution of β-CD was titrated with 4,4'-BPS, which were indicative of the formation of the 4,4'-BPS@β-CD complex (Figure 44a-c).

<sup>102</sup> K. Hirose, *J. Incl. Phenom. Macrocycl. Chem.*, **2001**, 39, 193–209.

<sup>103</sup> K. Hirose, *Analytical Methods in Supramolecular Chemistry*; Schalley, C. A., Eds.; WILEY-VCH: Weinheim, **2007**.

Considering as example the 1:1 mixture, a complexation induced shift (CIS,  $\Delta\delta = \delta_{compl} - \delta_{free}$ ) was found for both guest and host after mixing. As can be seen from Figure 44b, a single set of averaged  $^1\text{H}$  NMR signal was observed, indicating a fast exchange equilibrium between free and bound species on the NMR time scale. This is a clear indication of the formation of a host-guest complex. The same results were obtained by mixing different quantities of  $\beta$ -CD *host* and 4,4'-BPS *guest*.

In the above example of 1:1 mixture of  $\beta$ -CD *host* and 4,4'-BPS *guest* in  $\text{D}_2\text{O}$ , a CIS of  $-0.42$  ppm for the H5-atom of  $\beta$ -CD located inside the cavity was observed. A smaller CIS of  $-0.15$  ppm was found for the other two protons located inside the cavity, H3 and H6, while a CIS of  $-0.07$  was observed for H2. A CIS was also observed for the aromatic H-atoms of 4,4'-BPS after the inclusion inside the  $\beta$ -CD cavity where both  $\text{H1}^G$  and  $\text{H2}^G$  H-atoms were up-field shifted by  $-0.04$  and  $-0.10$  ppm, respectively.

The inclusion of 4,4'-BPS was confirmed by 2D NOESY spectra (Figure 44f). The aromatic  $\text{H2}^G$  (in *meta* to OH group) of 4,4'-BPS *guest* showed diagnostic dipolar couplings with the H3 and H5 atoms of  $\beta$ -CD, while the aromatic  $\text{H1}^G$  (in *ortho* to OH group) showed dipolar couplings with protons H6 and H5 of  $\beta$ -CD. These latter NOEs clearly indicate the proximity of the *guest* with the primary face of  $\beta$ -CD. As expected, the atoms of  $\beta$ -CD which are oriented outside of the cavity, H2 and H4, did not show dipolar couplings with the *guest*.

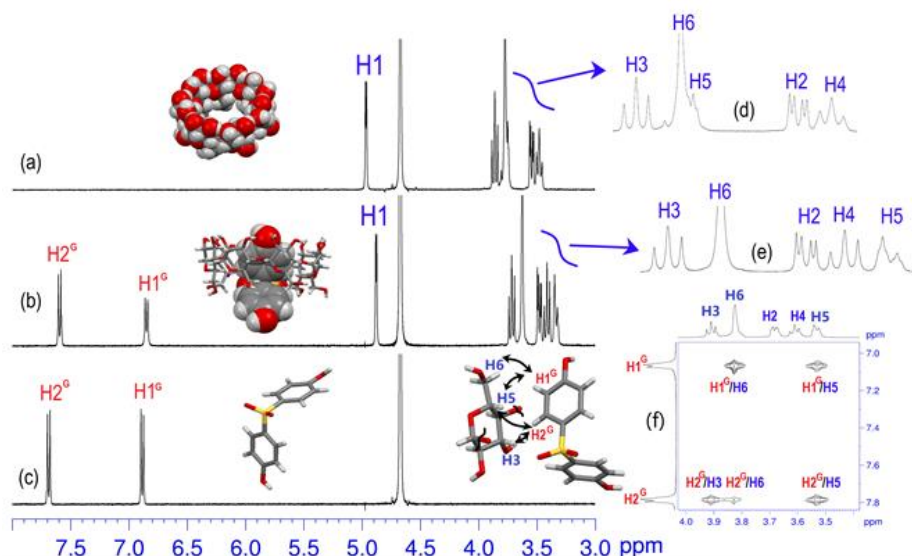


Figure 44. (a-e)  $^1\text{H}$  NMR spectra (400 MHz, 298 K,  $\text{D}_2\text{O}$ ) of: a)  $\beta$ -CD; b) Equimolar mixture of  $\beta$ -CD and 4,4'-BPS (3.0 mM); c) 4,4'-BPS; d) Expansion from 3.0 to 4.0 ppm of the  $^1\text{H}$  NMR spectrum of  $\beta$ -CD in (a); e) Expansion from 3.0 to 4.0 ppm of the  $^1\text{H}$  NMR spectrum of the 4,4'-BPS@ $\beta$ -CD complex in (b); f) Most relevant portion of the 2D NOESY spectrum of the 4,4'-BPS@ $\beta$ -CD complex. In (b) the solid-state structure of the 4,4'-BPS@ $\beta$ -CD complex is reported.

Similar shifts were observed in the  $^1\text{H}$  NMR signals of 2,4'-BPS@ $\beta$ -CD complex. In detail,  $\text{H1}^{\text{G}}$ ,  $\text{H5}^{\text{G}}$ , and  $\text{H6}^{\text{G}}$  of 2,4-BPS were up-field shifted, while  $\text{H2}^{\text{G}}$ ,  $\text{H3}^{\text{G}}$ , and  $\text{H4}^{\text{G}}$  were down-field shifted. A typical CIS of  $-0.1$  ( $\text{H3}$ ),  $-0.1$  ( $\text{H6}$ ),  $-0.27$  ( $\text{H5}$ ) ppm was also observed for the  $\beta$ -CD signals (Figure 45a-c).

The 2D NOESY spectrum evidenced that the 2-phenol unit of 2,4'-BPS did not show significant dipolar couplings with the H-atoms of  $\beta$ -CD. In contrast, there are strong dipolar couplings between  $\text{H5}$ ,  $\text{H3}$ , and  $\text{H6}$ -atoms on the inner cavity of  $\beta$ -CD and  $\text{H5}^{\text{G}}$  and  $\text{H6}^{\text{G}}$  aromatic atoms of the 4'-phenol unit of 2,4'-BPS *guest*. These results suggest that, in aqueous solution, the 4-phenol unit is included inside the cavity of the  $\beta$ -CD, while the 2-phenol unit is outside the cavity.

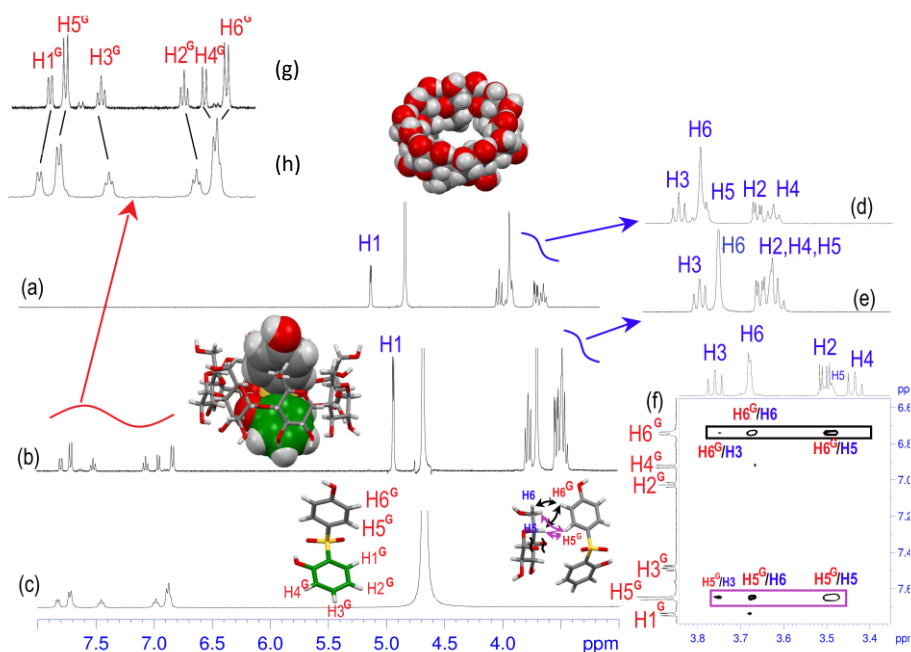


Figure 45. (a-c)  $^1\text{H}$  NMR spectra (600 MHz, 298 K,  $\text{D}_2\text{O}$ ) of: a)  $\beta$ -CD; b) Equimolar mixture of  $\beta$ -CD and 2,4-BPS (3.0 mM); c) 2,4-BPS; d) Expansion from 3.0 to 4.0 ppm of the  $^1\text{H}$  NMR spectrum of  $\beta$ -CD in (a); e) Expansion from 3.0 to 4.0 ppm of the  $^1\text{H}$  NMR spectrum of the 2,4-BPS@ $\beta$ -CD complex in (b); f) Most relevant portion of the 2D NOESY spectrum of the 2,4-BPS@ $\beta$ -CD complex; g) Expansion from 6.5 to 8.0 ppm of the  $^1\text{H}$  NMR spectrum of the 2,4-BPS@ $\beta$ -CD complex in (b); h) Expansion from 6.5 to 8.0 ppm of the  $^1\text{H}$  NMR spectrum of the 2,4-BPS in (c). In (b) the solid-state structure of the 2,4-BPS@ $\beta$ -CD complex is reported.

Diffusion-Ordered Spectroscopy (DOSY) NMR was used to study the complexation processes and the stoichiometry of BPS@ $\beta$ -CD complexes.<sup>104,105</sup>

Analysis of the DOSY spectrum of a 1:1 mixture of 4,4'-BPS/ $\beta$ -CD (2.66 mM, 298 K,  $\text{D}_2\text{O}$ ) provided a diffusion coefficient of  $2.95 \pm 0.05 \times 10^{-10} \text{ m}^2/\text{s}$  for the complexed 4,4'-BPS (Table 12), significantly lower of the free 4,4'-BPS under the same condition ( $4.88 \pm 0.04 \times 10^{-10} \text{ m}^2/\text{s}$ ), but similar to that of free  $\beta$ -CD

<sup>104</sup> Y. Cohen, L. Avram, L. Frish, *Angew. Chem., Int. Ed.*, **2005**, *44*, 520–554.

<sup>105</sup> P. Timmerman, J.L. Weidmann, K.A. Jolliffe, L.J. Prins, D.N. Reinhoudt, S. Shinkai, L. Frish, Y. Cohen, *J. Chem. Soc., Perkin Trans.*, **2000**, *2*, 2077–2089.

$(2.70 \pm 0.03 \times 10^{-10} \text{ m}^2/\text{s})$ .<sup>106</sup> This result strongly corroborated the formation of a stable inclusion complex between  $\beta$ -CD and 4,4'-BPS in which the *guest* diffuses more slowly than in the free state (Figure 46).

The ratio of diffusion coefficients for two different molecular species is inversely proportional to the cubic root of the ratio of their molecular masses for spherical molecules.<sup>105</sup> Based on this relationship, the diffusion coefficients measured for the complexed 4,4'-BPS and free 4,4'-BPS, were consistent with a 1:1 stoichiometry of the 4,4'-BPS@ $\beta$ -CD complex.

Table 12. Diffusion coefficient ( $10^{-10} \text{ m}^2/\text{s}$ ) at different concentration of 4,4'-BPS/ $\beta$ -CD at 298K in  $D_2O$

| $\beta$ -CD equivalents | [ $\beta$ -CD] (mM) | $D_{\text{obs 4,4'-BPS}}$ |
|-------------------------|---------------------|---------------------------|
| 0                       | -                   | 4.88                      |
| 0.25                    | 0.664               | 4.18                      |
| 0.50                    | 1.328               | 3.77                      |
| 0.75                    | 1.992               | 3.30                      |
| 1.00                    | 2.656               | 2.95                      |
| 1.50                    | 3.984               | 2.37                      |
| 2.00                    | 5.313               | 2.03                      |

<sup>106</sup> K. Betlejewska-Kielak, E. Bednarek, A. Budzianowski, K. Michalska, J.K. Maurin, *Molecules*, **2021**, *26*, 4089–4110.

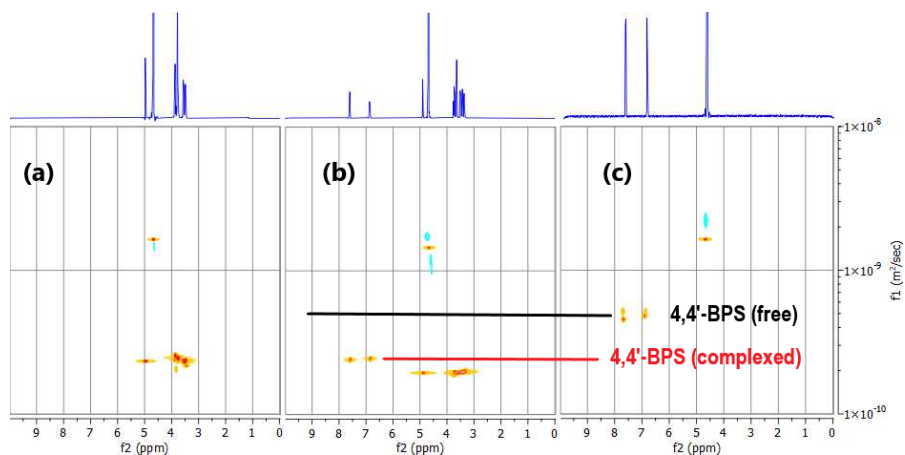


Figure 46. 2D-DOSY spectra (400 MHz,  $D_2O$ , 298 K) of: (a)  $\beta$ -CD; (b) 1:1 mixture of  $\beta$ -CD and 4,4'-BPS (15 mM each one); and (c) 4,4'-BPS (15 mM).

An analogous DOSY study was performed for the 1:1 mixture of 2,4'-BPS/ $\beta$ -CD (Table 13). Again, the diffusion coefficient for the complexed 2,4'-BPS is significantly lower ( $2.88 \pm 0.05 \times 10^{-10} \text{ m}^2/\text{s}$ ) than that of free 2,4'-BPS ( $4.88 \pm 0.04 \times 10^{-10} \text{ m}^2/\text{s}$ ). The results confirm a 1:1 stoichiometry of the 2,4'-BPS@ $\beta$ -CD complex (Figure 47).

Table 13. Diffusion coefficient ( $10^{-10} \text{ m}^2/\text{s}$ ) at different concentration of 2,4'-BPS/ $\beta$ -CD at 298 K in  $D_2O$

| $\beta$ -CD equivalents | $[\beta\text{-CD}]$ (mM) | $D_{\text{obs } 2,4'\text{-BPS}}$ |
|-------------------------|--------------------------|-----------------------------------|
| 0                       | -                        | 4.88                              |
| 0.25                    | 0.664                    | 3.99                              |
| 0.50                    | 1.328                    | 3.71                              |
| 0.75                    | 1.992                    | 3.08                              |
| 1.00                    | 2.656                    | 2.88                              |
| 1.50                    | 3.984                    | 2.47                              |
| 2.00                    | 5.313                    | 2.45                              |

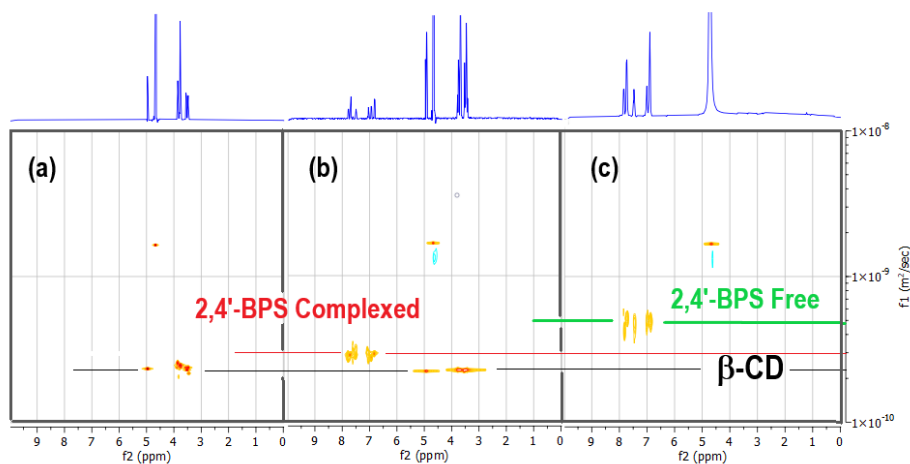


Figure 47. 2D-DOSY spectra (400 MHz,  $D_2O$ , 298 K) of: (a)  $\beta$ -CD; (b) 1:1 mixture of  $\beta$ -CD and 2,4'-BPS (15 mM each one); and (c) 2,4'-BPS (15 mM).

#### 4.2.2 Thermodynamic insights on the complexation of 4,4'-BPS and 2,4-BPS in solution by ITC

Isothermal titration calorimetry (ITC) measurements were performed in collaboration with Prof. C. Sgarlata of the University of Catania, allowing us to determine thermodynamic parameters such as enthalpy, Gibbs free energy and, indirectly, entropy for the BPS@ $\beta$ -CD complexes.

To determine the complex species formed in solution two different sets of titrations, exploring both small and large host-guest ratios, were carried out for each BPS/ $\beta$ -CD system. The first set of experiments was performed to quantify the 1:1 species, while the second set was performed to assess the possibility of further aggregation with the formation of complexes with different stoichiometry.

The thermodynamic parameters and the binding equilibria for the complex formation are reported in Table 14.

Table 14. LogK values and thermodynamic parameters for the formation of the 4,4'-BPS@ $\beta$ -CD, 4,4'-BPS@( $\beta$ -CD)<sub>2</sub> and 2,4'-BPS@ $\beta$ -CD complexes at 25 °C in neutral aqueous solution (pH 7, phosphate buffer 50 mM).

| Guest    | Equilibrium                                  | LogK     | $\Delta H^0$<br>(kJ mol <sup>-1</sup> ) | $\Delta S^0$<br>(J deg <sup>-1</sup> mol <sup>-1</sup> ) |
|----------|--|----------|---|--|
| 4,4'-BPS | H + G $\rightleftharpoons$ HG                | 4.23 (4) | -28.72 (1)                              | -15.4 (7)  |
|          | HG + H $\rightleftharpoons$ H <sub>2</sub> G | 2.6 (2)  | -9.44 (2)                               | 18 (5)   |
| 2,4'-BPS | H + G $\rightleftharpoons$ HG                | 3.43 (1) | -32.57 (1)                              | -43.5 (1)  |

ITC titrations for 2,4'-BPS/ $\beta$ -CD and 4,4'-BPS/ $\beta$ -CD systems in neutral aqueous solution (pH 7, phosphate buffer) at 25 °C are shown in Figure 48 and Figure 49, respectively.

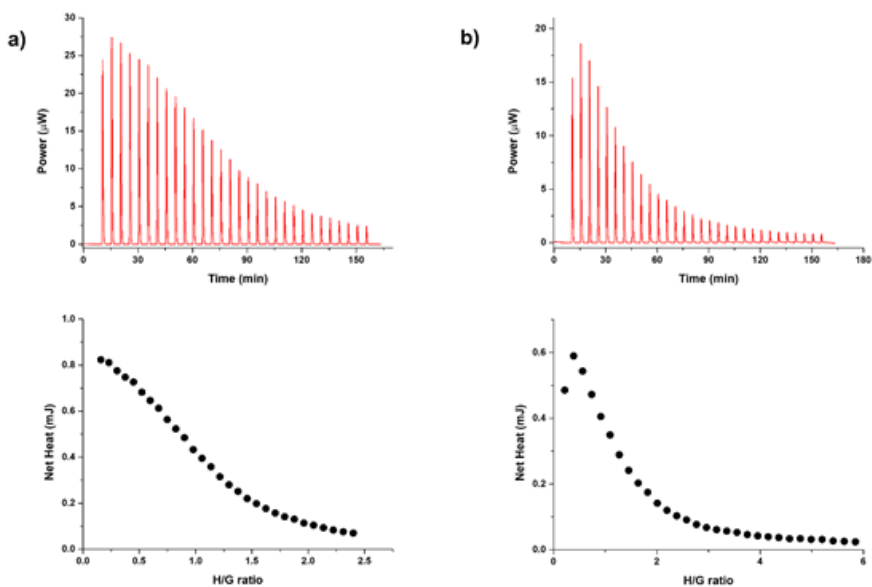


Figure 48. a) ITC titration curve of  $\beta\text{-CD}$  (4 mM) into 4,4'-BPS (0.5 mM) at 25 °C in aqueous solution (pH 7, phosphate buffer) with final H/G ratio of 2.5 (top) and relative integrated heat data (bottom); b) ITC titration curve of  $\beta\text{-CD}$  (5 mM) into 4,4'-BPS (0.2 mM) at 25 °C in aqueous solution (pH 7, phosphate buffer) with final H/G ratio of 6 (top) and relative integrated heat data (bottom).

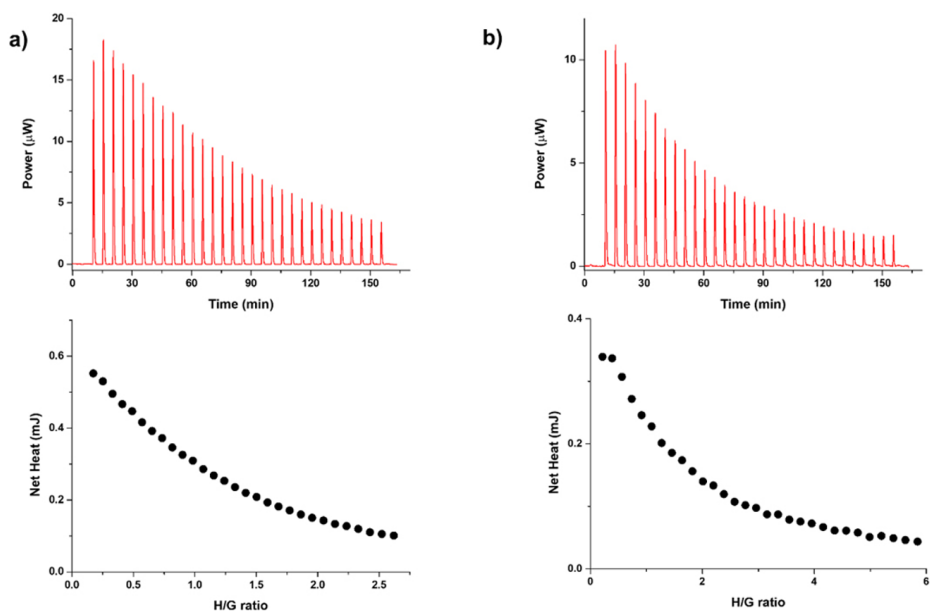


Figure 49. a) ITC titration curve of  $\beta\text{-CD}$  (4 mM) into 2,4'-BPS (0.5 mM) at 25 °C in aqueous solution (pH 7, phosphate buffer) with final H/G ratio of 2.6 (top) and relative integrated heat data (bottom); b) ITC titration curve of  $\beta\text{-CD}$  (5 mM) into 2,4'-BPS (0.2 mM) at 25 °C in aqueous solution (pH 7, phosphate buffer) with final H/G ratio of 6 (top) and relative integrated heat data (bottom).

It was found that both BPSs isomers form inclusion complexes with  $\beta\text{-CD}$  host although shape and size of the guests affect their binding features.

Weak non-covalent interactions drive the *host-guest* complex formation for both BPSs. For both guests, the formation of the 1:1 species results enthalpically favored by weak non-covalent interactions, such as dipole-dipole and hydrogen bonding formation. The unfavorable entropic term is the result of a balance between host and guest desolvation ( $\Delta S^\circ > 0$ ) and the loss of degrees of freedom due to the complex formation ( $\Delta S^\circ < 0$ ) which is the prevalent contribution (Figure 50,  $H + G = HG$ ).

The presence of the -OH group in the *para* position (4,4'-BPS) gives rise to the formation of an additional 1:2 complex species due to the increase of the binding constant value (of about one log unit). The complex 4,4'-BPS@( $\beta\text{-CD}$ )<sub>2</sub> (Figure 50,  $HG+G = H_2G$ ) is both enthalpically and entropically

favoured. The main cause of the enthalpy gain is additional interactions with the second  $\beta$ -CD cavity together with a favourable entropic contribution. Thus, the presence of the -OH groups in the *para* position enhances the binding affinity for enthalpy factors as they are able to establish dipole-dipole or hydrogen bonding interactions. In addition, a favourable enthalpy contribution indicates that specific interactions are occurring between the binding partners and this is an excellent way to ensure the specificity, selectivity and adaptability of the ligand.<sup>107</sup>

It can be supposed that the complex  $4,4'$ -BPS@( $\beta$ -CD)<sub>2</sub> assumes a capsular-like arrangement with two  $\beta$ -CD units capping both ends of the *guest*,<sup>108</sup> conversely.

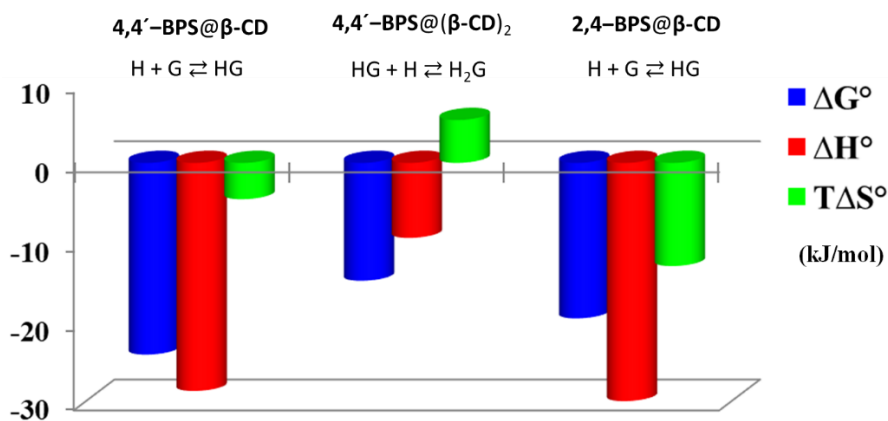


Figure 50. Thermodynamic parameters for the formation of complexes at 25 °C in neutral aqueous solution.

ITC study clearly shows that the  $\beta$ -CD *host* has greater affinity for  $4,4'$ -BPS guest with respect to its  $2,4'$ -isomer. The  $4,4'$ -BPS/ $2,4'$ -BPS selectivity ratio is 6.3 (calculated as the ratio between the  $K$  values for the formation of 1:1 complexes in Table 14).

<sup>107</sup> A.V. Campoy, E. Freire, *Biophys. Chem.*, **2005**, *115*, 115-124.

<sup>108</sup> (a) C. Bonaccorso, G. Brancatelli, G. Forte, G. Arena, S. Geremia, D. Sciotto, C. Sgarlata, *RSC Adv.*, **2014**, *4*, 53575-87; (b) C. Bonaccorso, R. Migliore, M.A. Volkova, G. Arena, C. Sgarlata, *Thermochim. Acta*, **2017**, *656*, 47-52.

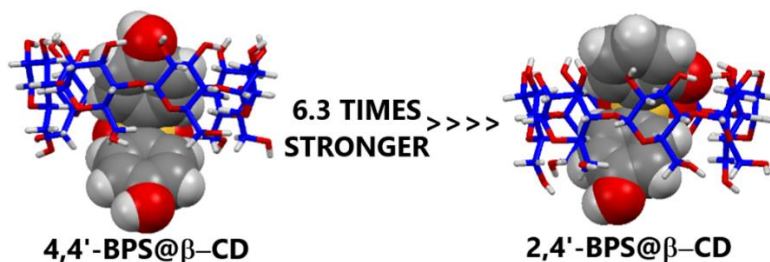


Figure 51. Selectivity ratio of 4,4'-BPS/2,4'-BPS calculated as ratio between the  $K$  values for the formation of 1:1 complexes.

### 4.2.3 Complexation study of 4,4'-BPS and 2,4'-BPS in the gas phase by FT ICR MS investigation

The gas-phase investigation was performed by HR ESI-FT-ICR mass spectrometry. The use of this technique allows us to study the structure of inclusion complexes without the complicating effect of solvent molecules.<sup>109</sup>

In the gas phase the *hydrophobic effect*, which is the main stabilizing effect of  $\beta$ -CD-inclusion complexes in solution, is absent.<sup>110</sup> Consequently the stability of the  $\beta$ -CD-complexes is strongly affected under this condition: in fact, some  $\beta$ -CD-inclusion complexes are not observed in the gas phase even if they are present in solution.<sup>111</sup>

In agreement with the molecular formula of the complex  $[4,4'\text{-BPS@}\beta\text{-CD} + 2\text{Na}]^{2+}$  (calcd for  $\text{C}_{54}\text{H}_{80}\text{Na}_2\text{O}_{39}\text{S}$ , 715.1891) the mass spectrum of a 1:1 mixture of 4,4'-BPS and  $\beta$ -CD in water showed a molecular ion peak at  $m/z$  715.1881 (Figure 52a). The same molecular ion peak was found for the complex  $[2,4'\text{-BPS@}\beta\text{-CD} + 2\text{Na}]^{2+}$  (Figure 52b). This suggests a high stability of these supramolecular complexes in the gas phase.

<sup>109</sup> (a) B. Baytekin, T.H. Baytekin, C.A. Schalley, *Org. Biomol. Chem.*, **2006**, *4*, 2825–2841. (b) C.A. Schalley, *Mass Spectrom. Rev.*, **2001**, *20*, 253–309. (c) D.P. Weimann, M. Kogej, C.A. Schalley, In *Mass Spectrometry and Gas Phase Chemistry of Supramolecules, Analytical Methods in Supramolecular Chemistry*, C.A. Schalley, Eds.; WILEY-VCH: Weinheim, **2012**, Chapter 5, pp 129–196.

<sup>110</sup> (a) J. Szejtli, *Chemistry. Chem. Rev.*, **1998**, *98*, 1743–1753. (b) G.A. Crini, *Chem. Rev.*, **2014**, *114*, 10940–10975.

<sup>111</sup> J.B. Cunniff, P. Vouros, D.M. Desiderio, *Rapid Commun. Mass Spectrom.*, **1994**, *8*, 715–719.

Furthermore, a Collision-Induced Dissociation (CID) experiment of supramolecular *guest@host* complexes in the gas phase was carried out to gain information on activation energies for dissociation processes.<sup>112</sup> In fact, it is known that, in the gas phase, the supramolecular *guest@host* complexes are associated until they are energetically activated by collision with neutral reagent gases.<sup>109,110</sup>

The ESI-CID MS/MS experiments of BPS@ $\beta$ -CD complexes were performed at different acceleration voltages, and thereby at different average collision energies. Using the same low voltage (1V) for both complexes, we found that a lower energy was required to dissociate the supramolecular complexes with 2,4'-BPS with respect to those with 4,4'-BPS (Figure 52).

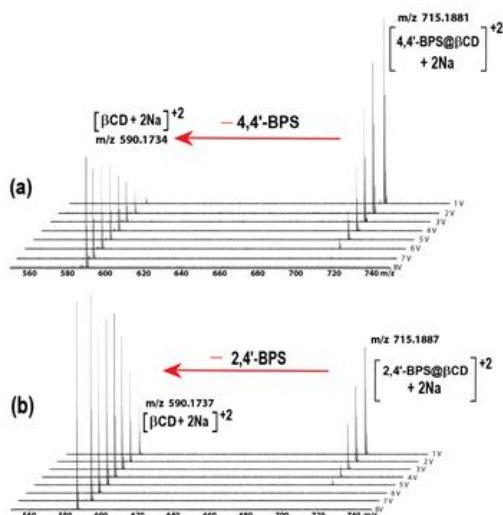


Figure 52. Series of ESI FT ICR CID mass spectra of: (a) 1:1 mixture of  $\beta$ -CD and 4,4'-BPS; and (b) 1:1 mixture of  $\beta$ -CD and 2,4'-BPS. After collisions with argon at acceleration voltages of 1-8 V.

In fact, the intensity ratio of the complex with 2,4'-BPS is 2/1 while the spectrum of 4,4'-BPS@ $\beta$ -CD shows an intensity ratio of 20/1.

<sup>112</sup> C. Talotta, C. Gaeta, Z. Qi, C.A. Schalley, P. Neri, *Angew. Chem. Int. Ed.*, **2013**, 52, 7437–7441.

$$\frac{I_{4,4'-BPS@β-CD}}{I_{β-CD}} = \frac{20}{1} \text{ at } 1 \text{ Volt}$$

$$\frac{I_{2,4'-BPS@β-CD}}{I_{β-CD}} = \frac{2}{1} \text{ at } 1 \text{ Volt}$$

Likewise, across the range 2-6 V the intensity ratio  $I_{(4,4'-BPS@β-CD)}/I_{(β-CD)}$  is more than 10 times larger than the analogous intensity ratio of the isomeric 2,4'-BPS@β-CD complex. That means that 4,4'-BPS has a higher kinetic barrier to escape from the β-CD cavity than the isomeric 2,4'-BPS.<sup>112</sup>

#### 4.2.4 DSC and TGA analysis of the inclusion complexes 4,4'-BPS@β-CD and 2,4'-BPS@β-CD.

DSC analysis was used to highlight the formation of β-CD inclusion complexes. In fact, when a guest molecule is included inside the β-CD cavity, the melting, boiling, and sublimation points are shifted to different temperatures or simply disappear.<sup>113</sup>

The DSC curve of β-CD showed a broad endothermic peak ( $T_{max} = 106 \text{ } ^\circ\text{C}$ ), attributable to the release of co-crystallized water molecules (Figure 53a) while the thermogram of the BPSs highlighted a sharp endothermic peak ( $T_{max} = 248.3 \text{ } ^\circ\text{C}$  for 4,4'-BPS and ,  $T_{max} = 183.7 \text{ } ^\circ\text{C}$  for 2,4'-BPS) associated to their melting event (Figure 53e).

The formation of the BPSs@β-CD inclusion complex in the mixture 1:1 was highlighted by the disappearance of the endothermic peaks attributable to the free BPSs and β-CD starting materials (Figure 53c and d). Additionally, the DSC curve of the 1:2 mixtures showed a wide peak between 60 and 120 °C (Figure 53b and f) attributable to the water releasing from free β-CD. Furthermore, in the 1:2 BPSs/β-CD mixtures, the peaks of free BPSs were detected, an evidence that not all the BPSs were included inside the β-CD-cavity (Figure 53d and h).

---

<sup>113</sup> H. Liu, X. Cai, Y. Wang, J. Chen, *Water Research*, **2011**, *45*, 3499–3511.

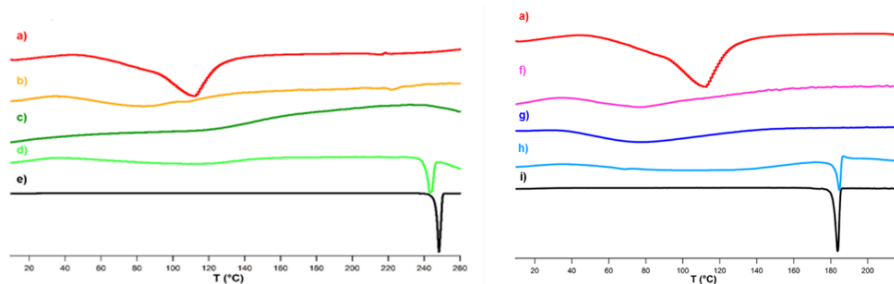


Figure 53. DSC curves. (Left) (a)  $\beta$ -CD; (b-d) 1:2, 1:1, and 2:1 mixtures of 4,4'-BPS and  $\beta$ -CD (e) 4,4'-BPS. (Right) (a)  $\beta$ -CD; (f-h) 1:2, 1:1, and 2:1 mixtures of 2,4-BPS and  $\beta$ -CD. (i) 2,4-BPS.

Thermogravimetric analysis (TGA) was carried out for BPSs@ $\beta$ -CD inclusion complexes. According to literature,<sup>114</sup> free  $\beta$ -CD showed weight loss of 11% w/w up to 105 °C attributable to the evaporation of both surface water and internal water associated with the macrocycle while the thermic degradation starts at 304.3 °C (Figure 54 red). For 4,4'-BPS was possible to observe a main degradation process where the mass of the molecule is reduced of about 85% at 363.4 °C (Figure 54 black).

Thermogravimetric curve of 1:1 mixture 4,4'-BPS/ $\beta$ -CD showed distinct features with respect to the free components. In detail, it showed a first event attributable to the loss of water at  $T < 105$  °C which is strongly reduced, in accordance with DSC results, while the degradation takes place at ca. 317 °C, earlier than the BPS alone. In addition, there is no evidence of free 4,4'-BPS in the 1:1 mixture, confirming that the guest is completely included into the cyclodextrin cavity (Figure 54 green).

The mixture 2,4'-BPS/ $\beta$ -CD showed a similar behaviour with a main event at 326 °C (Figure 55 blue). In this case, the degradation takes place later respect the 2,4'-BPS raw material.

<sup>114</sup> R.L. Abarca, F. J. Rodríguez, A. Guarda, M.J. Galotto, J.E. Bruna, *Food Chem.*, **2016**, *196*, 968-975.

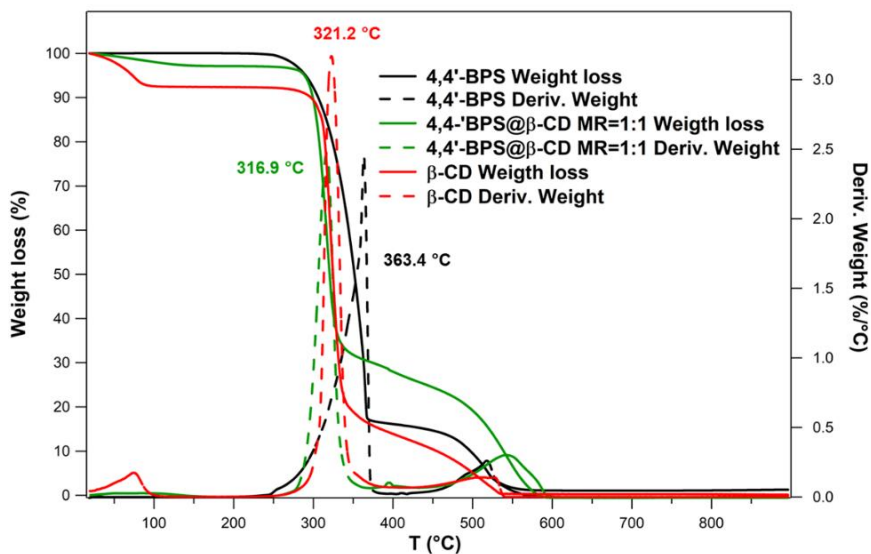


Figure 54. TGA heating curves of (red) β-CD; (green) 1:1 mixture of 4,4'-BPS and β-CD and (black) 4,4'-BPS.

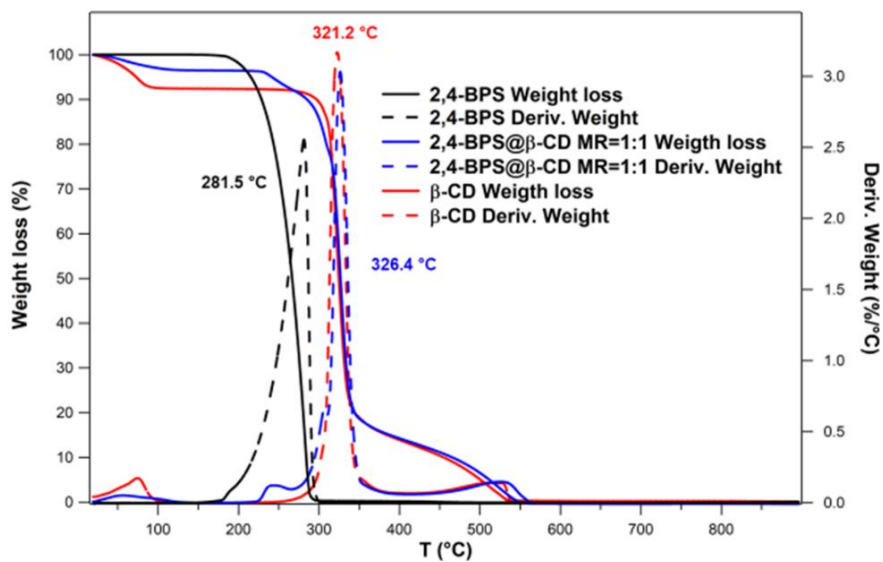


Figure 55. TGA heating curves of (red) β-CD; (blue) 1:1 mixture of 2,4'-BPS and β-CD and (black) 2,4'-BPS.

#### 4.2.5 FT IR spectra of BPSs@ $\beta$ -CD complexes

Infrared spectroscopy is a useful tool to study the interaction between cyclodextrin and guest molecules in the solid state. In fact, the formation of guest@ $\beta$ -CD inclusion complexes can be highlighted by the changes in the peak shape, position, and intensity.

FT IR spectrum of the  $\beta$ -CD show the band at  $3372\text{ cm}^{-1}$  attributable to the symmetrical and asymmetrical stretching of the OH groups, and another band at  $2921\text{ cm}^{-1}$  was associated with the C–H stretching. The absorption bands at  $1158\text{ cm}^{-1}$  and  $1030\text{ cm}^{-1}$  are attributable to the asymmetric and symmetrical stretching of the C–O–C unit, respectively. Regarding the 4,4'-BPS, the SO<sub>2</sub> group shows two peculiar bands at  $1291\text{ cm}^{-1}$  and  $1139\text{ cm}^{-1}$  attributable to asymmetrical and symmetrical stretching, respectively. The FT IR spectrum of the 1:1 complex  $\beta$ -CD/4,4'-BPS, shows a weak shift of the SO<sub>2</sub> stretching band from  $1291$  to  $1298\text{ cm}^{-1}$ , probably due to the inclusion of BPS inside the cavity of  $\beta$ -CD, unfortunately the second SO<sub>2</sub> group band shift ( $1139\text{ cm}^{-1}$ ) is covered by the  $1158\text{ cm}^{-1}$   $\beta$ -CD band. Analogous shifts were observed for S=O stretching band of 2,4'-BPS upon inclusion inside the  $\beta$ -CD cavity.

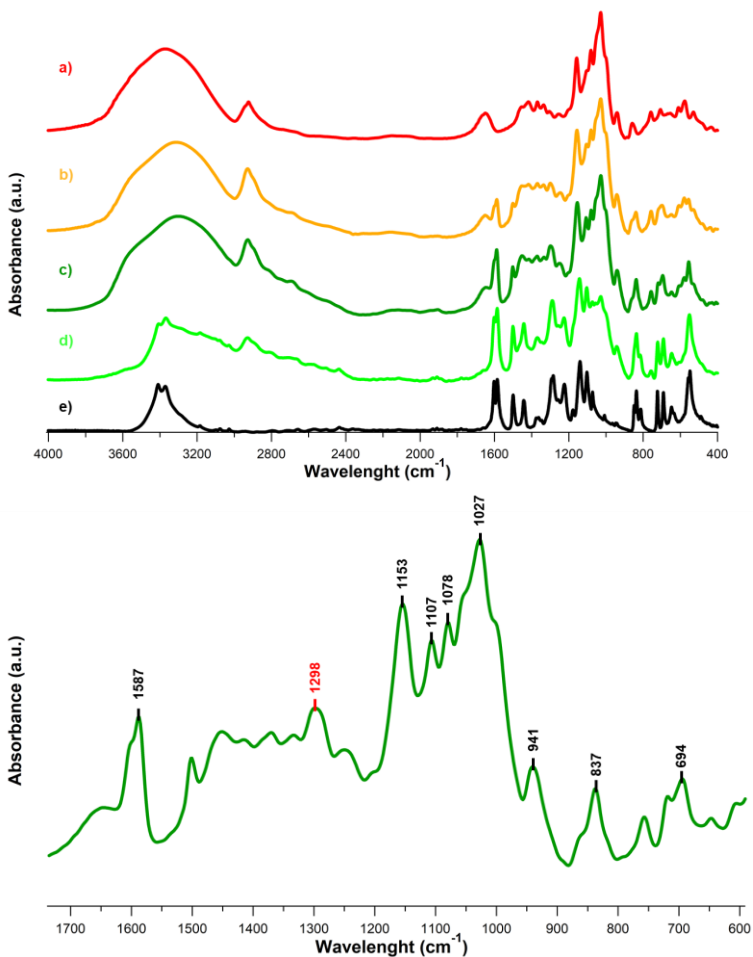


Figure 56. (top) FT-IR spectra of: (a)  $\beta$ -CD; (b) 1:2 mixture of 4,4'-BPS and  $\beta$ -CD; (c) 1:1 mixture of 4,4'-BPS and  $\beta$ -CD; (d) 2:1 mixture of 4,4'-BPS and  $\beta$ -CD; (e) 4,4'-BPS. (bottom) detail of FT IR spectrum in (c) 1:1 mixture of 4,4'-BPS and  $\beta$ -CD.

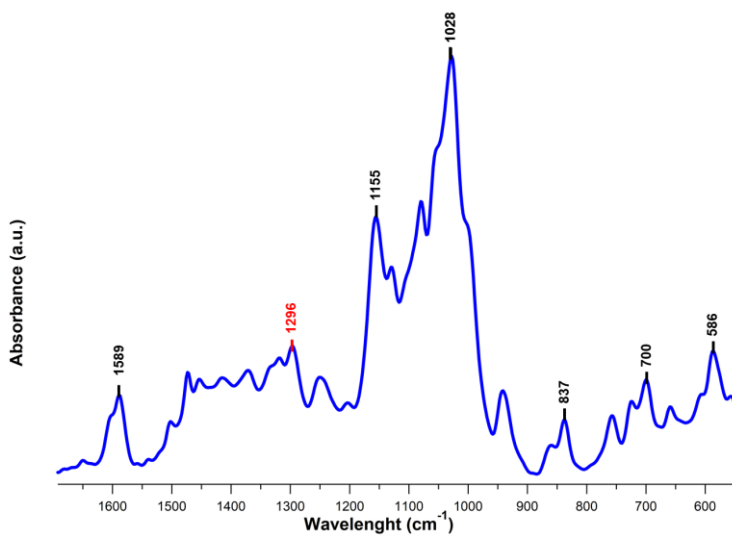
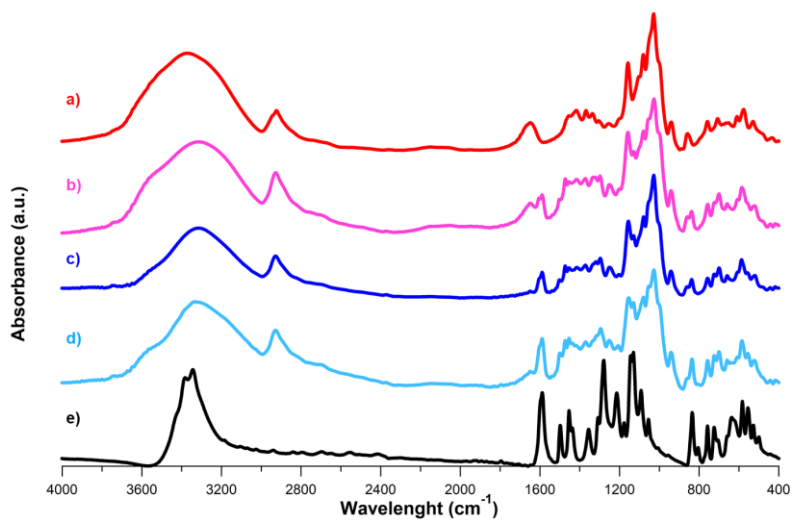


Figure 57. (top) FT-IR spectra of: (a)  $\beta$ -CD; (b) 1:2 mixture of 2,4'-BPS and  $\beta$ -CD; (c) 1:1 mixture of 2,4'-BPS and  $\beta$ -CD; (d) 2:1 mixture of 2,4'-BPS and  $\beta$ -CD; (e) 2,4'-BPS. (bottom) detail of FT IR spectrum in (c) 1:1 mixture of 2,4'-BPS and  $\beta$ -CD.

#### 4.2.6 Complexation study of 4,4'-BPS and 2,4'-BPS in the solid state

The X-ray study was performed in collaboration with Prof. S. Geremia and N. Hickey of the center of excellence in Biocristallography of the University of Trieste. The X-ray gave us additional information about the structure of the inclusion complexes in solid state: the 4,4'-BPS@ $\beta$ -CD complex crystallizes in the orthorhombic system, while 2,4'-BPS@ $\beta$ -CD crystallizes in the triclinic system (Figure 58).

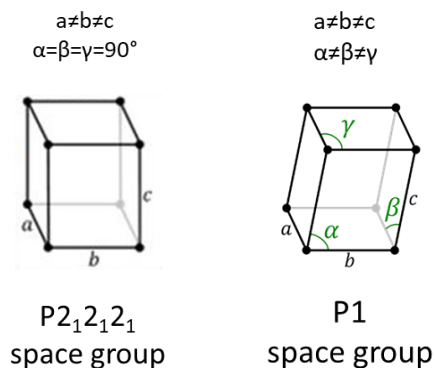


Figure 58. Orthorhombic crystalline system (left) and triclinic crystalline system (right).

The asymmetric unit of 4,4'-BPS@ $\beta$ -CD consists of a common head-to-head dimer formed by two  $\beta$ -CD macrocycles, which hosts two 4,4'-BPS guests. The glucose-CD units show the typical chair conformation with a pseudo- $C_7$ -symmetry. The two  $\beta$ -CD units are sealed by seven strong H-bonding interactions involving exclusively the secondary O3 hydroxyl groups of the two  $\beta$ -CD units (Figure 59).

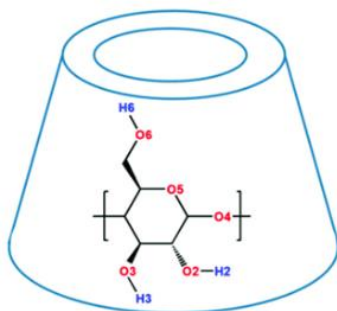


Figure 59.  $\beta$ -Cyclodextrin oxygen assignation.

The two-independent 4,4'-BPS units are included into the macrocycles in similar ways with one phenolic group exposed outside the  $\beta$ -CDs (Figure 60). In fact, the central sulfur atoms are 2.526 and 2.619 Å out of the respective planes defined by the O4 glycosidic atoms.

Interestingly, no direct strong H-bonds are observed between *host* and *guest*, including the sulphone group. Indeed, at the interface of the dimer, we found five water molecules which form a hydrogen-bonded network between the  $\beta$ -CD dimeric assembly (with the O2 and O3 atoms) which also involves two phenolic groups of the 4,4'-BPS *guests*. This encapsulated network of water molecules contributed to stabilize the dimeric structure in the solid state (Figure 60).

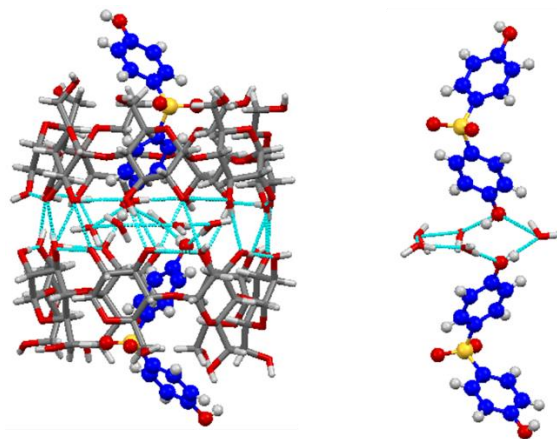


Figure 60. Side views of the solid state of  $(4,4'\text{-BPS@}\beta\text{-CD})_2$  dimeric complex.

The 2,4'-BPS@ $\beta$ -CD complex also forms a head-to-head dimeric structure in the solid state in which two  $\beta$ -CD macrocycles are sealed by four H-bonding interactions and a hydrogen-bonded bridge between one water molecule and the two  $\beta$ -CDs (Figure 61). But, in contrast to that observed in the case of the 4,4'-BPS complex, no water molecules were detected in the dimer interface. Moreover, respect the 4,4'-BPS, the central sulfur atoms of the 2,4'-BPS units are more deeply inserted. This allows the formation of a  $\pi\cdots\pi$  interaction between the 2-phenol rings of the 2,4'-BPS *guests*. Again, no direct strong H-bonds are observed between *host* and *guest*.

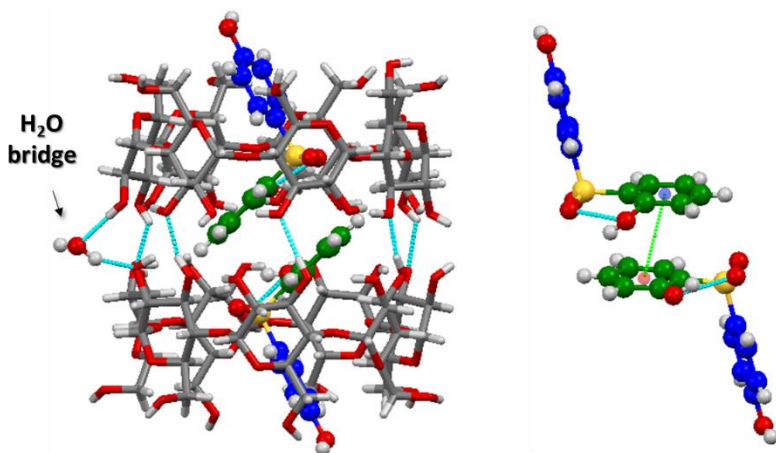


Figure 61. Side view of the solid state of  $(2,4'\text{-BPS@}\beta\text{-CD})_2$  dimeric complex.

All the details about crystallographic data for the complex  $4,4'\text{-BPS@}\beta\text{-CD}$  and  $2,4'\text{-BPS@}\beta\text{-CD}$  are reported in the experimental section (Table 15).

### 4.3 Conclusions

In conclusion, the characterization of the inclusion complexes between  $\beta\text{-CD}$  host and the two isomeric 4,4'-dihydroxydiphenyl sulfone and 2,4'-dihydroxydiphenyl sulfone (BPSs) was carried out in liquid solution, gas phase, and solid state. In solution, the formation of the inclusion complexes  $4,4'\text{-BPS@}\beta\text{-CD}$  and  $2,4'\text{-BPS@}\beta\text{-CD}$  was demonstrated by 1D and 2D NMR (NOESY and DOSY) experiments. The ITC investigation evidenced that the  $\beta\text{-CD}$  host shows a greater affinity for 4,4'-BPS with respect to its 2,4'-isomer, with a 4,4'-BPS/2,4'-BPS selectivity ratio of 6.3. In gas phase, collision-induced dissociation experiments (FT ICR ESI MS studies) indicate that 4,4'-BPS has a higher kinetic barrier to escape from the  $\beta\text{-CD}$  cavity than the isomeric 2,4'-BPS. In the solid state, the  $2,4'\text{-BPS@}\beta\text{-CD}$  complex forms a tubular dimeric assembly in the solid state in which two 2,4'-BPS guests are included in the cavity. Analogously the  $4,4'\text{-BPS@}\beta\text{-CD}$  complex forms a head-to-head dimer constituted by two  $\beta\text{-CD}$  macrocycles, which hosts two 4,4'-BPS guests. The dimer of  $\beta\text{-CD}$  is sealed by seven strong H-bonding interactions involving exclusively the secondary O3 hydroxyl groups. The inclusion of the 4,4'-BPS guest inside the  $\beta\text{-CD}$  cavity results in the

entrapment of several water molecule in the dimeric interface. DSC curves evidenced significant changes in material properties of 4,4'-BPS@ $\beta$ -CD and 2,4'-BPS@ $\beta$ -CD complexes in comparison to the starting raw materials. The formation of inclusion complexes between 4,4'-BPS or 2,4'-BPS and  $\beta$ -CD was also confirmed by FT IR, DSC, and TGA analysis (experimental section 4.4).

#### 4.4 Experimental section

The two isomers 4,4'-dihydroxydiphenyl and 2,4-dihydroxydiphenyl sulfones were purchased from TCI (GC grade > 98%) and were used without further purification. The  $\beta$ -cyclodextrin ( $\beta$ -CD) was obtained from Roquette (Kleptose® GC grade  $\geq$  93%) and used after being dried by freeze-drying. Reaction temperatures were measured externally.

The synthesis of BPSs@ $\beta$ -CD pseudorotaxane complexes was conducted in a flask under atmospheric pressure.  $\beta$ -CD (9.0 mg,  $8.0 \times 10^{-3}$  mmol) was solubilized in 10 mL of deionized water. Then, an appropriate amount of the BPS guest was added (1.8 mg,  $8.0 \times 10^{-3}$  mmol), and the resulting mixture was stirred at 25 °C for 30 min. Finally, the water was evaporated under vacuum, and the product was further dried and stored at room temperature.

**NMR spectra** were recorded on a 600 MHz spectrometer [600 ( $^1\text{H}$ ) and 150 MHz ( $^{13}\text{C}$ )], 400 [400 ( $^1\text{H}$ ) and 100 MHz ( $^{13}\text{C}$ )] and 300 [300 ( $^1\text{H}$ ) and 75 MHz ( $^{13}\text{C}$ )]. Chemical shifts are reported relative to the residual solvent peak. DOSY experiments were performed on a Bruker 400 spectrometer equipped with 5mm PABBO BB| 19F-1H\D Z-GRD Z114607/0109. The standard Bruker pulse program, ledbpgp2s, employing a double stimulated echo sequence and LED, bipolar gradient pulses for diffusion, and two spoil gradients was utilized. Individual rows of the quasi-2D diffusion databases were phased, and the baseline was corrected.

**$^1\text{H}$  NMR** (400 MHz, 298 K,  $\text{D}_2\text{O}$ ) of the equimolar mixture of  $\beta$ -CD and 4,4'-BPS (3.0 mM);  $\delta$  7.71 ( $\text{H}_2^{\text{G}}$ , d,  $J = 8.8$  Hz, 4H), 6.97 (d,  $\text{H}_1^{\text{G}}$ ,  $J = 8.8$  Hz, 4H), 5.00 ( $\text{H}_1$ , d,  $J = 3.6$  Hz, 7H), 3.83 (dd,  $\text{H}_3$ ,  $J_1 = J_2 = 9.5$  Hz, 7H), 3.74 (d,  $\text{H}_6$ ,  $J = 2.0$  Hz, 14 H), 3.60 (dd,  $\text{H}_2$ ,  $J_1 = 9.9$  Hz,  $J_2 = 3.6$  Hz, 7H), 3.53 (dd,  $\text{H}_4$ ,  $J_1 = J_2 =$

9.0 Hz, 7H), 3.47-3.44 (broad, H5, 7H). **<sup>13</sup>C NMR** (75 MHz, 298 K, D<sub>2</sub>O): 162.0, 132.1, 129.4, 116.6, 102.3, 81.3, 73.6, 72.4, 72.2, 60.2. **HRMS (ESI)**: m/z [4,4'-BPS@β-CD + 2Na]<sup>2+</sup> calculated for C<sub>54</sub>H<sub>80</sub>Na<sub>2</sub>O<sub>39</sub>S, 715.1891; found: 715.1881. **<sup>1</sup>H NMR** (600 MHz, 298 K, D<sub>2</sub>O) of the equimolar mixture of β-CD and 2,4-BPS (3.0 mM); δ 7.89 (H1<sup>G</sup>, dd, J<sub>1</sub> = 8.4 Hz, J<sub>2</sub> = 1.8 Hz, 1H), 7.81 (d, H5<sup>G</sup>, J = 8.8 Hz, 2H), 7.62 (ddd, H3<sup>G</sup>, J<sub>1</sub> = J<sub>2</sub> = 8.0 Hz, J<sub>3</sub> = 1.7 Hz, 1H), 7.17 (dd, H2<sup>G</sup>, J<sub>1</sub> = J<sub>2</sub> = 7.8 Hz, 1H), 7.06 (d, H4<sup>G</sup>, J = 8.4 Hz, 1H), 6.92 (d, H6<sup>G</sup>, J = 8.8 Hz, 2H), 5.04 (H1, d, J = 3.7 Hz, 7H), 3.89 (dd, H3, J<sub>1</sub> = J<sub>2</sub> = 9.3 Hz, 7H), 3.81 (d, H6, J = 2.7, 14 H), 3.65-3.62 (overlapped, H2+H4, 14H), 3.57 (broad, H5, 7H). **<sup>13</sup>C NMR** (75 MHz, 298 K, D<sub>2</sub>O): 162.7, 155.9, 137.5, 132.4, 130.6, 129.7, 126.6, 121.8, 119.4, 116.7, 102.9, 82.2, 74.2, 73.2, 72.9, 61.2. **HRMS (ESI)**: m/z [2,4-BPS@β-CD + 2Na]<sup>2+</sup> calculated for C<sub>54</sub>H<sub>80</sub>Na<sub>2</sub>O<sub>39</sub>S, 715.1891; found: 715.1887.

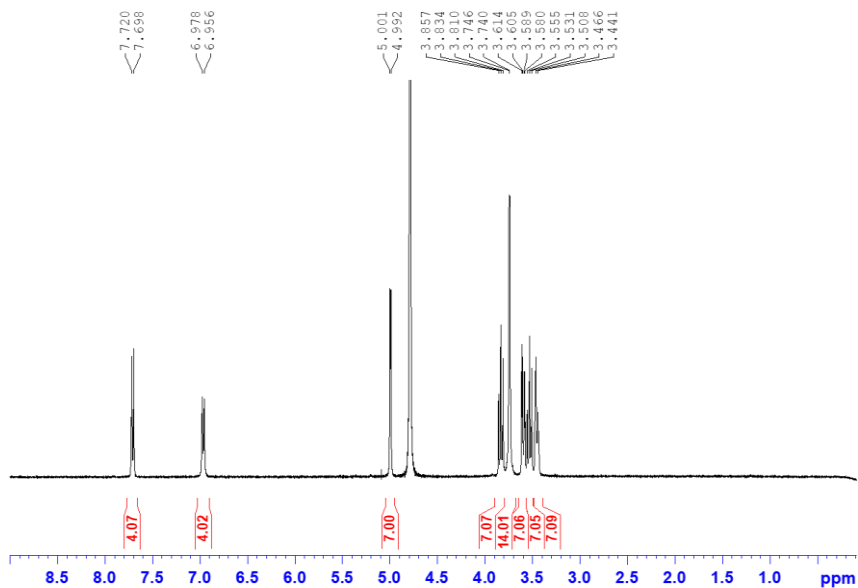


Figure 62.  $^1\text{H}$  NMR spectrum of 1:1 mixture of  $\beta$ -CD and 4,4'-BPS ( $\text{D}_2\text{O}$ , 400 MHz, 298 K).

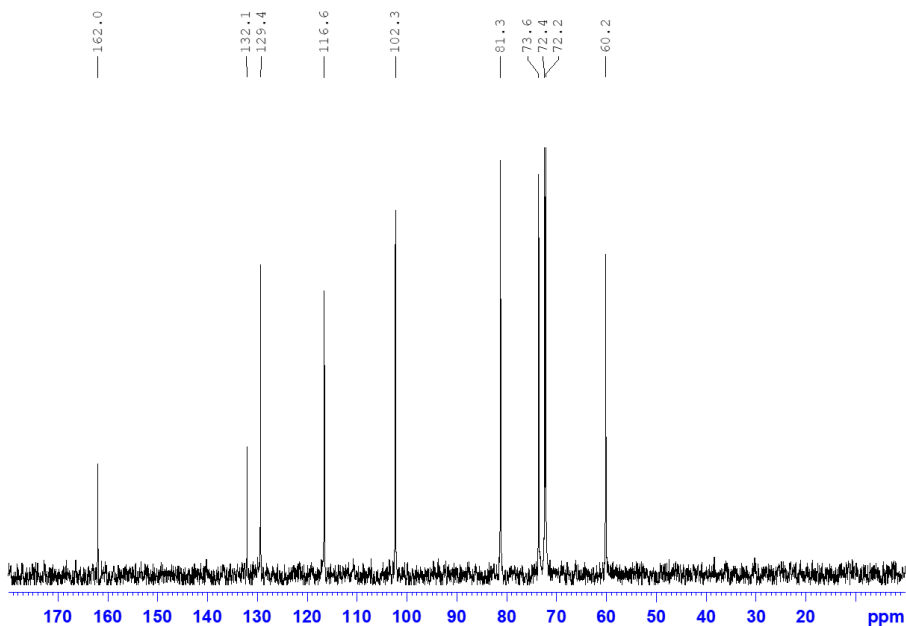


Figure 63.  $^{13}\text{C}$  NMR spectrum of 1:1 mixture of  $\beta$ -CD and 4,4'-BPS ( $\text{D}_2\text{O}$ , 75 MHz, 298 K).

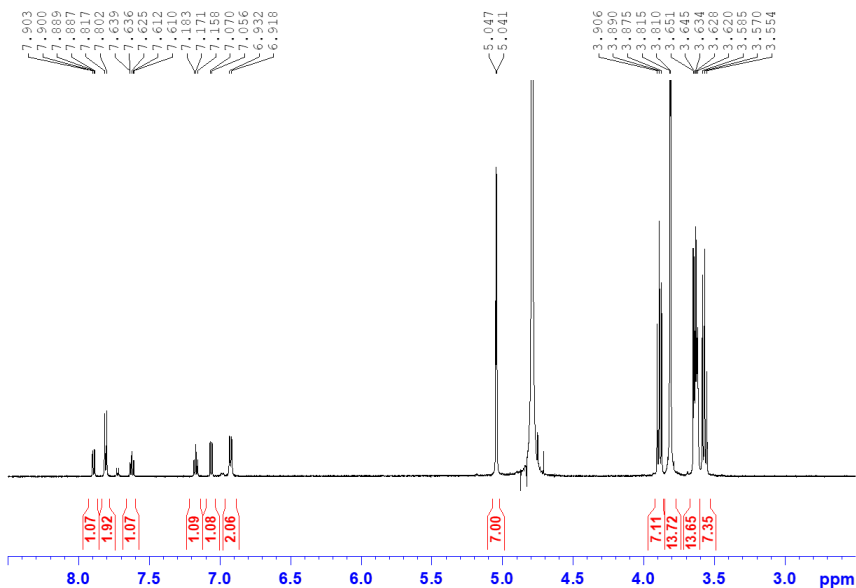


Figure 64.  $^1\text{H}$  NMR spectrum of 1:1 mixture of  $\beta$ -CD and 2,4'-BPS ( $\text{D}_2\text{O}$ , 600 MHz, 298 K).

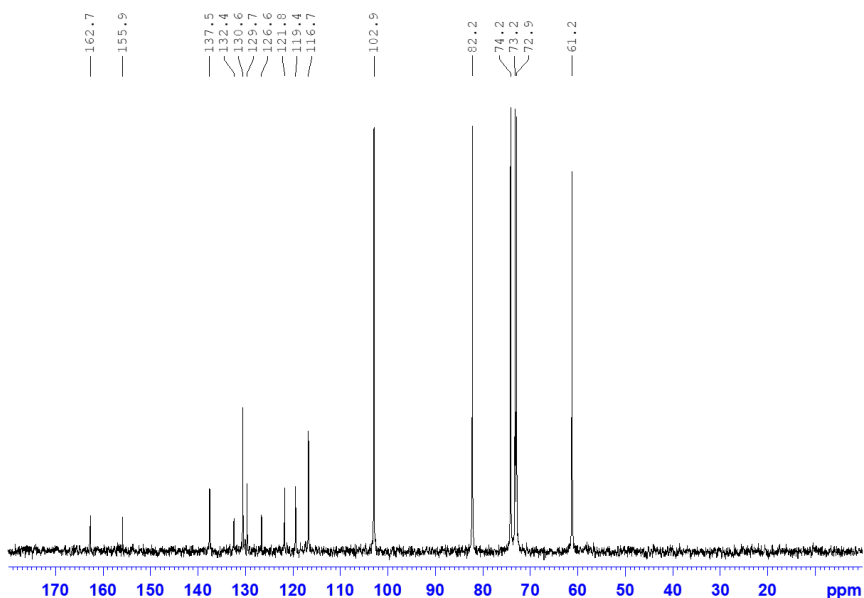


Figure 65.  $^{13}\text{C}$  NMR spectrum of 1:1 mixture of  $\beta$ -CD and 2,4'-BPS ( $\text{D}_2\text{O}$ , 75 MHz, 298 K).

**Calorimetric titrations (ITC)** were carried out at 25 °C with a nano-isothermal titration calorimeter Nano-ITC (TA Instruments, USA) having an active cell volume of 0.988 mL and a 250  $\mu$ L injection syringe. The reaction mixture in the sample cell was continuously stirred at 250 rpm during the titration. Measurements were run in the overfilled mode, which does not require any correction for liquid evaporation and for the presence of the vapour phase.<sup>115</sup> The power curve was integrated by NanoAnalyze software (TA Instruments, USA) to obtain the gross heat evolved/absorbed in the reaction. The instrument was calibrated chemically using a test HCl/TRIS reaction following the procedure previously described<sup>116</sup> and was also checked by running an electrical calibration.

Calorimetric experiments were carried out by titrating a 4,4'-dihydroxydiphenyl sulphone (4,4'-BPS) or a 2,4'-dihydroxydiphenyl sulphone (2,4'BPS) solution (0.2-0.5 mM) with an aqueous solution of  $\beta$ -CD (4-5 mM).

Both  $\beta$ -CD and guests were dissolved in 50 mM phosphate buffer (pH 7). The buffer was chosen to minimize any contribution resulting from the interaction of the reactants with the proton. Before each experiment, all solutions were degassed and stirred under vacuum for about 15 minutes. Typically, 4–5 independent titrations were run for each  $\beta$ -CD – guest system to explore both smaller (about 2.5) and larger (up to 6) host/guest ratios and thus collect a suitable number of points to investigate the possible formation of multiple species; the two sets of curves were refined together to obtain the final parameters. The heats of dilution were determined in separate blank experiments by titrating a solution containing phosphate buffer only with solutions of  $\beta$ -CD (prepared in phosphate buffer).

The net heats of reaction, obtained by subtracting the heat evolved/absorbed in the blank experiments, were treated by HypCal,<sup>30</sup> a software that allows for the determination of equilibrium constants and formation enthalpies of complex species in solution by a non-linear least-

---

<sup>115</sup> L.D. Hansen, G.W. Fellingham, D.J. Russell, *Anal. Biochem.*, **2011**, 409, 220-229.

<sup>116</sup> C. Sgarlata, V. Zito, G. Arena, *Anal. Bioanal. Chem.* **2013**, 405, 1085-1094.

squares analysis of calorimetric data. Thermodynamic parameters were determined by handling simultaneously data obtained from different titrations.

**HR ESI mass spectra** were recorded on a FT-ICR mass spectrometer equipped with a 7 T magnet. The samples were ionized in positive ion mode using ESI positive mode. The mass spectra were calibrated externally, and a linear calibration was applied. All chemicals of reagent grade were used as purchased without further purification.

**FT IR spectra** in the medium infrared region (MIR) were obtained with a 4100 Type A spectrometer (JASCO Europe) equipped with a triglycine sulfate (TGS) detector at a resolution of  $4\text{ cm}^{-1}$ . MIR measurements were derived by averaging 1000 scans obtained on samples dispersed in anhydrous KBr tablets. Baseline correction was performed with the Jasco FT-IR spectrometer software.

**Thermogravimetric analysis** was carried out with a TGA Q500 thermobalance (TA Instruments). A working air flux of  $100\text{ cm}^3/\text{min}$  was used. The TG profile was recorded in the  $25 < T\text{ (}^\circ\text{C)} < 900$  temperature range, using open platinum pans loaded with ca. 7 mg of each sample. The heating rate was of  $10\text{ }^\circ\text{C}/\text{min}$ . The balance resolution is  $1\text{ }\mu\text{g}$ .

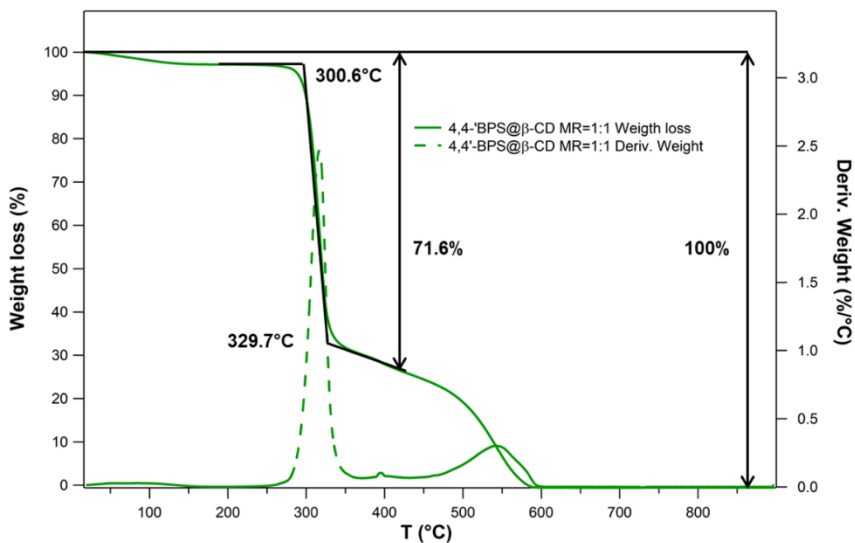


Figure 66. TGA heating curves of 1:1 mixture of 4,4'-BPS and  $\beta$ -CD, detail of onset temperatures and weight loss.

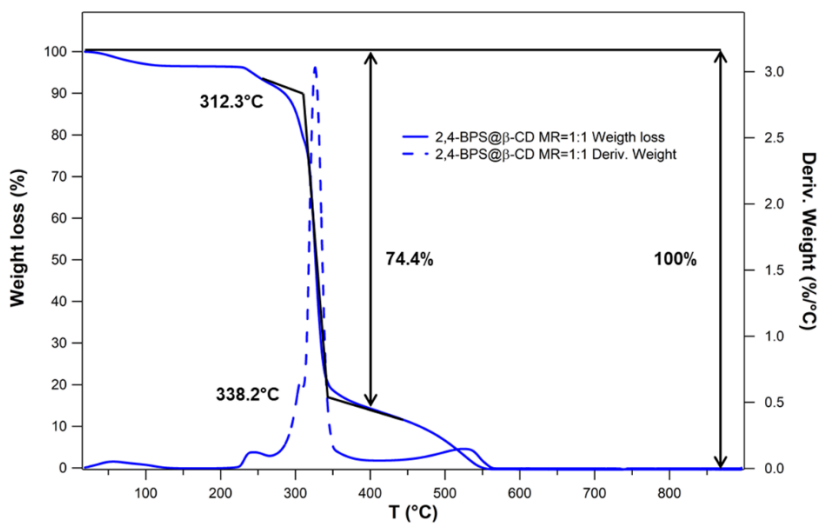


Figure 67. TGA heating curves of 1:1 mixture of 2,4'-BPS and  $\beta$ -CD, detail of onset temperatures and weight loss.

**Differential Scanning Calorimetry (DSC)** measurements were carried out with a DSC 25P Scanning Calorimeter (TA Instrument). Heating rate of 10°C/min, in the temperature range (5 - 260) °C, using approx. 5 mg of sample hermetically sealed in an aluminium pan.

**Determination of the crystallographic structures** of 4,4'-BPS@ $\beta$ -CD and 2,4'-BPS@  $\beta$  -CD. Single crystals of 4,4'-BPS@ $\beta$ -CD and 2,4-BPS@  $\beta$  -CD suitable for X-ray diffraction structure analysis were obtained by evaporation of aqueous solutions containing 1:1 molar mixture of  $\beta$  -CD and the 4,4'-BPS or 2,4'-BPS guest molecules. Data collection was carried out at the Macromolecular crystallography XRD1 beamline of the Elettra synchrotron (Trieste, Italy), employing the rotating-crystal method with a Dectris Pilatus 2M area detector. Single crystals were dipped in paratone cryoprotectant, mounted on a nylon loop and flash-frozen under a nitrogen stream at a 100 K. Diffraction data were indexed and integrated using the XDS package,<sup>117</sup> while scaling was carried out with XSCALE.<sup>118</sup> Structures were solved using the SHELXT program<sup>119</sup> and structure refinement was performed with SHELXL-18/3,<sup>120</sup> operating through the WinGX GUI,<sup>121</sup> by full-matrix least-squares (FMLS) methods on F2. Non-hydrogen atoms were refined anisotropically, with the exception of some disordered groups with low occupancy factors. Hydrogen atoms were added at the calculated positions and refined using the riding model.

---

<sup>117</sup> W. Kabsch, *Acta Crystallogr., Sect. D: Biol. Crystallogr.* **2010**, *66*, 125–132.

<sup>118</sup> W. Kabsch, *Acta Crystallogr D Biol. Crystallogr.* **2010**, *66*, 133-134.

<sup>119</sup> G.M. Sheldrick, *Acta Cryst. Section A*, **2015**, *71*, 3-8.

<sup>120</sup> G.M. Sheldrick, *Acta Cryst. Section A*, **2008**, *64*, 112-122.

<sup>121</sup> L. Farrugia, *J. Appl. Cryst.* **2012**, *45*, 849-854.

Table 15. Crystal data and structure refinement for compounds 4,4'-BPS@ $\beta$ -CD (CCDC code = 2085678) and 2,4-BPS@ $\beta$ -CD (CCDC code = 2085677).

|   | <b>4,4'-BPS@<math>\beta</math>-CD</b>   | <b>2,4-BPS@<math>\beta</math>-CD</b>  |
|---|---|---|
| Empirical formula                           | 2[C <sub>42</sub> H <sub>70</sub> O <sub>35</sub> , C <sub>12</sub> H <sub>10</sub> O <sub>4</sub> S]<br>27.7H <sub>2</sub> O | 2[C <sub>42</sub> H <sub>70</sub> O <sub>35</sub> , C <sub>12</sub> H <sub>10</sub> O <sub>4</sub> S] 21.4H <sub>2</sub> O                    |
| Formula weight                              | 3269.52   | 3156.02   |
| Temperature (K)                             | 100(2)  | 100(2)  |
| Wavelength (Å)                              | 0.7   | 0.7   |
| Crystal system                              | Orthorhombic  | Triclinic   |
| Space group                                 | P 2 <sub>1</sub> 2 <sub>1</sub> 2 <sub>1</sub>  | P 1   |
| Unit cell dimensions (Å, °)                 | <i>a</i> = 16.849(3)<br><i>b</i> = 29.247(4)<br><i>c</i> = 29.901(2)<br>$\alpha$ = 90<br>$\beta$ = 90<br>$\gamma$ = 90        | <i>a</i> = 15.317(1)<br><i>b</i> = 15.421(1)<br><i>c</i> = 17.681(1)<br>$\alpha$ = 99.011(4)<br>$\beta$ = 112.497(4)<br>$\gamma$ = 103.737(7) |
| Volume (Å <sup>3</sup> )                    | 14735(4)  | 3602.8(4)   |
| $\rho_{\text{calcd}}$ (g/cm <sup>3</sup> )  | 1.474   | 1.455   |
| $\mu$ (mm <sup>-1</sup> )                   | 0.15  | 0.15  |
| Z / F(000)                                  | 4 / 6964  | 1 / 1678  |
| Reflections collected                       | 138895  | 98518   |
| Independent reflections                     | 43260[R <sub>int</sub> = 0.0157]  | 39396[R <sub>int</sub> = 0.0123]  |
| Data/restr./param.                          | 43260/0/2238  | 39396/19/2121   |
| Goof  | 1.022   | 1.054   |
| Final <i>R</i> indices [I > 2 $\sigma$ (I)] | <i>R</i> <sub>1</sub> = 0.0519, <i>wR</i> <sub>2</sub> = 0.1426   | <i>R</i> <sub>1</sub> = 0.0552, <i>wR</i> <sub>2</sub> = 0.1537   |
| <i>R</i> indices (all data)                 | <i>R</i> <sub>1</sub> = 0.0527, <i>wR</i> <sub>2</sub> = 0.1437   | <i>R</i> <sub>1</sub> = 0.0554, <i>wR</i> <sub>2</sub> = 0.154  |

## 5. Bio-based re-tanning agent by sodium alginate

### 5.1 General Overview

#### 5.1.1 Sodium alginate as a green alternative

Alginate is an abundant carbohydrate found in the outer wall cell of brown macroalgae with a multitude of applications in drug delivery, textile printing and food industry.<sup>122</sup> Calcium, sodium, ammonium, and potassium salts of alginates have been affirmed as GRAS (Generally Recognized as Safe) by U.S. Food and Drug Administration.

Alginates are natural, anionic linear polysaccharides made up of different proportions of (1,4)-linked  $\beta$ -D-mannuronate (M) and (1,4)-linked  $\alpha$ -L-guluronate (G) residues (Figure 68).<sup>123</sup> In alginate, M and G are homogeneously or heterogeneously linked through 1 $\rightarrow$ 4 glycosidic bonds, thus forming linear dimers within the larger polymer: homodimers GG and MM occur as do heterodimers MG/GM.<sup>124</sup> The amount and distribution of each monomer depends on the species, location, and age of seaweed from which the alginate is isolated.<sup>125</sup>

Alginates rich in GG blocks have higher water solubility than those rich in MM blocks.<sup>126</sup> At low pH, alginates with more MG/GM blocks are soluble, whereas MM or GG block-rich alginates are insoluble.<sup>127</sup>

---

<sup>122</sup> M. Nasrollahzadeh, N. Shafiei, Z. Nezafat, N.S.S. Bidgol, *Carbohydr. Polym.*, **2020**, *241*, 116353.

<sup>123</sup> V. Ravichandran, A. Jayakrishnan, *Int. J. Biol. Macromol.*, **2018**, *108*, 1101–1109.

<sup>124</sup> J. Liu, S. yang, X. Li, Q. Yan, M.J.T. Reaney, Z. Jiang, *Compr. Rev. Food Sci. Food Saf.* **2019**, *18*, 1859-1881.

<sup>125</sup> O. Smidsrød, Skjak-Bræk, *Trends Biotech*, **1990**, *8*, 71–78.

<sup>126</sup> A. Jiménez-Escrig, F.J. Sánchez-Muniz, *Nutr Res*, **2000**, *20*, 585-598.

<sup>127</sup> T. Shimokawa, S. Yoshida, T. Takeuchi, K. Murata, T. Ishii, I. Kusakabe, *Biosci. Biotech. Biochem.*, **1996**, *60*, 1531-1534.

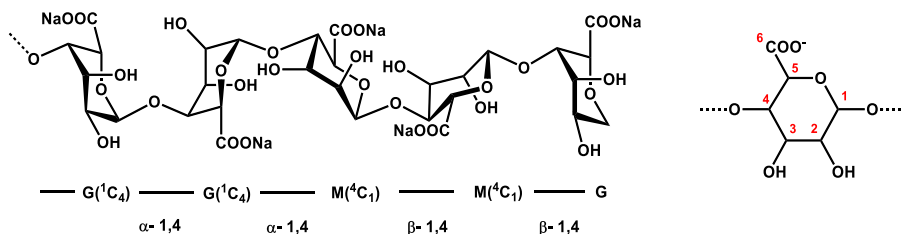


Figure 68. Sodium alginate structure (left) and its monomeric unit (right).

Food, cosmetics and pharmaceutical applications lies on alginates' gelling ability, their stabilizing properties and high viscosity in aqueous solutions.<sup>128</sup> In fact, alginates have the ability to form strong gels with divalent and trivalent cations, and these gels can be readily converted into aerogels by supercritical drying.<sup>129</sup>

A limit in the use of this material in the textile field is its viscosity. According to Rashid,<sup>130</sup> the viscosity of sodium alginate (SA) can be divided into three categories: (1) low viscosity, <240 cP; (2) medium viscosity, 240–3500 cP; and (3) high viscosity, >3500 cP.<sup>131</sup> Commercial SAs may have different viscosity depending on their origin and extraction method.

A factor which can influence the viscosity of the SA is the salt presence. In 2020 Castellano<sup>132</sup> demonstrated that using the right quantity of NaCl allows to decrease the viscosity of the polymer. Indeed, SA is reported to behave as nearly rigid polymers assuming a rodlike conformation in salt free environments due to the strong electrostatic repulsions between the charges (Figure 69b). The use of NaCl salt (0.025 mol/L with SA 0.005g/mL) was useful to completely screen the negative charges of alginate and force the chains to assume a random coil conformation (Figure 69c).

<sup>128</sup> J.L. Drury, D.J. Mooney, *Biomaterials*, **2003**, *24*, 4337–4351.

<sup>129</sup> R.R. Mallepally, I. Bernardm M.A. Marin, K.R.Ward, M.A. McHugh, *J. Supercrit. Fluids*, **2013**, *79*, 202–208.

<sup>130</sup> A. Rasyid, *Oseana*, **2003**, *28*, 33–38.

<sup>131</sup> N. Devina, Y.K. Eriwati, A.S. Santosa, *Phys.: Conf. Ser.*, **2018**, ser. 1073, 052012.

<sup>132</sup> A. Doderò, S. Vicini, M. Alloisio, M. Castellano, *Rheol. Acta*, **2020**, *59*, 365–374.

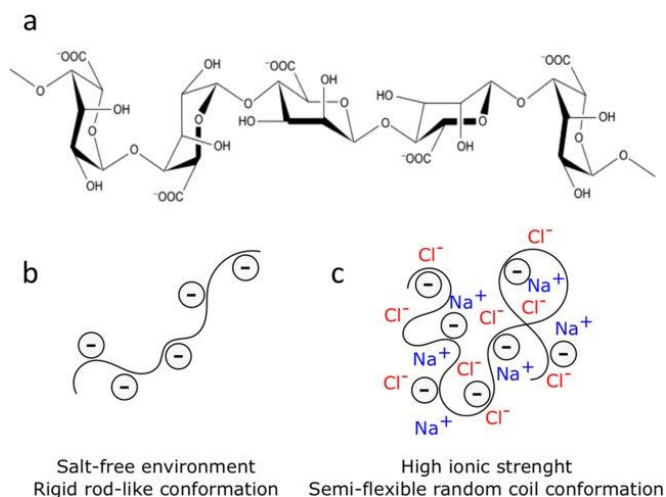


Figure 69. Chemical structure of sodium alginate (a), chain conformations assumed in a salt free environment (b) and in the presence of added salt (c).<sup>133</sup>

An efficient green alternative to reduce the viscosity and, consequently, the molecular weight of alginates is represented by the use of ultrasound. In 2017, Cao et al.<sup>134</sup> showed that ultrasonic treatment of alginates at different frequencies caused degradation, rearrangement, and changes in their properties such as molecular weight and viscosity. They showed that ultrasonic treatment of alginate could also increase its hydrophobic interaction and interfacial activity. Furthermore, an ultrasonic treatment was successfully employed to reduce the molecular mass of two sodium alginates in salt solutions by Dodero and Castellano in 2020.<sup>135</sup>

The tanning efficacy of oxidised sodium alginate was firstly reported by Ding and co-workers in 2018.<sup>136</sup> The selective oxidation of sodium alginate (SA) using  $\text{NaIO}_4$  was applied to obtain oxidized sodium alginate (OSA) whose ability to increase the thermal stability of leather powder was then tested. Through oxidation, the C2-C3 bond between two adjacent hydroxyl groups in the glucuronic or mannuronic units is cleaved, the 1,2-diol group is

<sup>133</sup> A. Dodero, S. Vicini, M. Alloisio, M. Castellano, *Rheol. Acta*, **2020**, *59*, 365–374.

<sup>134</sup> L. Feng, Y. Cao, D. Xu, S. Wang, J. Zhang, *Ultrason. Sonochem.*, **2017**, *34*, 609–615.

<sup>135</sup> A. Dodero, S. Vicini, M. Castellano, *Food Hydrocoll.*, **2020**, *109*, 106128.

<sup>136</sup> W. Ding, Y. Yi, Y. Wang, J. Zhou, B. Shi, *ChemistrySelect*, **2018**, *3*, 12330–12335.

converted into dialdehyde. OSA is an open chain biopolymer containing dialdehyde groups. The degree of oxidation may be varied in function of the molar ratio of monomer unit of the substrate and oxidizing agent. It is therefore possible to provide a wide variety of oxidised sodium alginate derivatives (Figure 70).

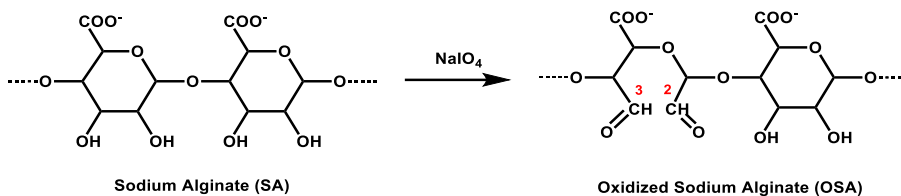


Figure 70. Reaction to obtain OSA using  $\text{NaIO}_4$ .

OSA has the advantage of higher solubility compared to SA due to the high degree of depolymerization and the presence of carboxyl groups and aldehyde functionalities. It was assumed that the use of OSA derivatives with various molecular weight would provide leather with different characteristics. For example, lower molecular weight and viscosity OSA derivatives have the ability to better penetrate inside leather structure and more efficiently bind to collagen. Meanwhile, the function of relatively high molecular weight components in OSA is also essential because they can fill into the interspaces between collagen fibres bundles and further reinforce the crosslinking network (Figure 71).

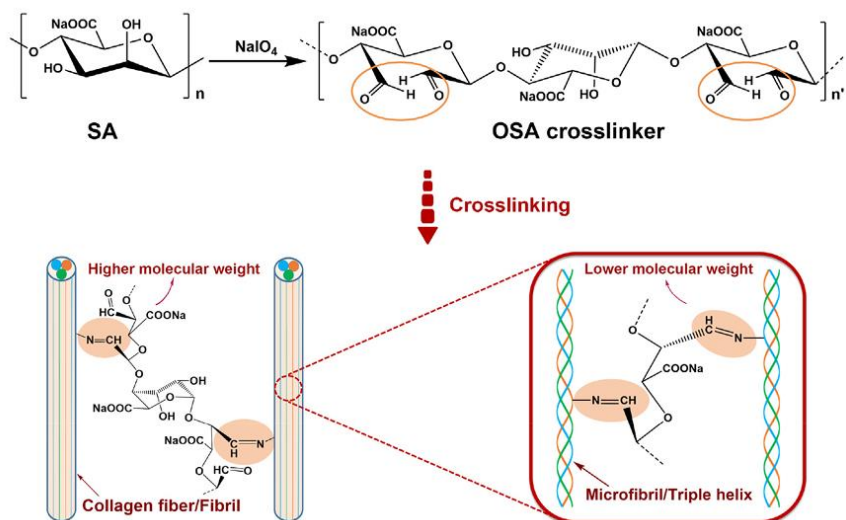


Figure 71. Crosslinking process and reaction of OSA with collagen fibre.<sup>137</sup>

However, the industrial use of  $\text{NaIO}_4$  is limited by its relatively high cost. In addition, industrial use of  $\text{NaIO}_4$  requires a lot of caution because it may cause severe skin burns, eye damage, organ damage in case of prolonged exposure, is very toxic to aquatic organisms and may cause fire or explosion (ECHA). This substance is registered under REACH<sup>138</sup> and may not be used/imported into the European Economic Area in quantities exceeding 1000 tonnes per year.<sup>139</sup>

Therefore, according to the restrictive EU regulations on the use of chemicals (REACH regulation), environmental impact [Waste Framework Directive 2008/98/EC, Water Framework Directive 2000/60/EC, Industrial Emissions Directive 2010/75/EU, the Circular Economy Package], the use of sodium periodate must be restricted.<sup>140</sup>

The present work concerns with the development of SA-based biodegradable re-tanning agent easy to be adopted in the tanning industry

<sup>137</sup> W. Ding, J. Zhou, Y. Zeng, Y. Wang, B. Shi, *Carbohydr. Polym.*, **2017**, *157*, 1650-1656.

<sup>138</sup> <https://echa.europa.eu/registration-dossier/-/registered-dossier/5745/3/1/2>

<sup>139</sup> <https://echa.europa.eu/it/substance-information/-/substanceinfo/100.029.270>

<sup>140</sup> [https://www.buyersguidechem.com/chemical\\_supplier/Sodium\\_periodate](https://www.buyersguidechem.com/chemical_supplier/Sodium_periodate)

without requiring changes in current technology. In addition, the use of renewable, biodegradable, non-toxic resources would significantly reduce the chemical and environmental footprint of leather production and could pave the way to obtain biodegradable leather.

The research was performed in the first year of the three-year European Eureka project “*Biodegradable and Antimicrobial Re-tanning Agent and Coating for Ecological and Safe Leather*”. The project is in the development phase of the envisaged products and the tests are now carried out on pilot scale at the facilities of A3 Leather Innovation Center, University of Lleida, Igualada, Spain.

Therefore, in the first part of this work, newly and completely safe/non-toxic and biodegradable re-tanning agents (SADs) with a broad molecular weight distribution were developed from bio-renewable sodium alginate derivatives, obtained using ultrasound technology (US).<sup>141,142</sup> Furthermore, in order to reduce the viscosity of the solutions and increase the oxidation degree, a combination of US and oxidising agents ( $\text{H}_2\text{O}_2/\text{NaIO}_4$ )<sup>143</sup> and catalysts was tested.

All SAD samples were tested on raw hide and the interaction between collagen matrix and SADs, in terms of increase of the hydrothermal stability of collagen-SAD matrix, was studied by micro-differential scanning calorimetry (micro-DSC). Attenuated total reflection infrared spectroscopy (FTIR-ATR) was used to characterise the various SADs. To this purpose SADs spectra were compared to that of SA and OSA obtained by selective oxidation with  $\text{NaIO}_4$ .

### 5.1.2 *The ultrasounds and the cavitation phenomenon*

Ultrasound is a mechanical oscillating sound wave that requires an elastic medium to support it. Being mechanical waves, they propagate in the medium with energy transfer and not particles. Matter particles simply

---

<sup>141</sup> A. Doderò, S. Vicini, M. Castellano, *Food Hydrocoll.*, **2020**, *109*, 106128.

<sup>142</sup> L. Feng, Y. Cao, D. Xu, S. Wang, J. Zhang, *Ultrason. Sonochem.*, **2017**, *34*, 609-615.

<sup>143</sup> S. Mao, T. Zhang, W. Sun, X. Ren, *Pharm. Dev. Technol.*, **2011**, *17*, 763-769.

oscillate around their equilibrium position, with energy transfer from one particle to another.

The fundamental effect of ultrasound on a fluid is to impose an acoustic pressure on top of the hydrostatic pressure already acting on the medium.

When ultrasound reaches high thresholds of intensity, the acoustic pressure wave drops below the vapour pressure of the liquid, causing the growth of small bubbles created by gaseous nuclei in the liquid.<sup>144</sup> A further increase in intensity generates a negative pressure in the fluid, causing a succession of compression and rarefaction phases. This leads to the formation of further bubbles caused by the negative pressure exceeding the attractive force of the molecules in the medium during the rarefaction cycle (Figure 72).<sup>145</sup>

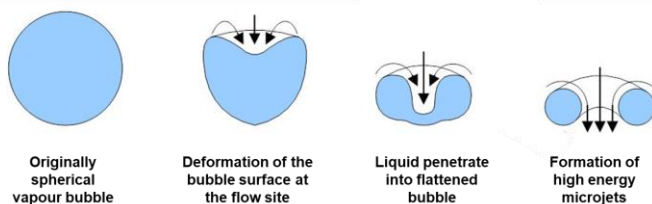


Figure 72. Effect of the negative pressure.<sup>146</sup>

During the compression cycle, the bubbles shrink and their contents are reabsorbed into the liquid. As the surface of the bubble has expanded, not all the vapour is reabsorbed so, after a number of cycles, the bubble grows. The bubble oscillates according to the applied frequency up to a certain critical value and then, in a compression cycle, implodes.<sup>147</sup> This process is known as the cavitation phenomenon (Figure 73).

<sup>144</sup> T.J. Mason, L. Paniwnyk, F. Chemat, M. Abert Vian, *Alternatives to Conventional Food Processing*, Andrew Proctor (ed.), RSC Green Chemistry Series, **2010**.

<sup>145</sup> M. Vinatoru, T.J. Mason, I. Calinescu, *TrAC Trends Anal. Chem.*, **2017**, 97, 159–78.

<sup>146</sup> <https://slideplayer.com/slide/9649811/>

<sup>147</sup> A. Patist, D. Bates, *Innov. Food Sci. Emerg. Technol.*, **2008**, 9, 147–154.

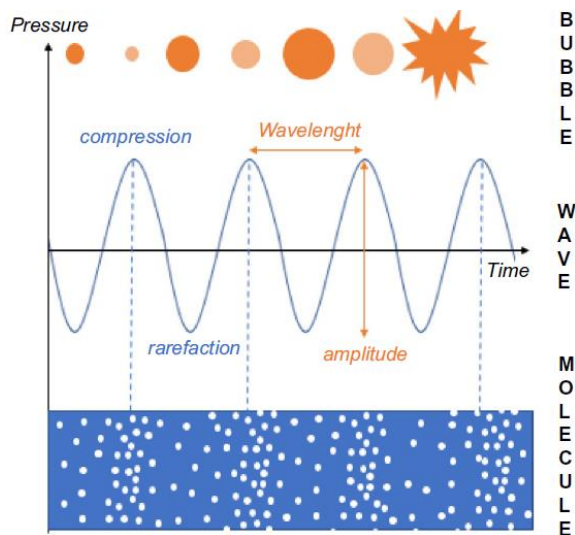


Figure 73. The cavitation phenomenon.

As the gas bubbles implode, a large amount of localised energy is released, leading to very high pressures and temperatures and the formation of hot spots characterised by temperatures of over 5000 K, pressures of around 1000 atmospheres and a lifetime of less than  $\mu\text{s}$ .<sup>148</sup> Localized hot spots can significantly accelerate the chemical reactivity of a medium.<sup>149</sup>

The chemical effects caused by ultrasound can be of various types. Three distinct parts of the reaction environment can be identified: the area inside the cavitation bubble (gaseous environment), the liquid-bubble interface and the liquid itself.<sup>150</sup>

The most used medium in reactions involving ultrasound is water. Radicals at the bubble interface and in the liquid bulk can recombine with each other to form hydrogen peroxide and water. The formation of radicals in water is influenced by the presence of dissolved gases, especially oxygen. Only a small fraction of the radical species produced has a sufficiently long lifetime

<sup>148</sup> C. Wen, J. Zhang, H. Zhang, C.S. Dzah, M. Zandile, Y. Duan, *Ultrason. Sonochem.*, **2018**, *48*, 538–549.

<sup>149</sup> K.S. Suslick, *Sci. Am.*, **1989**, *260*, 80–6.

<sup>150</sup> T.J. Mason, *Chemistry with Ultrasound*. Amsterdam: Elsevier Applied Science, **1990**.

to diffuse into the liquid. The only species, originating from radical processes and able to diffuse easily away from the bubble, is hydrogen peroxide. The formation of these radicals can lead to chemical reaction called sonochemical reactions (Figure 74).

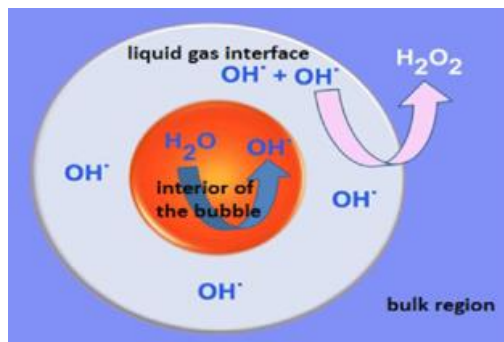


Figure 74. Sonochemical reaction.<sup>151</sup>

Two types of cavitation can be distinguished: in the first, the stable cavitation, the bubble remains stable around an equilibrium size for many compression-decompression cycles.<sup>152</sup>

On the other hand, when the bubble contains the vapour phase of the liquid and only lasts for one or a few pressure cycles, cavitation is called transient.<sup>153</sup>

### 5.1.3 Ultrasonic transducer

Ultrasonic transducers are devices which convert desired electrical signals to ultrasonic waves. The most widely used in industrial application are magnetostrictive and piezoelectric transducers.<sup>154</sup>

An example of piezoelectric transducer is the ultrasonic horn (Figure 75a) characterized by a small tip from which high intensity ultrasound is

<sup>151</sup> <http://www.ukacusat.in/sonochemistry/>

<sup>152</sup> T.G. Leighton, *The acoustic bubble*. San Diego. Academic Press, 312-426, **1994**.

<sup>153</sup> L. Vernès, M. Vian, F. Chemat, *Ultrasound and Microwave as Green Tools for Solid-Liquid Extraction*-chapter 12, Ed. Colin F. Poole, Elsevier, **2020**.

<sup>154</sup> K. Yasui, *Fundamentals of Acoustic Cavitation and Sonochemistry*. In: Pankaj, Ashokkumar M. (eds) *Theoretical and Experimental Sonochemistry Involving Inorganic Systems*. Springer, Dordrecht, **2010**.

radiated. It converts alternating electrical energy directly into mechanical energy through the *piezoelectric effect*. If an alternating electric field is applied along the axis of a piezoelectric crystal, the crystal expands and contracts along this axis. These vibrations are amplified by the resonant masses of the transducer and directed to the liquid.<sup>155</sup>

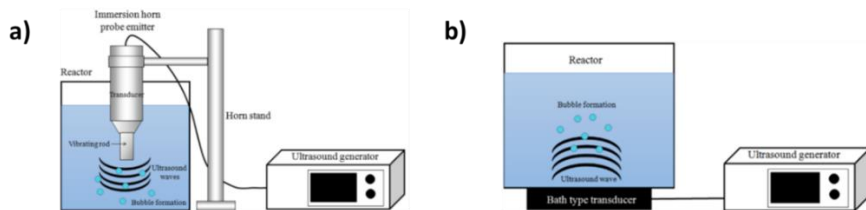


Figure 75. Type of ultrasonic transducer. a) Ultrasonic horn, b) bath type transducer.<sup>155</sup>

The bath type transducers (Figure 75b) use the principle of *magnetostriction*: an instantaneous application of an alternating magnetic field causes the ferromagnetic material to contract and stretch, producing a sound wave that passes through the sonicated liquid.<sup>156</sup>

## 5.2 Synthesis and characterization of SADs

### 5.2.1 Preliminary tests

Some preliminary trials were performed to test our research hypothesis, namely their capacity to interact with collagen from hide powder. Different types of transducers were tested as well as various treatment conditions (treatment duration, ultrasound frequency and intensity, temperature etc.) to decrease viscosity (i.e. obtain the appropriate depolymerization degree) and increase oxidation degree by forming aldehyde groups.

For example, the 2% SA solution was subjected to sonication using an ultrasonic Sonic vibracell VCX 750 (Figure 76) with the impulse sequence 5 second ON and 5 second OFF. The other sonication conditions (i.e. energy,

<sup>155</sup> B. Thokchom, A.B. Pandit, P. Qiu, B. Park, J. Choi, J. Khim, *Ultrason. Sonochem.*, **2015**, *27*, 210–234.

<sup>156</sup> Y. Yao, Y. Pan, S. Liu, *Ultrason. Sonochem.*, **2020**, *62*, 104772.

average power, frequency, amplitude, time and temperature) are reported in Table 16.



Figure 76. Sonic vibracell VCX 750 with a 13mm probe in titanium.

Table 16. Preliminary samples developed

| Sample  | Energy (J) | Average Power (W) | Sonication Time (min) | $T$ (°C) |
|---|------------|-------------------|-----------------------|----------|
| SAD1  | 72085      | 53.40             | 22.5                  | 20       |
| SAD2  | 74041      | 54.85             | 22.5                  | 50       |
| SA 2% w/w;<br>Frequency 20%;<br>Amplitude 50% |            |                   |                       |          |

SADs ability to interact with collagen was then tested by mixing the sonicated SA with hide powder (H) in the presence of NaCl and keeping the mixtures shaken in a bath oscillator (Thermo Scientific Compact Digital Rocker) at 100 rpm at room temperature for 2h (Figure 78 and Table 17). The mixtures were left to dry in air for 2 days. Before taking the samples for performing the shrinkage test, the hide was thoroughly washed with distilled water to eliminate the residual NaCl.

Table 17. Condition used for the testing the interaction of SADs with hide powder

| Test Name | Sample Used | Quantity (ml) | NaCl (g) | Hide powder (g) | Time (h) | RPM |
|-----------|-------------|---------------|----------|-----------------|----------|-----|
| H-SAD1    | SAD1        | 20            | 0.12     | 0.5             | 2        | 100 |
| H- SAD2   | SAD2        | 20            | 0.12     | 0.5             | 2        | 100 |
| H- SA     | SA 2%       | 20            | 0.12     | 0.5             | 2        | 100 |

The Shrinkage temperature ( $T_s$ ) was determined using the Micro Hot Table (MHT) method.<sup>157</sup> The shrinkage (contraction) activity of collagen fibres is described by a sequence of temperature intervals: no activity – A1 – B1 –  $\Delta C$  – B2 – A2 – complete shrinkage. Interval A is characterized by shrinkage activity in individual fibers, one fibre at a time and with pause in between the individual movements. When shrinkage activity in one fibre is immediately followed by shrinkage activity in another fibre without pause, interval B is reached. Interval  $\Delta C$ , known as the main shrinkage interval, is defined by the simultaneously and continuously shrinking of at least two fibres. Shrinkage temperature  $T_s$  refers to the starting temperature of the main shrinkage interval, while T first ( $T_f$ ) and T last ( $T_l$ ) are defined as the temperatures at which the first and last shrinkage activity of an individual fiber is observed. The total length of the shrinkage process is expressed as  $\Delta T = (T_l - T_f)$  (Figure 77). The shrinkage activity results obtained for H-SAD1 and H-SAD2 are reported in Table 18.

---

<sup>157</sup> R. Larsen, Microanalysis of Parchment, ed. *Archetype Publication Ltd*, 2002.

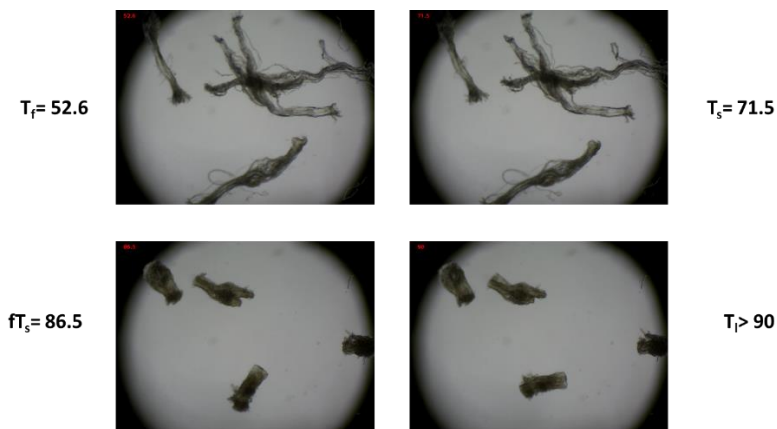


Figure 77. Images of fibres' shrinkage during the MHT measurement of H-SAD2.



Figure 78. Thermo Scientific Compact Digital Rocker.

Table 18. Shrinkage activity by MHT method for H-SAD1 and H-SAD2 compared to the shrinkage activity of hide powder reacted with the initial SA solution H-SA

| Test Name   | Sample tested | $T_f$ (°C) | $T_s$ (°C) | $ft_s$ (°C) | $T_l$ (°C) |
|-------------|---------------|------------|------------|-------------|------------|
| Hide Powder | -             | 40.3       | 56.4       | 66.6        | 78.4       |
| H-SAD1      | SAD1          | 51.8       | 59.1       | 69.8        | 87.1       |
| H-SAD2      | SAD2          | 52.6       | 71.5       | 86.5        | >90        |
| H-SA        | SA 2%         | 41.4       | 54.9       | 68.5        | 82.6       |

From the results in Table 18, only the SA solution treated at 50°C (SAD-2), shows ability to increase the shrinkage temperature and intervals, thus conferring increased thermal stability to collagen. These preliminary results confirm the suitability of US treatment to adequately modify the SA solution so that increase its ability to interact with collagen within hide powder.

## 5.2.2 *Synthesis of samples*

### 5.2.2.1 *Experiments with the ultrasonic horn Sonic vibracell VCX 750*

The temperature of the solvent also plays a key role in the use of ultrasound. The use of high temperatures helps to disrupt solute-matrix interactions, which involve van der Waals forces, hydrogen bonding, and dipole attractions between solute molecules. On the other hand, at lower temperatures, a better cavitation phenomenon is obtained since, when the temperature of the solvent increases, its vapour pressure also increases and therefore more solvent vapour fills the cavitation bubbles which will then tend to collapse less violently.

For this reason, the first set of samples was made trying different combination of temperature and time to achieve a compromise between temperature and cavitation.<sup>158</sup>

Starting from the US conditions used to obtain the SAD2 sample, we repeated the preliminary tests by increasing all process parameters, i.e. energy, amplitude, time and temperature as reported in Table 19.

---

<sup>158</sup> L. Capelo, M.M Galesio, G.M. Felisberto, C. Vaz, J. Costa Pessoa, *Talanta*, **2005**, *66*, 1272–1280.

Table 19. US tests with Sonic vibracell VCX 750 and the sonication conditions

| Sample | Energy (J) | Amplitude (%) | Sonication time (min) | T (°C) |
|--------|------------|---------------|-----------------------|--------|
| SAD2   | 83381      | 50            | 22.5                  | 50     |
| SAD3   | 170338     | 60            | 30                    | 50     |
| SAD4   | 363700     | 75            | 60                    | 75     |
| SAD5   | 975406     | 75            | 120                   | 75     |

SA 2% w/w;  
Frequency 20%

### 5.2.2.2 Experiments with bath type transducers

Two different types of bath transducers were used: the Advanced sonic processing system (Figure 79), which has the advantage of combining high amplitude and low frequency, and the Meinhardt Ultraschalltechnik device, which can operate at different frequencies but with low amplitude.

The Advanced sonic processor system has also the advantage of enabling gas / air bubbling in the system. In our specific case, air bubbling could be beneficial to increase the efficiency of the US treatment.



Figure 79. Advanced sonic processor system.

By increasing the gas content in the liquid increases the gas/vapour ratio within the bubbles and, due to the kinetics of dissolution, the gas acts as a buffer, cushioning the collapse of the bubbles and reducing the intensity of the shock wave.<sup>159</sup> In addition, gas molecules or microbubbles provide the

<sup>159</sup> O. Behrend, H. Schubert, *Ultrason. Sonochem.*, **2001**, *8*, 271-276.

basis for the formation and growth of bubbles, allowing the activation of the oxidation process.

Table 20. Preliminary US tests with Advanced sonic processing system and the sonication conditions

| Sample                        | Amplitude (%) | Sonication Time (min) | T (°C) | Air bubble (L/h) |
|-------------------------------|---------------|-----------------------|--------|------------------|
| SAD6                          | 100           | 30                    | 40     | 600              |
| SAD7                          | 100           | 60                    | 40     | 600              |
| SAD8                          | 100           | 90                    | 40     | 600              |
| SA 2% w/w;<br>Frequency 20kHz |               |                       |        |                  |

As the Meinhardt Ultraschalltechnik can operate at different frequencies, it is possible to make a further subdivision of ultrasound treatment depending on the frequency at which US are generated, the power (W) and the sound intensity (W/cm<sup>2</sup>) used:<sup>160,161</sup>

- A) high energy ultrasounds: characterised by low frequencies (20 kHz - 100 kHz) and I= 10 to 1000 W/cm<sup>2</sup>;
- B) medium energy ultrasounds: characterised by medium frequencies (100 kHz - 1 MHz) and I= 5-300 W/cm<sup>2</sup>;
- C) low energy ultrasounds: characterized by high frequencies (1 MHz - 10 MHz) and I < 1 W/cm<sup>2</sup>.

By using an intermediate frequency, we expect a weaker physical effect, but an increased formation of free radicals.

---

<sup>160</sup> H. Feng, H. Lee, Effect of Power Ultrasound on Food Quality, *Ultrasound Technologies for Food and Bioprocessing*, Ed. Springer, 559-582, 2011.

<sup>161</sup> F.J.O. Landa, S.R. Penacoba, F. Montero de Espinosa, D. Razansky, X.L. Deán-Ben, *Ultrasonics*, 2019, 94, 117-123.

Table 21. Preliminary US tests with Meinhardt Ultraschalltechnik system and the sonication conditions

| Sample    | Energy (J) | Amplitude | Frequency (kHz) | Sonication Time (min) | T (°C) |
|-----------|------------|-----------|-----------------|-----------------------|--------|
| SAD9      | 180000     | 7         | 1146            | 60                    | 45     |
| SAD10     | 180000     | 7         | 864             | 60                    | 45     |
| SAD11     | 180000     | 7         | 580             | 60                    | 45     |
| SA 2% w/w |            |           |                 |                       |        |

### 5.2.3 SADs characterization

#### 5.2.3.1 The oxidation degree

The amount of the aldehyde groups formed by the US treatment was evaluated through titration using hydroxylamine hydrochloride, according to the method of evaluating the oxidized degree (OD) of OSA.<sup>162</sup> The OD values measured for our SADs are listed in Table 22.

---

<sup>162</sup> L. Yuan, Y. Wu, J. Fang, X. Wei, Q. Gu, H. El-Hmashary, S.S. Al-Deyab, Y. Morsi, X. Mo, *Artif. Cells Nanomed. Biotechnol.*, **2017**, *45*, 76-83.

Table 22. Oxidation degree (OD) values measured for the variously US treated SA solutions (SADs) compared to the oxidation degree of SA solution oxidised using  $\text{NaIO}_4$  (OSA).

| Sample | Oxidation degree (%) |
|--------|----------------------|
| OSA    | 78                   |
| SAD2   | 24                   |
| SAD3   | 28                   |
| SAD4   | 37                   |
| SAD5   | 58                   |
| SAD6   | 12                   |
| SAD7   | 20                   |
| SAD8   | 21                   |
| SAD9   | 26                   |
| SAD10  | 10                   |
| SAD11  | 45                   |

As from the Table 22, the SAD5 derivative obtained at high temperature under air bubbling has the higher OD value compared to the ones obtained in mild conditions (e.g. SAD2 and SAD3). The SAD6, SAD7, SAD8 derivatives obtained at the highest amplitude (100%) but at lower temperature have low OD values. The use of medium frequency (e.g. SAD11) gave better results compared to the higher frequencies (e.g. SAD9 and SAD10).

### 5.2.3.2 Viscosity

The viscosity of SADs was measured to evaluate the depolymerization degree (Table 23).

Table 23. Viscosity values measured for the variously US treated SA solutions (SADs) compared to that of the initial SA 2% solution. The viscosity of SA solution oxidised using NaIO<sub>4</sub> (OSA) is also reported for comparison, too.

| Sample | Final Viscosity (cp) |
|--------|----------------------|
| SA 2%  | 3950                 |
| OSA    | 6.5                  |
| SAD2   | 2915                 |
| SAD3   | 2340                 |
| SAD4   | 2140                 |
| SAD5   | 403.3                |
| SAD6   | 636                  |
| SAD7   | 1913                 |
| SAD8   | 1503                 |
| SAD9   | 30.8                 |
| SAD10  | 40.2                 |
| SAD11  | 46.1                 |

### 5.2.3.3 ATR-FTIR analysis

The molecular fingerprint of the SA derivatives was obtained by ATR-FTIR with the aim of identifying the aldehydic function. To this purpose, their spectra were compared with those of SA and OSA (oxidised SA obtained using NaIO<sub>4</sub>).

All SADs spectra present the bands corresponding to the stretching vibrations of O–H bonds in the range of 3000–3600 cm<sup>-1</sup>, while the bands corresponding to stretching vibrations of aliphatic C–H were observed at 2920–2850 cm<sup>-1</sup>.<sup>163</sup>

The peak at 1738 cm<sup>-1</sup> is indicative of the formation of the aldehyde group and well correlates with the oxidation degree.<sup>164</sup>

<sup>163</sup> H. Daemi, M. Barikani, *Sci. Iran.*, **2012**, *19*, 2023–2028.

<sup>164</sup> Y. Wu, L. Yuan, N. Sheng, Z. Gu, W. Feng, H. Yin, Y. Morsi, X. Mo, *Front. Mater. Sci.*, **2017**, *11*, 215–222.

The asymmetric stretching vibration of the carboxylate group occurs at 1597–1592  $\text{cm}^{-1}$  for all SADs, while the symmetric stretching is visible near 1405  $\text{cm}^{-1}$ .<sup>165</sup> According to Barikani,<sup>163</sup> the weak signal at 1459  $\text{cm}^{-1}$ , we identified in the OSA spectrum, corresponds to the symmetric stretching vibrations of carboxylate salt ion. The band at 1295  $\text{cm}^{-1}$  could be assigned to the deformation of C-C-H and O-C-H stretching vibrations of the pyranose ring.<sup>166</sup>

The bands around 1300  $\text{cm}^{-1}$  were assigned to the  $\nu$  C-O stretching vibrations<sup>167</sup> and the signal at 1143  $\text{cm}^{-1}$  correspond to the glycosidic bond.<sup>168</sup>

The bands near 1120 and 940  $\text{cm}^{-1}$  were attributed to the C–O stretching vibration of pyranosyl ring and the C–O stretching with contributions from C–C–H and C–O–H deformation.<sup>163</sup> The bands around 1025  $\text{cm}^{-1}$  could be also assigned to C–O stretching vibrations.<sup>169</sup> It was reported that in the spectrum of alginate G ((1  $\rightarrow$  4) linked  $\alpha$ -L-gulopyranuronic acid) fraction the C–O stretching vibration occurs at 943  $\text{cm}^{-1}$ , while the band at 885  $\text{cm}^{-1}$  was assigned to deformation vibration of  $\beta$ -C<sub>1</sub>–H mannuronic acid residues.<sup>170</sup>

Absorption peaks around 815  $\text{cm}^{-1}$  and 780  $\text{cm}^{-1}$  were attributed to deformation vibrations of COH, CCH and OCH moieties in the  $\alpha$ -L-guluronic acid residues, with contributions of the bending deformation vibration of the C–O–C glycosidic linkage in homopolymeric blocks.<sup>169</sup>

Figure 80 illustrates the spectra of SAD5 compared to that of OSA. The second derivative of both spectra was done to maximize and better identify the significant signals not easily observable in the ATR-FTIR spectra.

---

<sup>165</sup> W. Ding, Y. Yi, Y. Wang, J. Zhou, B. Shi, *ChemistrySelect*, **2018**, 3, 12330–12335.

<sup>166</sup> R.G. Huamani-Palomino, C.R. Jacinto, H. Alarcón, I. Mejía, R.C. López, *Int. J. Biol. Macromol.*, **2019**, 129, 1056–1068.

<sup>167</sup> S.R. Derkach, N.G. Voron'ko, N.I. Sokolan, D.S. Kolotova, Y.A. Kuchina, *J. Dispers. Sci. Technol.*, **2020**, 41, 690–698.

<sup>168</sup> T. Aguirre Calvo, P. Santagapita, *Qual. Reliab. Eng. Int.*, **2016**.

<sup>169</sup> A. Zimoch-Korzycka, D. Kulig, Z. Król-Kilinska, B. Zarowska, L. Bobak, A. Jarmoluk, *Polymers*, **2021**, 13, 2258–2274.

<sup>170</sup> D. Leal, B. Matsuhiro, M. Rossi, F. Caruso, *Carbohydrate Research*, **2008**, 343, 308–316.

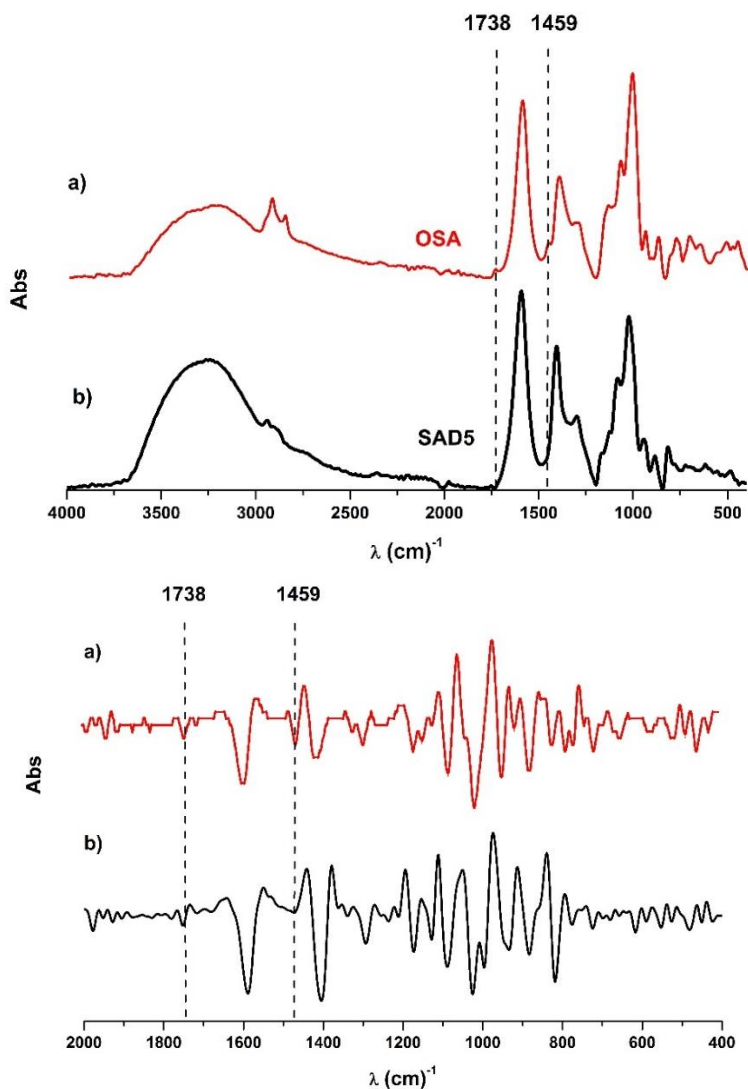


Figure 80. (top) ATR- FTIR spectra of (a) OSA, (b) SAD5; (bottom) ATR-FTIR second derivative spectra of (a) OSA, (b) SAD5.

### 5.3 Lab-scale tanning tests

Tanning tests were performed at lab-scale using sheep raw hide. To simulate the movement of a real tanning drum, we used a rotator drive

stirrer STR4 (Stuart). The scheme of the wet-white tanning process is reported in Figure 81.



Figure 81. Scheme of the lab-scale wet-white tanning process.

The raw hide was initially pre-treated to fully hydrate and reach a pH around 6 ( $\pm 0.5$ ) and then was introduced in the stirrer vessel together with the SAD and the necessary amount of NaCl. The hide was stirred in the tanning float for 6 hours and then left in the tanning bath overnight. The second day, it was stirred for 6h and again left in the tanning bath overnight to optimise penetration and bonding. In the third day, NaHCO<sub>3</sub> was added in the tanning float to increase pH up to about 8. The hide was stirred for 3h to allow SAD to fix in the leather structure. Leather was then washed and left to dry in air at room temperature. All SADs were tested using a raw hide – tanning bath ratio of 100:2000 and 24% NaCl. The amount of NaHCO<sub>3</sub> used for the neutralization (pH= 8) varied from one test to another.

#### 5.4 Sodium alginate derivatives SADs tanning ability - Denaturation temperature evaluation by micro- DSC

To evaluate the tanning ability of SADs we registered the denaturation curves of SAD-tanned leather using micro-DSC technique and measured the denaturation parameters, i.e. denaturation temperature  $T_{\max}$  of denaturation enthalpy,  $\Delta H$ .<sup>171</sup> The results obtained are reported in Table 24.

Considering the intrinsic heterogeneity of natural hide, only a  $T_{\max}$  variation higher than 5 °C was considered enough to state with good certainty that

---

<sup>171</sup> A.D. Covington, W.R. Wise, *Tanning Chemistry The science of Leather*, Ed. Royal Society of Chemistry, Croydon, 2020.

an increase in the hydrothermal stability of the hide was induced by the interaction of collagen with the tested SAD.

Table 24. Denaturation parameters of SAD-tanned hides measured by micro-DSC

| Leather symbol | SAD   | Transducer type                 | $T_{max}$ (°C) | $\Delta H$ (J/g) |
|----------------|-------|---------------------------------|----------------|------------------|
| Raw hide       | -     | -                               | 53.7           | 26.0             |
| L-SAD2         | SAD2  | Sonic vibracell<br>VCX 750      | 61.2           | 36.7             |
| L-SAD3         | SAD3  | Sonic vibracell<br>VCX 750      | 59.9           | 42.8             |
| L-SAD4         | SAD4  | Sonic vibracell<br>VCX 750      | 59.2           | 34.8             |
| L-SAD5         | SAD5  | Sonic vibracell<br>VCX 750      | 57.9           | 25.3             |
| L-SAD6         | SAD6  | Advanced sonic<br>processor     | 60.6           | 47.6             |
| L-SAD7         | SAD7  | Advanced sonic<br>processor     | 61.6           | 40.6             |
| L-SAD8         | SAD8  | Advanced sonic<br>processor     | 60.2           | 42.6             |
| L-SAD9         | SAD9  | Meinhardt<br>Ultraschalltechnik | 60.5           | 43.4             |
| L-SAD10        | SAD10 | Meinhardt<br>Ultraschalltechnik | 61.2           | 48.4             |
| L-SAD11        | SAD11 | Meinhardt<br>Ultraschalltechnik | 60.1           | 49.9             |

The increase in the hydrothermal stability of hides after the tanning tests with SADs is reflected by the increase of both temperature and enthalpy of denaturation. Such increase could be ascribed to the ability of SADs to interact with collagen. Considering the presence of numerous -OH groups and some aldehydic functions in SADs, it is very likely that the collagen-SAD matrix is stabilised through hydrogen bonds.

It is worth mentioning that, as illustrated in the chapter 3.3.1.1, a heterogeneous tanning process results in a heterogeneous distribution of thermal stability in the leather structure, evidenced by the co-existence of various collagen populations with distinct thermal stability. The variability in thermal stability may be ascribed to various factors, the most important being the tannin penetrability and tannin ability to interact with collagen. The heterogeneity of the tanning process can be evaluated by micro-DSC which provide an asymmetric calorimetric signal, that is a multi-component peak, or a rather symmetric, but broad peak.

In Figure 82-Figure 85, the denaturation curves of the SAD-tanned hides are grouped depending on the type of transducer used.

In Figure 82 the leathers tanned with SAD2 – SAD5, obtained using the Sonic vibracell VCX 750 are compared.

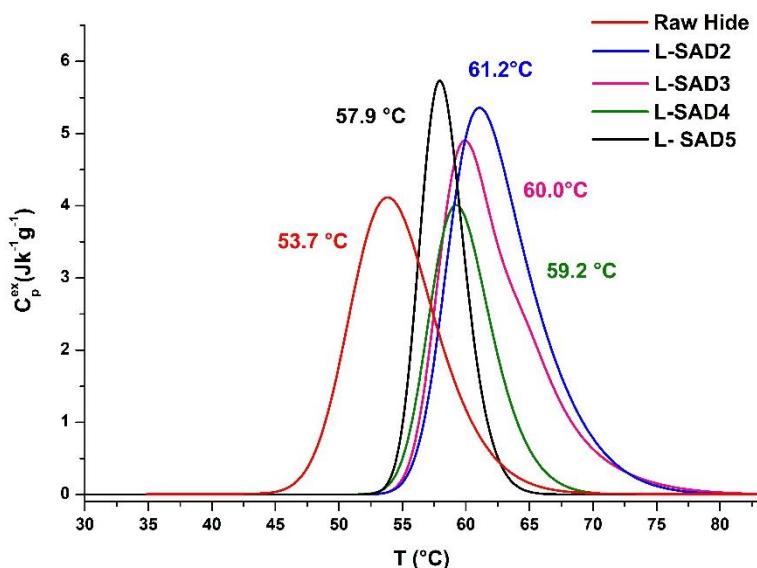


Figure 82. Denaturation curves of leathers tanned with the SADs obtained using the ultrasonic horn VCX 750.

Tanning with SAD5, the SA derivative obtained using the longest sonication time (120 minutes) and the highest temperature (75 °C), resulted in the product with the lowest  $T_{max}$  and  $\Delta H$  values. It would seem unexpected if

we were to correlate this behavior with the lowest viscosity and higher OD of SAD5. On the other part, SAD2, SAD3 and SAD4 gave similar results in terms of  $T_{\max}$ . However, we should note that SAD2, obtained using the shortest US treatment (22.5 minutes) at mild temperature (50 °C), conferred the leather the highest hydrothermal stability ( $T_{\max}= 61$  °C), even though it has the highest viscosity and the lowest OD compared to the other SADs of this group.

Regarding the group of SA derivatives obtained using the Advanced sonic processor system (bath type reactor with air bubbling), all conferred leather a similar thermal stability in terms of denaturation temperature (Figure 83). However, in terms of peak symmetry, L-SAD8 shows the more symmetrical signal, meaning that SAD8 has a more homogeneous distribution of the molecular mass. On the other part, the denaturation peak of L-SAD7 shows the presence of at least two collagen-SAD7 population, most likely ascribable to an uneven penetration of SAD7 in the leather structure due to its high viscosity.

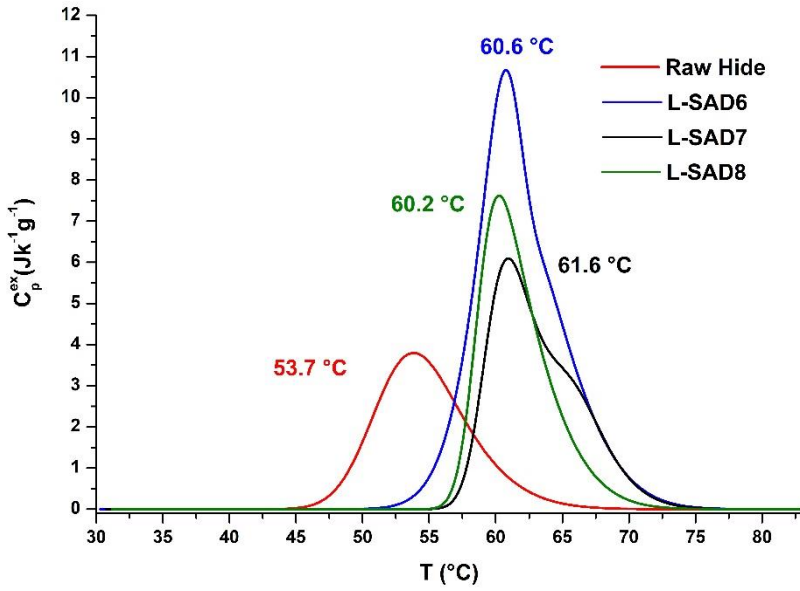


Figure 83. Denaturation curves of leathers tanned with the SADs obtained using the Advanced sonic processor system with air bubbling.

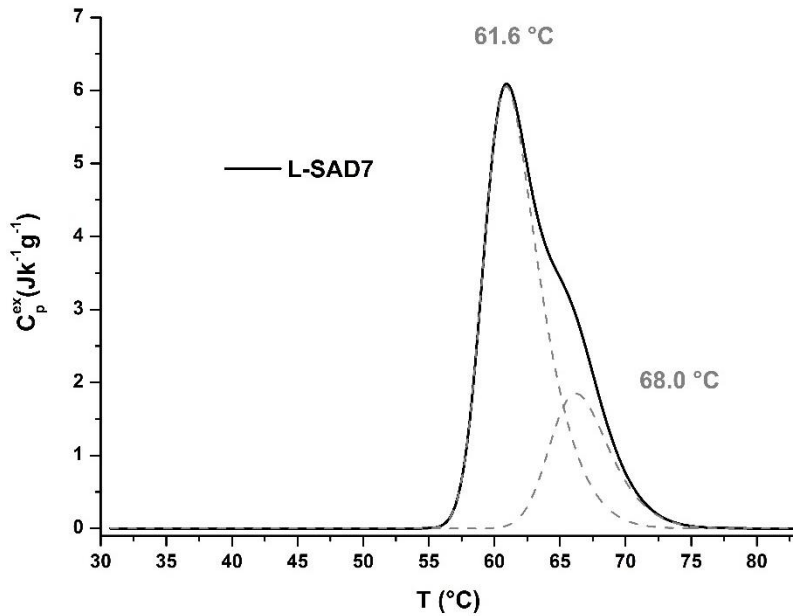


Figure 84. Deconvolution of denaturation curve obtained for L-SAD7 samples.

On the contrary, the denaturation peaks of leather samples tanned with the SA derivatives (SAD9-11), obtained using the Meinhardt Ultraschalltechnik system at decreasing frequency, are symmetric and a little bit sharper (Figure 85). This indicates a much more evenly penetration of SADs in the structure of hide. Noteworthy, the frequency does not appear to significantly affect the viscosity and tanning ability of SADs. In addition, it appears that the higher oxidation degree of SAD11 (induced by the low frequency US treatment) has no influence either.

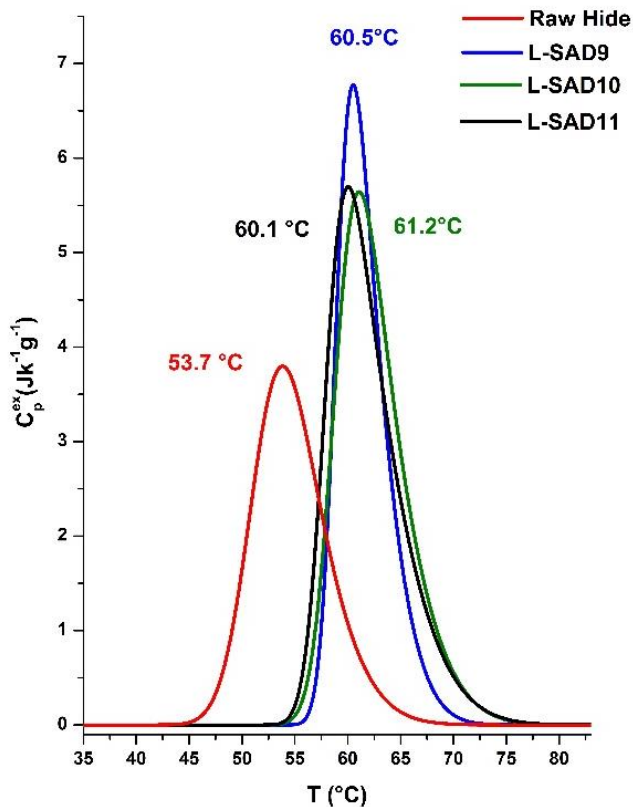


Figure 85. Denaturation curves of leathers tanned with the SADs obtained using the Meinhardt Ultraschalltechnik at various frequencies.

## 5.5 Upscaling the US reactor

Considering the above results and the feasibility of scaling up the US reactor, we selected the SAD7 obtained using the Advanced sonic processor system with the air bubbling for preparing the quantity necessary for a re-tanning test at micro pilot scale.

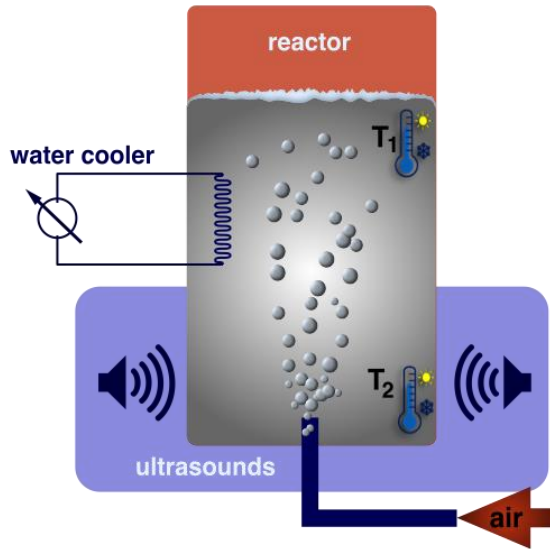


Figure 86. Micro pilot scale US reactor.

The viscosity of the sample (SAD7p) obtained at micro pilot US reactor illustrated in Figure 86 was performed to confirm the reproducibility of the US treatment at micro pilot scale. As shown in Table 25, the viscosity is comparable to the viscosity of SAD7 (Table 25).

Table 25. Viscosity measurement of the SAD7p sample obtained at micro pilot scale

| Measurement No. | 1                          | 2                          | 3                          |
|-----------------|----------------------------|----------------------------|----------------------------|
| Spindle         | 21                         | 21                         | 21                         |
| Viscosity       | 1908 cP                    | 1987 cP                    | 1983 cP                    |
| Torque          | 76.3%                      | 59.6%                      | 59.5%                      |
| Speed           | 20 RPM                     | 15 RPM                     | 15 RPM                     |
| Temperature     | 20.8 °C                    | 21 °C                      | 21 °C                      |
| Time            | 30 s                       | 30 s                       | 30 s                       |
| SS              | 354.8 dyne/cm <sup>2</sup> | 277.1 dyne/cm <sup>2</sup> | 276.7 dyne/cm <sup>2</sup> |
| SR              | 18.6 1/s                   | 13.95 1/s                  | 13.95 1/s                  |
| Accuracy        | 25 cP                      | 33.33 cP                   | 33.33 cP                   |

SAD7p sample is going to be tested within a wet-white tanning process on micro pilot scale at the facilities of A3 Leather Innovation Center, University of Lleida, Igualada, Spain.

### 5.6 *Optimisation of depolymerisation and aldehyde group formation.*

After studying the effect of the various factors on the US ability to convert SA in derivatives capable to interact with collagen within hide and increase the hydrothermal stability of the treated hide (“almost-tanned” leather), a further effort has been directed towards maximising the depolymerization degree of sodium alginate to improve its penetrability into leather structure, and hence its performance as a re-tanning agent. Therefore, in this second part of the project, various depolymerization methods were used in combination with the ultrasounds. The same US reactors and work parameters were used for synthesizing new SA derivatives.

The depolymerisation of polysaccharides occurs through the cleavage of glycosidic bonds which may encounter different mechanisms of

degradation, such as oxidative free radicals depolymerisation, acid,<sup>172</sup> alkaline and enzymatic-catalysed hydrolysis.<sup>173</sup>

The oxidative–reductive free radical depolymerization (ORD) of alginates involves a series of free radical reactions that lead to chain scission.<sup>174</sup> Compounds like H<sub>2</sub>O<sub>2</sub>, NaIO<sub>4</sub> and transition metal ions acting as catalysts can initiate the ORD. Based on this, we tried to synthesize SADs with smaller and more homogeneous molecular weight using the synergistic effects of inorganic catalysis and ultrasound. A further step of oxidation by H<sub>2</sub>O<sub>2</sub> and NaIO<sub>4</sub> followed.

Two different catalysts, [FeSO<sub>4</sub> · 7H<sub>2</sub>O] and [Co(CH<sub>3</sub>COO)<sub>2</sub> · 4H<sub>2</sub>O], were used with a 1 : 0.025 ratio between SA and the catalyst.

H<sub>2</sub>O<sub>2</sub> was added in low (0.1% w/w of the total mass of the solution) and high quantity (3% w/w of the total mass of the solution) to evaluate the concentration influence on the properties of SAD.

Catalysts and H<sub>2</sub>O<sub>2</sub> were added directly in the ultrasound reactor.

Although the SA oxidation using NaIO<sub>4</sub> ensures optimal tanning ability of the oxidised sodium alginate (OSA), its use is restricted by REACH regulation, as already explained in chapter 5.1.1. Up to now, a ratio of 1 : 0,8 between SA and NaIO<sub>4</sub> was reported by Ding<sup>175</sup> while a lower rate of 1 : 0,2 = SA : NaIO<sub>4</sub> was successfully used by Badea<sup>176</sup> to obtain highly thermostable automotive leather.

Starting from the premises of a synergistic action of US and NaIO<sub>4</sub>, we decreased ten to twenty times the NaIO<sub>4</sub> quantity compared to the one used in the mentioned studies, i.e. 0.08:1; 0.02:1 and 0.01:1 w/w ratios of

---

<sup>172</sup> O. Smidsrød, B. Larsen, T. Painter, A. Haug, *Acta Chem. Scand.*, **1969**, 23, 1573-1580.

<sup>173</sup> H.K. Holme, K. Lindmo, A. Kristiansen, O. Smidsrød, *Carbohydr. Polym.*, **2003**, 54, 431–438.

<sup>174</sup> O. Smidsrød, A. Haug, B. Larsen, *Acta Chem. Scand.*, **1963**, 17, 2628-2637.

<sup>175</sup> E. Badea, M. Crudu, C. Carsote, C. Sendrea, M.C. Lupas, L. Miu, Stabilisation of collagen by alginate dialdehyde for eco-sustainable tanning. XL National Conference on Calorimetry, Thermal Analysis and Chemical Thermodynamics, Pisa, Italy. 17-19 December **2018**.

<sup>176</sup> E. Badea, M. Crudu, C. Carsote, C. Sendrea, M.C. Lupas, L. Miu, Stabilisation of collagen by alginate dialdehyde for eco-sustainable tanning. XL National Conference on Calorimetry, Thermal Analysis and Chemical Thermodynamics, Pisa, Italy. 17-19 December **2018**.

NaIO<sub>4</sub>:SA. The oxidant was added after the US treatment following the procedure previously described reported.<sup>177</sup>

The SA derivatives obtained by combining US and catalysts or oxidants are reported in in Table 26. The US treatment was performed using the same parameters, i.e. amplitude 100%; frequency 20 kHz; temperature 40 °C; time 60 minutes; air bubbling 600 L/h.

Table 26. SADs obtained by combining US and catalysts and/or oxidants

| Sample  | Catalyst /oxidant  | Oxidation degree (%) | Viscosity (cp) |
|---|--|----------------------|----------------|
| SAD12   | FeSO <sub>4</sub> · 7H <sub>2</sub> O                    | 45.9                 | 27.25          |
| SAD13   | Co(CH <sub>3</sub> COO) <sub>2</sub> · 4H <sub>2</sub> O | 29.2                 | 260.0          |
| SAD14   | H <sub>2</sub> O <sub>2</sub> 0.1%                       | 50.3                 | 8.0            |
| SAD15   | H <sub>2</sub> O <sub>2</sub> 3%                         | -                    | 2.0            |
| SAD16   | NaIO <sub>4</sub> (NaIO <sub>4</sub> :SA = 0.01:1)       | 27.4                 | 192.3          |
| SAD17   | NaIO <sub>4</sub> (NaIO <sub>4</sub> :SA = 0.02:1)       | 23.5                 | 256.0          |
| SAD18   | NaIO <sub>4</sub> (NaIO <sub>4</sub> :SA = 0.08:1)       | 28.6                 | 110.0          |
| SA concentration 2% wt;<br>Amplitude 100%;<br>Frequency 20kHz;<br>Temperature 40°C;<br>Time 60 minutes;<br>Air bubble 600 L/h |  |                      |                |

For SAD15, synthesized using an excess of H<sub>2</sub>O<sub>2</sub>, the oxidation degree could not be determined. On the other hand, the presence of carboxylic acid was identified by ATR-FTIR spectroscopy at 1713 cm<sup>-1</sup> (Figure 87b). It is known that carboxylic groups interfere with the indicator used in the measurement.

<sup>177</sup> W. Ding, Y. Yi, Y. Wang, J. Zhou, B. Shi, *ChemistrySelect*, **2018**, 3, 12330– 12335.

Noteworthy, all SADs show a band at  $1738\text{ cm}^{-1}$  attributed to the aldehyde carbonyl (C=O) group as found for OSA.<sup>178</sup> (Figure 87).

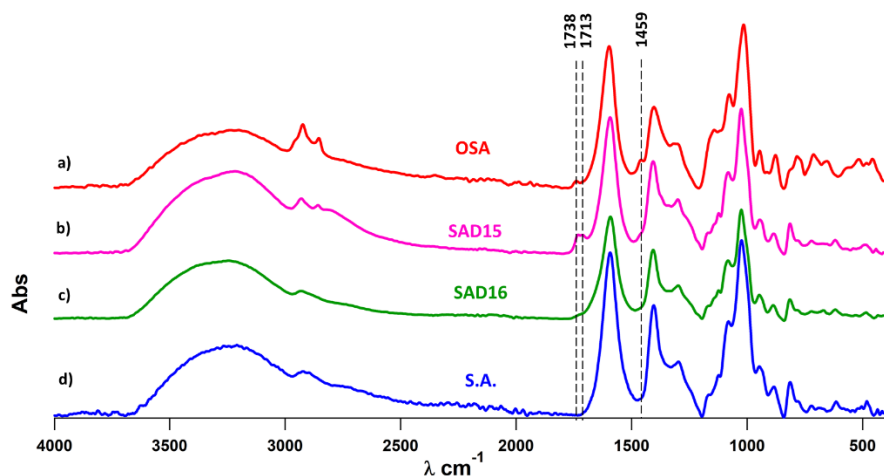


Figure 87. ATR-FTIR of a) OSA, b) SAD15, c) SAD16 and d) Sodium alginate.

### 5.6.1 Sodium alginate derivatives SADs tanning ability - Denaturation temperature evaluation by micro-DSC

All samples were tested in tanning tests on raw hide and micro-DSC measurements were performed on resulted leather samples.

In the tanning test, 100 g SAD was mixed with 1.2 g NaCl and stirred until the complete dissolution of the salt, when 5g hide was added and stirred for 6 hours/1<sup>st</sup> day + 6 hours/2<sup>nd</sup> day, while resting overnight. On the 3<sup>rd</sup> day, 1g of  $\text{NaHCO}_3$  was added and the tanning bath was stirred for 3 hours until a final pH= 8 was reached.

The denaturation parameters of SAD-tanned hides measured by micro-DSC are listed in Table 27, while the denaturation curves are illustrated in Figure 88 Figure 91.

---

<sup>178</sup> Y. Wu, L. Yuan, N. Sheng, Z. Gu, W. Feng, H. Yin, Y. Morsi, X. Mo, *Front. Mater. Sci.*, **2017**, *11*, 215–222.

Table 27. Denaturation parameters of SAD-tanned hides measured by micro-DSC

| Leather symbol | SAD   | $T_{max}$ (°C) | $\Delta H$ (J/g) |
|----------------|-------|----------------|------------------|
| L-SAD12        | SAD12 | 59.9           | 43.8             |
| L-SAD13        | SAD13 | 60.9           | 40.8             |
| L-SAD14        | SAD14 | 59.2           | 24.9             |
| L-SAD15        | SAD15 | 56.6           | 44.9             |
| L-SAD16        | SAD16 | 62.4           | 47.5             |
| L-SAD17        | SAD17 | 64.5           | 49.5             |
| L-SAD18        | SAD18 | 67.0           | 27.2             |

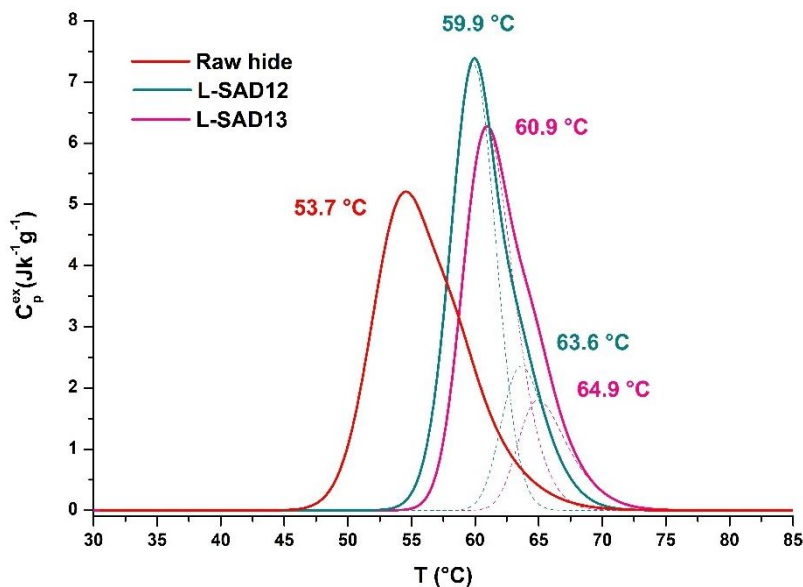


Figure 88. Denaturation curves of leathers tanned with the SADs synthesized by US treatment in the presence of inorganic catalysts.

Surprisingly, the use of the two inorganic catalysts did not improve the tanning capacity of the new derivatives compared to the US-only treated ones. However, a more stable collagen-SAD population occurred for both L-SAD12 and L-SAD13 (Figure 88), suggesting the presence of a “factor” able to make the collagen-SAD interaction more efficient.

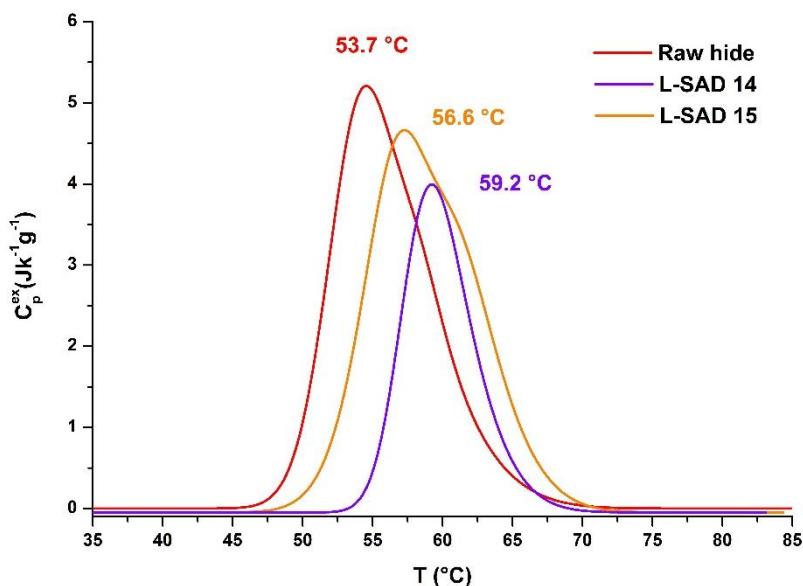


Figure 89. Denaturation curves of leathers tanned with the SADs synthesized by US treatment in the presence of various concentrations of H<sub>2</sub>O<sub>2</sub>.

Also, adding H<sub>2</sub>O<sub>2</sub> (Figure 89) in small concentration did not improve the tanning capacity of the new derivative (SAD14), compared to the US-only treated ones, while higher H<sub>2</sub>O<sub>2</sub> concentration (3% w/w) worsen the ability of SAD15 to interact with collagen.

As expected, the SA derivatives obtained by a two-step process, i.e. US treatment and oxidation by NaIO<sub>4</sub>, showed an improved ability to interact with collagen and increase leather thermal stability (Figure 90). Considering the tanners criterium on which it is determined whether the hide turns into leather, the only real tanning agents among all SADs synthesized are SAD16-18. Except from L-SAD17, the other two leathers, L-SAD 16 and L-SAD17, show asymmetrical denaturation peaks (Figure 90) with two maximums at (63-65) °C and (67-69) °C, respectively, indicating a wider distribution of molecular masses for SAD17/18 compared to SAD18 which conferred leather a good hydrothermal homogeneity. Consequently, lower average molecular mass and thus ability to more evenly penetrate the hide structure could be hypothesized for SAD18.

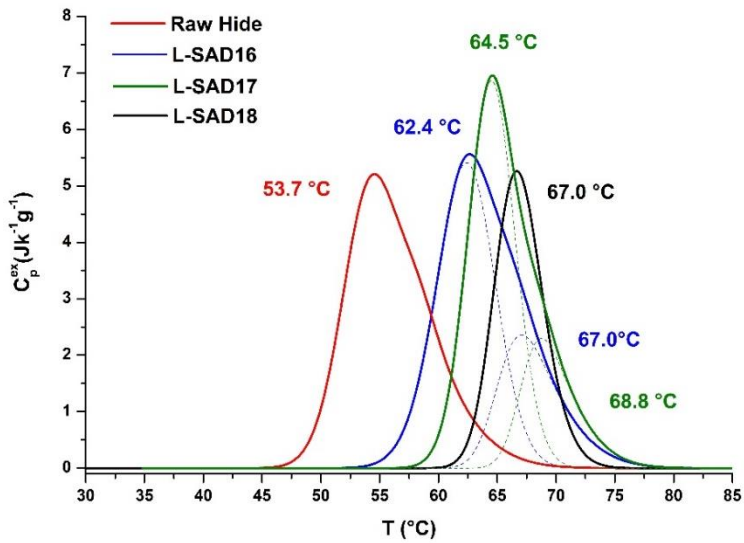


Figure 90. Denaturation curves of leathers tanned with the SADs synthesized by a two-step process: US treatment and oxidation with  $\text{NaIO}_4$ .

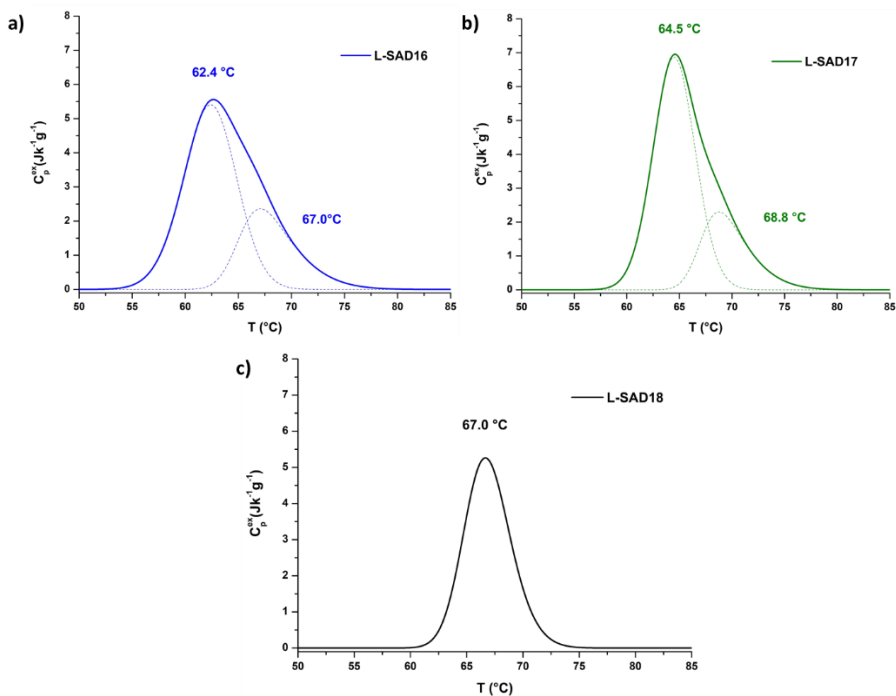


Figure 91. Bi-component denaturation curves of a) L-SAD16, b) L-SAD17, compared to mono-component denaturation curve of c) L- SAD18.

Even SAD16-18 do not yet achieve the performance of a commercial tanning agent, they can be highly competitive as commercial re-tanning agents. Furthermore, the quantity of the periodate used is really very low and this implies lower costs and environmental benefit in terms of wastewater organic loading.

## 5.7 Conclusion

The use of ultrasounds as “depolymerization agent” allows to obtain Sodium Alginate Derivatives (SADs) with different molecular weights and degree of oxidation. Compared to the oxidised sodium alginate (OSA) synthesized by oxidation with  $\text{NaIO}_4$ , our US treatments generated much less aldehydic groups. This limits the use of the US-synthesized SADs for the re-tanning process, where a higher distribution of molecular weights would

enable both the fullness of leather and grain evenness (by penetrating in the hide structure and filling the space between collagen fibres).

Moreover, the use of a technology entirely based on the use of ultrasound paves the way for greener industrial technology by reducing the use of more toxic and not biodegradable chemicals. Of course, the “US *synthesis*” can be considered a green process, and SADs are safe and biodegradable products with the additional advantage of their renewable raw matter.

Furthermore, a two-step synthesis based on US and very low quantities of  $\text{NaIO}_4$  allowed us to obtain a product that could become very competitive as a strong re-tanning agent. The very low concentration of  $\text{NaIO}_4$  significantly reduces its environmental and economic drawbacks.

The results obtained so far have confirmed the suitability of the various SADs as non-toxic re-tanning agents for increasing the biodegradability of leather and the environmental impact of end-of-life leather.

The next research step will concern with the upscaling of SADs production and re-tanning process on industrial pilot scale at the industrial facility of CURTIDOS BADIA SA tannery. The most effective SADs will be selected based on their validation tests at industrial level.

## **5.8 Experimental section**

The ultrasound experiments were performed at the Faculty of Applied Chemistry and Materials Science of the University Politehnica of Bucharest under the joint supervision of Professor Ioan Calinescu and Dr. Petre Chipurici.

**The ultrasonic horn** used was Sonic vibracell VCX 750 with a 13mm probe in titanium. The process for obtaining the samples was conducted in a flask under atmospheric pressure and the temperature was maintained constant using the ultra-low refrigerated circulators Thermo Scientific HAKEE G50.

**The bath type reactors** used were the Advanced sonic processing systems and the Meinhardt Ultraschalltechnik. The process for obtaining the samples was conducted under atmospheric pressure and the temperature was maintained constant using the thermostat MK70 MLW.

Tanning tests and physical-chemical analyses were performed at the Leather and Footwear Research Institute (ICPI), a branch of the National Research and Development Institute for Textiles and Lather (INCDTP), Bucharest under the supervision of Dr. Elena Badea.

**Micro Hot table (MHT)** measurements were performed with an equipment composed of a Linkam LTS120 micro heating plate (Linkam Scientific Instruments) equipped with an automatic heating rate adjustment system and a SMZ 745 Nikon stereomicroscope. The shrinking motion was registered by a Nikon D90 digital camera mounted on the microscope. Micro-samples of 10-15 fibres were thoroughly wetted and separated in demineralised water, placed on a microscope slide with a concavity and left 2 min to reach a homogeneous hydration level. Hydrated fibres were separated as much as possible under the microscope light using a pair of fine needles and then covered with a cover glass, placed on the hot table and heated at  $2^{\circ}\text{C per min}^{-1}$ . The shrinkage process was digitally recorded, and the various temperatures defining the shrinkage activity were visually determined.

**The viscosity** was measured using a Brookfield Ametek DV2T viscometer set at  $20^{\circ}\text{C}$  using different spindle depending on the viscosity of the sample.

**The Infrared Spectroscopy in Attenuated Total Reflection mode (FTIR-ATR)** analyses were carried out using an ALPHA spectrometer (Bruker Optics) equipped with a Platinum ATR module. The penetration depth, depending on the refractive indices of ATR crystal and sample, typically amounts to a few microns (ca.  $0.5\text{--}3\ \mu\text{m}$ ). Spectra were recorded in the  $4000\text{--}400\ \text{cm}^{-1}$  spectral range with a  $4\ \text{cm}^{-1}$  resolution, using 32 scans. Opus software (Bruker Optics, Germany) was used for the acquisition and elaboration of the spectra.

**Micro-Differential Scanning Calorimetry (micro-DSC)** measurements were carried out with a high-sensitivity Micro-DSC III calorimeter (SETARAM), in the temperature range ( $25\text{--}85$ )  $^{\circ}\text{C}$ , at  $0.5\ \text{K min}^{-1}$  heating rate, using  $850\ \mu\text{l}$  stainless steel (Hastelloy C) cells. This low scan rate was applied to provide the equilibrium condition for DSC analysis and accurately measure the denaturation parameters. Samples of about ( $5.0\text{--}10.0$ ) mg were suspended in  $0.5\ \text{M}$  acetate buffer ( $\text{pH} = 5.0$ ) directly in the measure cell and left for 30

minutes to assure their fully hydration and avoid  $T_{\max}$  and enthalpy variation with hydration level. Experimental DSC data acquired with the SETARAM SetSoft2000 software were analysed using PeakFit 4.1 (Jandel Scientific). DSC multiple peaks of the investigated samples were deconvoluted using the PeakFit asymmetric Gaussian fit function to improve the fit of the asymmetry in the peaks.

The industrial sodium alginate was procured from Kemia Tau, Italy. Ethylene glycol and sodium periodate were purchased from Sigma Aldrich. Sodium chloride, sodium bicarbonate and water were industrial grade reagents.

## 6. Final conclusions

The main goal of this PhD research project concerns with the synthesis of new classes of eco-friendly additives from renewable sources for a more sustainable tanning process.

The possibility of exploiting supramolecular complexes to derive a more eco-friendly and water soluble wet-white tanning agent from the widely used tannin MIDA DD<sup>®</sup>, a bisphenol S based polymer, through the use of  $\beta$ -cyclodextrin, a cyclic oligosaccharide, was explored.

The formation of new supramolecular systems based on the interaction of  $\beta$ -cyclodextrin with the commercial polymer (MIDA DD<sup>®</sup>) enabled us to obtain a new class of synthetic tannins (*SupraSynts*) which, in addition of being more environmentally friendly, conferred leather added safety and enhanced performance features. The physical-chemical and mechanical properties of crust leather prove that the *host-guest* synergy is advantageous in terms of quality, environmental impact, cost and end-of-life leather, and thus competitive advantage over the current product MIDA DD<sup>®</sup>.

Moreover, as the MIDA DD<sup>®</sup> is a polymer bisphenol S based, we evaluated the complexation ability between  $\beta$ -CD and the two isomers of BPS. The results clearly show that  $\beta$ -CD host can recognize the two isomers, 4,4'-

dihydroxydiphenyl sulfone and 2,4'-dihydroxydiphenyl sulfone (BPS) in solution, gas phase, and in the solid state with a 4,4'-BPS/2,4'-BPS selectivity ratio of 6.3.

Successively, due to the growing concerns related to the environmental impact of the commercial synthetic re-tanning agents currently on the market, the research was focused on the possibility to develop more sustainable additives derived entirely from renewable sources such as alginate.

Sodium Alginate Derivatives (SADs) able to interact with collagen within hide have been synthesized using the ultrasound technology (US). Periodate oxidation of SADs allowed us to enhance their ability to interact more strongly and evenly with collagen throughout the hide structure. Such re-tanning agents will also offer a competitive advantage over the synthetic ones through a balance between product performance and longer life-time, costs and environmental benefits.

## Scientific contributions:

- Gliubizzi, R.; Pauciulo, A., Bruno, I., Bartiromo, A., Quaratesi, I., Gaeta, C.; Neri, P.; Composto conciante o riconciante di pellame con composto di inclusione a base di ciclodestrina. **2022**, Patent submitted with application number 1020220000938.
- Quaratesi, I.; Della Sala, P.; Capacchione, C.; Talotta, C.; Geremia, S.; Hickey, N.; Gliubizzi, R.; Bruno, I.; Sgarlata, C.; Migliore, R.; Gaeta, C.; Neri, P.; Selective recognition of bisphenol S isomers in water by  $\beta$ -cyclodextrin. *Supramol Chem*, **2021**, 1061-0278. [DOI: 10.1080/10610278.2021.1991925]
- Capacchione, C.; Della Sala, P.; Quaratesi, I.; Bruno, I.; Pauciulo, A.; Bartiromo, A. R.; Neri, P.; Talotta, C.; Gliubizzi, R.; Gaeta, C.; Poly(Ethylene Glycol)/ $\beta$ -Cyclodextrin Pseudorotaxane Complexes as Sustainable Dispersing and Retarding Materials in a Cement-Based

Mortar. *ACS Omega* **2021**, *6* (8), 12250–12260. [DOI: 10.1021/acsomega.1c01133].

- 28<sup>th</sup> Progress in Organic and Macromolecular Compounds, MACRO lasi 2021, oral presentation: “ $\beta$ -cyclodextrin host for the selective recognition of isomers of bisphenol S in water.”
- 28<sup>th</sup> Progress in Organic and Macromolecular Compounds, MACRO lasi 2021, poster session: “Alginate-derived tanning agents for biodegradable leather.”
- Supramolecular chemistry days for young researchers. 13-15 October 2021- virtual edition, poster session: “Molecular Recognition of Isomers of Bisphenol S by  $\beta$ -Cyclodextrin Host.”